

**CATALYSTS SUPPORTED ON MCM-41 SYNTHESIZED  
FROM RICE HUSK SILICA: TITANIUM OXIDE FOR  
PHOTODEGRADATION OF ORGANIC POLLUTANTS  
AND POTASSIUM OXIDE FOR TRANSESTERIFI-  
CATION OF PALM OLEIN OIL**

**Surachai Artkla**

**A Thesis Submitted in Partial Fulfillment of the Requirements for the  
Degree of Doctor of Philosophy in Chemistry  
Suranaree University of Technology  
Academic Year 2008**

ตัวเร่งปฏิกิริยาบนตัวรองรับ MCM-41 ที่สังเคราะห์โดยใช้ซิลิกาจากแกลบ:  
ไทเทเนียมออกไซด์ สำหรับการสลายตัวด้วยแสงของสารมลพิษอินทรีย์ และ  
โพแทสเซียมออกไซด์สำหรับแทรนส์เอสเทอริฟิเคชันของน้ำมันปาล์มโอเลอิน

นายสุรชัย อากกล้า

วิทยานิพนธ์นี้เป็นส่วนหนึ่งของการศึกษาตามหลักสูตรปริญญาวิทยาศาสตรดุษฎีบัณฑิต  
สาขาวิชาเคมี  
มหาวิทยาลัยเทคโนโลยีสุรนารี  
ปีการศึกษา 2551

**CATALYATS SUPPORTED ON MCM-41 SYNTHESYZED FROM  
RICE HUSK SILICA: TITANIUM OXIDE FOR  
PHOTODEGRADATION OF ORGANIC POLLUTANTS AND  
POTASSIUM OXIDE FOR TRANSESTERIFICATION OF PALM  
OLEIN OIL**

Suranaree University of Technology has approved this thesis submitted in partial fulfillment of the requirements for the Degree of Doctor of Philosophy.

Thesis Examining Committee

---

(Assoc. Prof. Dr. Malee Tangsathitkulchai)

Chairperson

---

(Assoc. Prof. Dr. Jatuporn Wittayakun)

Member (Thesis Advisor)

---

(Prof. Dr. Wonyong Choi)

Member

---

(Assoc. Prof. Dr. Nurak Grisdanurak)

Member

---

(Dr. Sanchai Prayoonpokarach)

Member

---

(Prof. Dr. Pairote Sattayatham)

Vice Rector for Academic Affairs

---

(Assoc. Prof. Dr. Prapan Manyum)

Dean of Institute of Science

สุรัชย์ อาจกล้า : ตัวเร่งปฏิกิริยาบนตัวรองรับ MCM-41 ที่สังเคราะห์โดยใช้ซิลิกาจาก  
แกลบ : ไทเทเนียมออกไซด์ สำหรับการสลายตัวด้วยแสงของสารมลพิษอินทรีย์ และ  
โพแทสเซียมออกไซด์ สำหรับทรานส์เอสเทอร์ฟิเคชันของน้ำมันปาล์มโอเลอิน  
(CATALYSTS SUPPORTED ON MCM-41 SYNTHESIZED FROM RICE HUSK  
SILICA: TITANIUM OXIDE FOR PHOTODEGRADATION OF ORGANIC  
POLLUTANTS AND POTASSIUM OXIDE FOR TRANSESTERIFICATION OF  
PALM OLEIN OIL) อาจารย์ที่ปรึกษา : รองศาสตราจารย์ ดร. จตุพร วิทยาคุณ, 158 หน้า.

วิทยานิพนธ์นี้เน้นศึกษาตัวเร่งปฏิกิริยาบนตัวรองรับ RH-MCM-41 ซึ่งเป็นวัสดุมีโซพอร์  
ที่สังเคราะห์ได้จากซิลิกาจากแกลบข้าว ได้แก่ (1) Ti-RH-MCM-41 ซึ่งเตรียมได้จากการเติมเต  
ตระบิวทิล ออโทไทเทเนท (TBOT) ลงในเจลที่ใช้สังเคราะห์ RH-MCM-41 (2) TiO<sub>2</sub>/RH-  
MCM-41 เตรียมได้จากการปลูกถ่าย TBOT บน RH-MCM-41 ที่เตรียมไว้แล้ว (3) TiO<sub>2</sub>/RH-  
MCM-41 เตรียมได้จากการกระจายอนุภาคนาโนของ TiO<sub>2</sub> ลงไปบน RH-MCM-41 และ (4)  
K<sub>2</sub>O/RH-MCM-41 เตรียมได้โดยวิธีทำให้ RH-MCM-41 เอบ่มด้วยโพแทสเซียมอะซิเตต แล้ว  
วิเคราะห์ตัวเร่งปฏิกิริยาทั้งหมดด้วยเทคนิคหลายอย่าง เช่น การเลี้ยวเบนของรังสีเอกซ์ และการดูด  
ซับ-การคายไนโตรเจน

นำตัวเร่ง Ti-RH-MCM-41 และ TiO<sub>2</sub>/RH-MCM-41 เตรียมจากการปลูกถ่าย ที่มี  
ปริมาณ TiO<sub>2</sub> เท่ากัน คือ 10% โดยมวล มาทดสอบปฏิกิริยาการสลายตัวด้วยแสงของเมทิลออเรนจ์  
ได้ค่าการแปลงผันของเมทิลออเรนจ์ เท่ากับ 32.0% และ 87.10% ตามลำดับ ตัวเร่งตัวที่สองดีกว่า  
เพราะว่ามีปริมาณไททาเนียที่เป็นอะนาเทส ซึ่งเป็นเฟสที่ว่องไวสูงกว่าตัวแรก เมื่อทดสอบต่อไป  
โดยใช้อัตราส่วนน้ำหนักรของตัวเร่งต่อปริมาตรเมทิลออเรนจ์เท่ากับ 5 กรัมต่อลิตร และความ  
เข้มข้นเริ่มต้น 2 ส่วนในล้าน พบว่าการสลายตัวมีอันดับเทียมเท่ากับ 1 และค่าคงอัตราเท่ากับ 0.17  
ต่อนาที

นำตัวเร่ง TiO<sub>2</sub>/RH-MCM-41 ที่เตรียมจากการปลูกถ่าย และการกระจายอนุภาคนาโน มา  
ทดสอบปฏิกิริยาการสลายตัวด้วยแสงของอะลาคลอร์ ได้ค่าการแปลงผันของอะลาคลอร์หลังจาก  
20 นาที เท่ากับ 76.2% และ 100% ตามลำดับ ตัวเร่งที่เตรียมจากการกระจายอนุภาคนาโนดีกว่า  
เพราะประกอบไปด้วยไททาเนียที่มีทั้งเฟสอะนาเทต และรูไทล์ในอัตราส่วน 80:20 ซึ่งเป็น  
อัตราส่วนที่เหมาะสมที่ว่องไวที่สุด นอกจากนี้การทำงานของตัวเร่งนี้ดีกว่าไททาเนียเปล่าเล็กน้อย  
(100% และ 95% ตามลำดับ) เมื่อทดสอบปฏิกิริยาโดยใช้อัตราส่วนน้ำหนักรของตัวเร่งต่อ  
ปริมาตรอะลาคลอร์ 1 กรัมต่อลิตร ที่ความเข้มข้นของอะลาคลอร์ 80 ไมโครโมลาร์ และ pH ของ

สารละลายเท่ากับ 4 พบว่าการสลายตัวมีอันดับเทียมเท่ากับ 1 ค่าคงที่อัตราเท่ากับ 0.23 ต่อนาที และการดูดซับของอะลาคลอร์บนไททานเนียมที่กระจายบน RH-MCM-41 เป็นการดูดซับแบบฟรอนด์ลิช

จากนั้นนำ  $\text{TiO}_2/\text{RH-MCM-41}$  ที่เตรียมจากการกระจายอนุภาคนาโนของ  $\text{TiO}_2$  บน RH-MCM-41 มาทดสอบปฏิกิริยาการสลายตัวด้วยแสงของ เตตระเมทิลแอมโมเนียม (TMA) คลอไรด์ เพื่อเปรียบเทียบความว่องไวกับ  $\text{TiO}_2$  เปล่า พบว่า  $\text{TiO}_2/\text{RH-MCM-41}$  ดูดซับ TMA ดีกว่าบน  $\text{TiO}_2$  เปล่า (15% และ 5%) และตัวเร่ง 10%  $\text{TiO}_2/\text{RH-MCM-41}$  ให้ค่าการแปลงผันของ TMA เท่ากับ 100% หลังจาก 90 นาที ในขณะที่  $\text{TiO}_2$  เปล่า ในปริมาณที่เท่ากัน ให้ค่าการแปลงผันเพียง 20% การสลายตัวมีอันดับเทียมเท่ากับ 1 ค่าคงที่อัตราเท่ากับ 0.029 ต่อนาที และการดูดซับของ TMA บน 10%  $\text{TiO}_2/\text{RH-MCM-41}$  เป็นแบบแลงเมียร์

สุดท้าย นำตัวเร่ง  $\text{K}_2\text{O}/\text{RH-MCM-41}$  มาทดสอบกับปฏิกิริยาการผลิตไบโอดีเซลจากน้ำมันปาล์มโอเลอิน และเมทานอล ผ่านปฏิกิริยาทรานส์เอสเตอร์ฟิเคชันที่อุณหภูมิ 50 75 และ 100 °C การทดลองพบว่า 8%  $\text{K}_2\text{O}/\text{RH-MCM-41}$  ให้ค่าการแปลงผันสูงสุดในทุกอุณหภูมิ และที่ปริมาณการเติมเดียวกันนี้ ความว่องไวเพิ่มขึ้นตามอุณหภูมิ และให้ค่าการแปลงผันเฉลี่ย 84% ที่อุณหภูมิ 100 °C

SURACHAI ARTKLA : CATALYSTS SUPPORTED ON MCM-41  
SYNTHESIZED FROM RICE HUSK SILICA: TITANIUM OXIDE  
FOR PHOTODEGRADATION OF ORGANIC POLLUTANTS AND  
POTASSIUM OXIDE FOR TRANSESTERIFICATION OF  
PALM OLEIN OIL. THESIS ADVISOR : ASSOC. PROF.  
JATUPORN WITTAYAKUN, Ph.D. 158 PP.

RH-MCM-41/TiO<sub>2</sub>/K<sub>2</sub>O/HETEROGENEOUS CATALYSIS/BIODIESEL/TMA/  
ALACHLOR/FAME/ PHOTODEGRADATION/ TRANSESTERIFICATION

This thesis focused on catalysts supported on RH-MCM-41, a mesoporous material synthesized with rice husk silica. The catalysts were: (1) Ti-RH-MCM-41 prepared by adding tetrabutyl orthotitanate (TBOT) into the synthesis gel of RH-MCM-41; (2) TiO<sub>2</sub>/RH-MCM-41 prepared by grafting TBOT on preformed RH-MCM-41; (3) TiO<sub>2</sub>/RH-MCM-41 prepared by dispersing nanoparticles of TiO<sub>2</sub> on RH-MCM-41; and K<sub>2</sub>O/RH-MCM-41 prepared by impregnation of potassium acetate on RH-MCM-41. All catalysts were well characterized by various techniques such as X-ray diffraction and nitrogen adsorption-desorption.

The Ti-RH-MCM-41 and TiO<sub>2</sub>/RH-MCM-41 from grafting with TiO<sub>2</sub> loading of 10 wt%, were tested for photodegradation of methyl orange. The conversions on both catalysts after 20 min were 32.20% and 87.10%, respectively. The later was more active because it contained more anatase which is an active phase of titania. When tested further at a ratio of catalyst weight to methyl orange volume of 5 g/L and initial concentration of 2.0 ppm, the degradation obeyed pseudo-first order with a rate constant of 0.17 min<sup>-1</sup>.

The TiO<sub>2</sub>/RH-MCM-41 catalysts prepared from grafting and dispersing titania nanoparticles were tested for photodegradation ofalachlor. The conversions on both catalysts after 20 min were 76.2% and 100%, respectively. The second catalyst was better because it contained both anatase and rutile phases with ration of 80:20 which was the optimum ratio to give the highest catalytic activity. The performance of the titania dispersed on RH-MCM-41 was slightly better than the bare TiO<sub>2</sub> (conversion 100% vs 95%, respectively). The reaction tested at catalyst weight toalachlor volume of 1 g/L withalachlor concentration of 80 μM and solution pH of 4 obeyed pseudo-first order with rate constant of 0.23 min<sup>-1</sup>. The adsorption ofalachlor on the titania dispersed on RH-MCM-41 obeyed Freundlich isotherm.

The TiO<sub>2</sub>/RH-MCM-41 prepared by dispersing titania nanoparticles on RH-MCM-41 was tested for photodegradation of tetramethylammonium (TMA) chloride comparing photoactivity with bare TiO<sub>2</sub>. The TiO<sub>2</sub>/RH-MCM-41 had higher TMA adsorption (15% vs 5%) and activity than that of the bare TiO<sub>2</sub>. The highest TMA conversion of 100% was obtained from 10%Ti<sub>2</sub>/RH-MCM-41 after 90 min while only 20% conversion was obtained from the bare TiO<sub>2</sub> with the same TiO<sub>2</sub> loading. The kinetics obeyed pseudo-first order with rate constant of 0.029 min<sup>-1</sup>. Adsorption fitted well with Langmuir isotherm.

Finally, K<sub>2</sub>O/RH-MCM-41 catalysts were tested for biodiesel production from transesterification of palm olein oil and methanol at 50, 75 and 100 °C. The catalyst with 8%K<sub>2</sub>O/RH-MCM-41 gave the highest average conversion of 84% at 100 °C.

School of Chemistry

Academic Year 2008

Student's signature\_\_\_\_\_

Advisor's signature\_\_\_\_\_

## **ACKNOWLEDGEMENTS**

I am profoundly grateful to my advisor, Assoc. Prof. Dr. Jatuporn Wittayakun, for his patient guidance, support, encouragement and suggestions throughout this research. I would like to thank Assoc. Prof. Dr. Nurak Grisdanurak and Prof. Dr. Wonyong Choi for their facilitating, supervising and encouraging in parts of my experiment. Their guiding provided extensive knowledge and expanded my scientific point of view.

I would like to acknowledge other committee members including Assoc. Prof. Dr. Malee Tungsathikulchai and Dr. Sanchai Prayoonpokarach for their suggestions before and during my defense. I wish to thank all the lecturers at the School of Chemistry for their good attitude and advices, all of staffs at the Center for Scientific and Technology Equipments for their assistance and suggestion on the uses of instruments.

I also would like to thank all of my lab members at Material Chemistry Research Unit at SUT, National Center of Excellent for Environmental and Hazardous Waste Management at TU and Environmental Photoenergy application at POSTECH, Korea for their valuable discussions, helps and comments.

I acknowledge supports from Suranarree University of Technology (scholarship for student with outstanding academic record and research funding) and Research Synchrotron Light Research Institute (Public Organization) Research Grant 2-2548/PS01.

I am finally deeply grateful to my parents, my sisters and my love for support, understanding, encouragement, motivation and building up inspiration.

Surachai Artkla



## CONTENTS

	<b>Page</b>
ABSTRACT IN THAI.....	I
ABSTRACT IN ENGLISH.....	III
ACKNOWLEDGEMENTS.....	V
CONTENTS.....	VI
LIST OF FIGURES.....	XIV
LIST OF TABLES.....	XXI
LIST OF SCHEMES.....	XXII
LIST OF ABBRIVIATIONS.....	XXIII
<b>CHAPTER</b>	
<b>I INTRODUCTION.....</b>	<b>1</b>
1.1 Rationale of the study.....	1
1.1.1 Rice husk silica and MCM-41.....	1
1.1.2 Photodegradation of nitrogenous organic compounds.....	2
1.1.3 Transesterification of palm olein .....	4
1.2 Research objectives.....	4
1.3 References.....	5
<b>II LITERATURE REVIEWS</b>	
2.1 Introduction.....	8



## CONTENTS (Continued)

	<b>Page</b>
2.7.3 Separation of mixed products from transesterification.....	36
2.7.4 Heterogeneous catalysts.....	36
2.8 References.....	39
<b>III PHOTOCATALYTIC DEGRADATION OF METHYL ORANGE ON Ti-RH-MCM-41 AND TiO<sub>2</sub>/RH-MCM-41.....</b>	<b>50</b>
3.1 Abstract.....	50
3.2 Introduction.....	51
3.3 Experimental .....	54
3.3.1 Chemicals and materials.....	54
3.3.2 Apparatus and instruments.....	54
3.3.3 Preparation of rice husk silica.....	55
3.3.4 Synthesis of RH-MCM-41.....	55
3.3.5 Synthesis of Ti-RH-MCM-41.....	56
3.3.6 Preparation of TiO <sub>2</sub> /RH-MCM-41.....	56
3.3.7 Catalyst Characterization.....	57
3.3.8 Catalytic testing for photocatalytic degradation of methyl orange.....	58
3.3.9 Adsorption of methyl orange on TiO <sub>2</sub> /RH-MCM-41.....	59
3.4 Results and discussion.....	59



## CONTENTS (Continued)

	<b>Page</b>
4.3.5 Photocatalytic degradation of alachlor.....	87
4.3.6 Adsorption isotherm of alachlor.....	88
4.4 Results and Discussion.....	89
4.4.1 Characterization of catalysts by XRD.....	89
4.4.2 Characterization by Nitrogen adsorption-desorption.....	91
4.4.3 Characterization by TEM.....	93
4.4.4 Characterization by DR-UV.....	95
4.4.5 Characterization by zeta potential analysis.....	96
4.4.6 Photodegradation of alachlor on bare TiO <sub>2</sub> and TiO <sub>2</sub> /RH-MCM.....	97
4.4.6.1 Effect of TiO <sub>2</sub> loading on RH-MCM-41 to photodegradation.....	97
4.4.6.2 Comparison on catalytic activity of catalysts.....	98
4.4.6.3 Synergistic effect of support and UV light.....	100
4.4.6.4 Effect of alachlor concentration.....	101
4.4.6.5 Kinetics of reaction.....	103
4.4.6.6 Effect of pH to photodegradation of alachlor.....	104

## CONTENTS (Continued)

	<b>Page</b>
4.4.7 Adsorption isotherm ofalachlor.....	107
4.5 Conclusions.....	110
4.6 References.....	110
<b>V PHOTOCATALYTIC DEGRADATION OF TETRAMETHYL- AMMONIUM CHLORIDE ON TiO<sub>2</sub>/RH-MCM-41.....</b>	<b>114</b>
5.1 Abstract.....	114
5.2 Introduction.....	115
5.3 Experimental.....	117
5.3.1 Chemicals and materials.....	117
5.3.2 Apparatus and instruments.....	117
5.3.3 Photocatalytic degradation of TMA.....	117
5.3.4 Adsorption isotherm determination on catalysts.....	118
5.4 Results and discussion.....	119
5.4.1 Photodegradation of TMA on bare TiO <sub>2</sub> and TiO <sub>2</sub> /RH-MCM-41.....	119
5.4.1.1 Effect of TiO <sub>2</sub> content on RH-MCM-41 to photodegradation.....	119
5.4.1.2 Effect of catalyst concentration.....	119
5.4.1.3 Effect of pH to photodegradation of TMA on TiO <sub>2</sub> /RH-MCM-41.....	121
5.4.1.4 Synergic effect of support and UV light....	124

## CONTENTS (Continued)

	<b>Page</b>
5.4.1.5 Kinetics of reaction.....	128
5.4.2 Adsorption of TMA on bare TiO <sub>2</sub> and TiO <sub>2</sub> /RH-MCM-41.....	129
5.5 Conclusions.....	132
5.6 References.....	133
<b>VI TRANSESTERIFICATION OF PALM OLEIN WITH METHANOL ON K<sub>2</sub>O/RH-MCM-41.....</b>	<b>135</b>
6.1 Abstract.....	135
6.2 Introduction.....	136
6.3 Experimental.....	137
6.3.1 Chemicals and materials.....	137
6.3.2 Apparatus and instruments.....	138
6.3.3 Preparation of K <sub>2</sub> O/RH-MCM-41.....	138
6.3.4 Characterization of K <sub>2</sub> O/RH-MCM-41.....	138
6.3.5 Catalytic testing for transesterification.....	139
6.4 Results and discussion.....	140
6.4.1 Characterizations of K <sub>2</sub> O/RH-MCM-41.....	140
6.4.2 Catalytic Activity of K <sub>2</sub> O/RH-MCM-41 and K <sub>2</sub> O/RH-SiO <sub>2</sub> .....	147
6.5 Conclusions.....	150
6.6 References.....	150

**CONTENTS (Continued)**

	<b>Page</b>
<b>VII CONCLUSION.....</b>	153
<b>APPENDIX.....</b>	156
<b>CURRICULAR VITAE.....</b>	158



## LIST OF FIGURES

Figure	Page
2.1 Main processes occurring in a semiconductor particle upon absorption of photon energy larger than band gap energy ( $E_g$ ) to excite electron from valence (VB) to conduction band (CB): (a) electron–hole generation; (b) oxidation of donor ( $D_{ads}$ ); (c) reduction of acceptor ( $A_{ads}$ ); (d) and (e) electron–hole recombination at surface and in bulk, respectively.....	22
2.2 Structures of a) anatase and b) rutile.....	23
3.1 XRD of spectrum of RH-SiO <sub>2</sub> .....	60
3.2 A) low angle XRD patterns of Ti-RH-MCM-41 and TiO <sub>2</sub> /RH-MCM-41 and B) high angle XRD pattern of TiO <sub>2</sub> /RH-MCM-41.....	62
3.3 Ti K-edge XANES spectra of 10% Ti-RH-MCM-41, Ti foil and TiO <sub>2</sub> anatase references .....	64
3.4 Fourier-transform magnitude of the $k^3$ -weighted Ti EXAFS spectrum of 10% Ti-RH-MCM-41, calculated in the k range of 2.3-9.55 Å <sup>-1</sup> (dotted line-experimental curve, solid line-theoretical curve): <b>A</b> ) k space and <b>B</b> ) R space. <b>A</b> ) N <sub>2</sub> adsorption-desorption isotherm and <b>B</b> ) pore size distribution of RH-MCM-41 and 10% Ti-RH-MCM-41.....	65

## LIST OF FIGURES (Continued)

<b>Figure</b>	<b>Page</b>
3.5 A) N <sub>2</sub> adsorption-desorption isotherm and B) pore size distribution of RH-MCM-41 and 10%Ti-RH-MCM-41.....	68
3.6 FTIR of RH-MCM-41 and Ti-MCM-41.....	69
3.7 Catalytic activity of 10%Ti-RH-MCM-41 and 10%Ti-MCM-41: cat = 2.5 g/L, C <sub>0</sub> = 2 ppm, pH = 4.5, [H <sub>2</sub> O <sub>2</sub> ] = 0.01 M.....	71
3.8 Effect of catalyst concentration on photocatalytic degradation of methyl orange on 10%TiO <sub>2</sub> /RH-MCM-41: C <sub>0</sub> = 2 ppm, pH = 4.5, [H <sub>2</sub> O <sub>2</sub> ] = 0.01 M.....	72
3.9 Effect of methyl orange concentration to photocatalytic degradation on 10%TiO <sub>2</sub> /RH-MCM-41: [cat.] = 5.0 g/L, C <sub>0</sub> = 2 ppm, pH = 4.5, [H <sub>2</sub> O <sub>2</sub> ] = 0.01 M.....	73
3.10 Initial degradation rate of methyl orange degradation.....	74
3.11 Pseudo-first order plot of photocatalytic degradation of methyl orange on TiO <sub>2</sub> /RH-MCM-41.....	75
3.12 Adsorption of methyl orange on TiO <sub>2</sub> /RH-MCM-41; cat = 5 g/L, C <sub>0</sub> = 2, 4, 6 and 10 ppm, pH = 4.5, [H <sub>2</sub> O <sub>2</sub> ] = 0.01 M: A) Langmuir isotherm and B) Freundlich isotherm.....	78
4.1 Chemical structure of alachlor.....	83
4.2 XRD spectra; A) characteristic peaks of RH-MCM-41 and B) characteristic peaks of anatase and rutile phase of TiO <sub>2</sub> .....	90

## LIST OF FIGURES (Continued)

Figure	Page
4.3 A) N <sub>2</sub> adsorption-desorption isotherm; a) RH-MCM-41, b) 10% TiO <sub>2</sub> /RH-MCM-41, c) 20% TiO <sub>2</sub> /RH-MCM-41, d) 40% TiO <sub>2</sub> /RH-MCM-41, e) 60% TiO <sub>2</sub> /RH-MCM-41 and f) bare TiO <sub>2</sub> . B) Mesopore size distribution of RH-MCM-41 and 10% TiO <sub>2</sub> /RH-MCM-41.....	92
4.4 High-resolution TEM images of RH-MCM-41, TiO <sub>2</sub> and 10% TiO <sub>2</sub> /RH-MCM-41; A) Hexagonal structure of RH-MCM-41 (100k), B) unsupported bare TiO <sub>2</sub> nanoparticles (25k), C) and D) TiO <sub>2</sub> particles on RH-MCM-41 (25k).....	94
4.5 UV-visible diffuse reflectance spectra of a) TiO <sub>2</sub> , b) 60% TiO <sub>2</sub> /RH-MCM-41, c) 40% TiO <sub>2</sub> /RH-MCM-41, d) 20% TiO <sub>2</sub> /RH-MCM-41, e) 10% TiO <sub>2</sub> /RH-MCM-41, and f) RH-MCM-41.....	95
4.6 Zeta potential of RH-MCM-41, TiO <sub>2</sub> /RH-MCM-41 and TiO <sub>2</sub> suspended in water as a function of pH.....	97
4.7 Photocatalytic degradation ofalachlor on various TiO <sub>2</sub> /RH-MCM-41s; [TiO <sub>2</sub> /RH-MCM-41] = 1 g/L, pH = 4, [alachlor] = 80 μM, UV light = 300 nm.....	98
4.8 Comparison of photocatalytic activity of various TiO <sub>2</sub> /RH-MCM-41s for photodegradation ofalachlor; [modified TiO <sub>2</sub> ] = 1 g/L, [TiO <sub>2</sub> ] = 0.1 g/L, pH = 4, [alachlor] = 100 μM, UV light = 300 nm...	99

## LIST OF FIGURES (Continued)

<b>Figure</b>	<b>Page</b>
4.9 Photocatalytic degradation of alachlor on bare TiO <sub>2</sub> , TiO <sub>2</sub> /RH-MCM-41, dark control TiO <sub>2</sub> /RH-MCM-41 and RH-MCM-41; [TiO <sub>2</sub> /RH-MCM-41] = 1 g/L, pH = 4, [alachlor] = 80 μM, UV light = 300 nm.....	101
4.10 Effect of concentration influencing photocatalytic degradation of alachlor; [TiO <sub>2</sub> /RH-MCM-41] = 1 g/L, pH = 4, UV light = 300 nm.....	102
4.11 Initial degradation rate of alachlor by differential method; [TiO <sub>2</sub> /RH-MCM-41] = 1 g/L, pH = 4, UV light = 300 nm.....	103
4.12 Pseudo-first order plot from photocatalytic degradation of alachlor; [TiO <sub>2</sub> /RH-MCM-41] = 1 g/L, pH = 4, [alachlor] = 80 μM, UV light = 300 nm.....	104
4.13 Effect of pH influencing photocatalytic degradation of alachlor; [TiO <sub>2</sub> /RH-MCM-41] = 1 g/L, [alachlor] = 80 μM, UV light = 300 nm.....	105
4.14 Initial degradation rate of alachlor influencing by pH solution; [TiO <sub>2</sub> /RH-MCM-41] = 1 g/L, [alachlor] = 80 μM, UV light = 300 nm.....	106
4.15 Adsorption of alachlor on TiO <sub>2</sub> /RH-MCM-41; A) Langmuir isotherm A) Freundlich isotherm; [TiO <sub>2</sub> /RH-MCM-41] = 1 g/L, pH = 4, [alachlor] = 80 μM, UV light = 300 nm.....	109

## LIST OF FIGURES (Continued)

Figure	Page
5.1 Effect of TiO <sub>2</sub> loadings in TiO <sub>2</sub> /RH-MCM-41 on photocatalytic degradation rate of TMA; [TMA] = 100 μM, pH = 7.....	120
5.2 Effect of catalyst concentration on photocatalytic degradation of TMA; [TMA] = 100 μM, pH = 7.....	121
5.3 Effect of pH solution on photocatalytic degradation of TMA; [TMA] = 100 μM, [10% TiO <sub>2</sub> /RH-MCM-41] = 1 g/L.....	122
5.4 Effect of solution pH on degradation rate of TMA; [TMA] = 100 μM, [TiO <sub>2</sub> /RH-MCM-41] = 1 g/L, [TiO <sub>2</sub> ] = 0.1 g/L.....	123
5.5 Photocatalytic degradation of TMA on TiO <sub>2</sub> , RH-MCM-41 and TiO <sub>2</sub> /RH MCM-41; [RH-MCM-41] = 1 g/L, [TiO <sub>2</sub> /RH-MCM-41] = 1 g/L, [TiO <sub>2</sub> ] = 0.1 g/L, pH = 7.....	124
5.6 Product distribution from photodegradation of TMA: A) bare TiO <sub>2</sub> and B) TiO <sub>2</sub> /RH-MCM-41; [TMA] = 100 μM, [TiO <sub>2</sub> /RH-MCM-41] = 1 g/L, [TiO <sub>2</sub> ] = 0.1 g/L, pH7, UV light = 300 nm.....	126
5.7 TOC removal from photodegradation of TMA; [TMA] = 100 μM, pH =7, [TiO <sub>2</sub> /RH-MCM-41] = 1 g/L, [TiO <sub>2</sub> ] = 0.1 g/L, UV light = 300 nm.....	127
5.8 Reaction order of TMA photodegradation on TiO <sub>2</sub> /RH-MCM-41; [TMA] = 100 μM, [TiO <sub>2</sub> /RH-MCM-41] = 1 g/L, pH = 7.....	129

## LIST OF FIGURES (Continued)

Figure	Page
5.9 Adsorption of TMA on TiO <sub>2</sub> and TiO <sub>2</sub> /RH-MCM-41; [TiO <sub>2</sub> /RH-MCM-41] = 1 g/L, [TiO <sub>2</sub> ] = 0.1 g/L, pH = 7.....	130
5.10 Equilibrium adsorption isotherm of TMA adsorption on TiO <sub>2</sub> /RH-MCM-41 fitted to Langmuir model; [TiO <sub>2</sub> /RH-MCM-41] = 1 g/L, pH = 7.....	132
6.1 XRD patterns of (a) RH-MCM-41, (b) 4% K <sub>2</sub> O/RH-MCM-41, (c) 8% K <sub>2</sub> O/RH-MCM-41 and (d) 12% K <sub>2</sub> O/RH-MCM-41.....	141
6.2 N <sub>2</sub> adsorption-desorption isotherm of RH-MCM-41 and K <sub>2</sub> O/RH-MCM-41; (a) RH-MCM-41, (b) 4% K <sub>2</sub> O/RH-MCM-41, (c) 8% K <sub>2</sub> O/RH-MCM-41 and (d) 12% K <sub>2</sub> O/RH-MCM-41.....	143
6.3 Pore size distribution of RH-MCM-41 and K <sub>2</sub> O/RH-MCM-41; (a) 4% K <sub>2</sub> O/RH-MCM-41, (b) 8% K <sub>2</sub> O/RH-MCM-41 and (c) 12% K <sub>2</sub> O/RH-MCM-41.....	144
6.4 K K-edge XANES spectra of K <sub>2</sub> O/RH-MCM-41 and KI reference.....	146
6.5 Formation of methyl palmitate on K <sub>2</sub> O/RH-MCM-41 at various temperatures.....	148
6.6 Formation of unsaturated methyl esters (methyl oleate, C18:1; methyl linoleate, C18:2 and methyl linolenate, C18:3) on K <sub>2</sub> O/RH-MCM-41 at various temperatures.....	148
6.7 Formation of methyl stearate (C18:0) on K <sub>2</sub> O/RH-MCM-41 at various temperatures.....	149

**LIST OF FIGURES (Continued)**

<b>Figure</b>	<b>Page</b>
6.8 Catalytic activity of 8% K <sub>2</sub> O supported on RH-MCM-41 and RH-SiO <sub>2</sub> at 100 °C.....	149

## LIST OF TABLES

<b>Table</b>	<b>Page</b>
1.1 Methods of silica preparation from rice husks and yield.....	2
2.1 Basic strength of solid catalysts indicated by Hammett indicators.....	17
3.1 Textural properties of RH-MCM-41, 10% TiO <sub>2</sub> /RH-MCM-41 and 10% Ti-RH-MCM-41.....	61
3.2 Pre-edge and edge energy of 10% Ti-RH-MCM-41 from normalized absorption of XANES.....	66
3.3 Structure parameters of the nearest coordination shell around Ti atom in 10% Ti-RH-MCM-41 with the amplitude reduction factor ( $S^2_0$ ) = 0.42.....	66
3.4 Raw data from adsorption of methyl orange on 10% TiO <sub>2</sub> /RH-MCM-41.....	76
4.1 BET surface area and average mesopore diameters of TiO <sub>2</sub> , RH-MCM-41 and TiO <sub>2</sub> /RH-MCM-41 at STP.....	93
6.1 Structure properties data of RH-MCM-41 and K <sub>2</sub> O/RH-MCM-41.....	142
6.2 Pore volume and surface area of RH-SiO <sub>2</sub> , RH-MCM-41, K <sub>2</sub> O/RH-SiO <sub>2</sub> and K <sub>2</sub> O/RH-MCM-41.....	145



## LIST OF SCHEMES

<b>Scheme</b>	<b>Page</b>
2.1 Transesterification reaction of vegetable oil with alcohol to ester and glycerol.....	34
2.2 The reaction mechanism of alkali-catalyzed transesterification of triglyceride with alcohol.....	35
3.1 Photodegradation process of organic carbon on TiO <sub>2</sub> .....	52

## LIST OF ABBREVIATIONS

°C	Degree celsius
Å	Angstrom
a	Unit cell width
AOPs	Advanced oxidation processes
BET	Brunauer-Emmett-Teller
BJH	Barret-Joyner-Halenda
C	Concentration
CB	Conduction band
C <sub>e</sub>	Equilibrium concentration of adsorbate in solution
cm <sup>2</sup>	Square meter
cm <sup>3</sup>	Cubic centimeter
d	Differentiate operator
D	Pore diameter
D <sub>100</sub>	Interplanar distance of (100)
DR-UV	Diffuse reflectance ultra violet
e <sub>CB</sub> <sup>-</sup>	Electron on conduction band
E <sub>g</sub>	Band gap energy
et al	et alia (and other)
etc.	et cetera
eV	Electron volt
EXAFS	Extended X-Ray absorption fine structure

**LIST OF ABBREVIATIONS (Continued)**

FFA	Free fatty acid
FTIR	Fourier transform infrared
g	gram
h	hour
$h_{VB}^+$	Hole on valence band
i.e.	id est (that is)
K	Adsorption capacity constant
$k$	Wave vector
$K_{ad}$	Apparent adsorption equilibrium concentration
kPa	kilopascal
L	liter
m	meter
MCM-41	Mobile crystalline material No. 41
mg	milligram
min	minute
mL	milliliter
n	Adsorption layer of adsorbate
nm	nanometer
$P/P_0$	Relative pressure
ppm	Part per million
PZC	Point of zero charge
$q_e$	Amount of adsorbate on the catalyst at the equilibrium

**LIST OF ABBREVIATIONS (Continued)**

$q_{\max}$	Maximum adsorption amount of adsorbate
$r$	Distance from absorber atom
R	Alkyl group
RH	Rice husk
$S_{\text{BET}}$	Specific surface area
TEM	Transmission electron microscope
TOC	Total organic carbon
UV-vis	Ultra violet visible
VB	Valence band
$V_p$	Pore width
$V_s$	Versus
W	Watt
Wt%	Weight percentage
XANES	X-Ray absorption near edge structure
XAS	X-Ray absorption spectrometry
XRD	X-Ray diffraction
$\mu\text{M}$	micromolar
$\mu\text{m}$	micrometer

# CHAPTER I

## INTRODUCTION

### 1.1 Rationale of the study

#### 1.1.1 Rice husk silica and MCM-41

Silica can be found in rice husk which is cheap and can be considered as a waste material. Rice husk can be burned mostly as a fuel after milling processes and can be fermented to produce fertilizer. Researchers, especially in rice producing countries, try to investigate the possibility to increase the rice husk value. Among several available uses, one possibility is to extract silica with high purity from rice husk. The silica extraction process is simple and inexpensive, making it beneficial to use rice husk as a natural silica source instead of commercial ones. Silica with high purity in amorphous form and only trace amount of other inorganic impurities can be obtained by leaching with acid or base and calcination (Conradt et al., 1992 ; Real et al., 1996; Yalcin and Sevinc, 2001; Della et al., 2002; Liou, 2004). Examples of rice silica preparation methods and the product purity are shown in Table 1.1.

The rice husk silica can be utilized in syntheses of mesoporous materials which are materials with pore size in the range of 20-100 Å, especially, MCM-41 which possesses ordered hexagonal structure with specific surface area as high as 1000-1400 m<sup>2</sup>/g and uniform pore diameter (Grisdanurak et al., 2003; Chiarakorn et al., 2007; Nur et al., 2004; Nur et al., 2006; Poh et al., 2006; Chumee et al., 2009). The MCM-41 is suitable for various applications such as molecular sieves, adsorbents and catalytic supports. In this thesis rice husk silica was used in the

synthesis of MCM-41, notated as RH-MCM-41 which served as a support for titania ( $\text{TiO}_2$ ) and potassium oxide ( $\text{K}_2\text{O}$ ). The  $\text{TiO}_2/\text{RH-MCM-41}$  catalysts were tested for photodegradation of various nitrogenous organic pollutants (Chapter III – V) and the  $\text{K}_2\text{O}/\text{RH-MCM-41}$  was tested for transesterification of palm olein (Chapter VI).

**Table 1.1** Methods of silica preparation from rice husks and yield.

Researchers	Methods	Treating substances	Purity (wt%)
Conradt et al., 1992	Pre-treatment with enzyme or chemicals and thermal treatment	Cellulose enzyme, HCl, $\text{H}_2\text{SO}_4$ or NaOH	99.8
Real et al., 1996	Acid leaching and thermal treatment	HCl	99.5
Yalcin and Sevinc, 2001	Chemical and thermal treatment	HCl, $\text{H}_2\text{SO}_4$ or NaOH	99.6
Della et al., 2002	Thermal treatment	-	95
Liou, 2004	Acid leaching and Thermal treatment	HCl	99.7

### 1.1.2 Photodegradation of nitrogenous organic compounds

An increase in the world's population and the demands in consumption have resulted in the biological and chemical contamination of water supplies, pollution of rivers and air. Nitrogenous organic compounds including ammine

surfactant, azo dye and herbicides can be found in ecosystem and wastewater. These chemicals in water may raise many problems to environment and human health. In the case of azo dye and surfactant ammine, they can contaminate aquatic lives, exist in adsorbed sludge and initiate carcinogenicity. In the case of herbicides, they have several disadvantages such as carcinogenicity, neurotoxicity and effect on cell development and reproduction (Burrows et al., 2002). Because of these problems, several researchers have devoted to removal of these nitrogenous compounds for the sake of ecosystem and human health. Conventional methods to remove organic compounds including biological degradation, physical adsorption and chemical treatment are not effective in practice (Konstantinou and Albanis, 2004).

Advanced oxidation processes (AOPs) are newer method that are useful for degradation of nitrogenous compounds. These processes use  $\text{TiO}_2$  and UV light to effectively generate oxidative species such as hydroxyl radicals (Konstantinou and Albanis, 2004). However, there are many problems that retard the photoactivity, especially, electron-hole recombination and catalyst separation (Carp et al., 2004; Ryu et al., 2003). The goal of this work was to overcome these problems in the removal of nitrogenous compounds by using mesoporous, RH-MCM-41 as a catalytic support for  $\text{TiO}_2$  to provide hydroxyl functionalized surface to suppress the problems mentioned above. Titania was dispersed on the surface of RH-MCM-41 in three different methods. The first method was mixing a titanium precursor in the preparative gel of RH-MCM-41 to produce Ti-RH-MCM-41. The second method was grafting the titanium precursor on preformed RH-MCM-41 to produce a grafted  $\text{TiO}_2/\text{RH-MCM-41}$  catalyst. Both Ti-RH-MCM-41 and  $\text{TiO}_2/\text{RH-MCM-41}$  were tested for the degradation of methyl orange and the details are provided in Chapter III. The third

method was dispersion of commercial  $\text{TiO}_2$  nanoparticles on RH-MCM-41 to produce a dispersed  $\text{TiO}_2$ /RH-MCM-41 catalyst. This catalyst was tested for photodegradation of tetramethylammonium (TMA) chloride and alachlor and details are included in Chapter IV and V, respectively.

### **1.1.3 Transesterification of palm olein**

The last part of this thesis concerned a biodiesel production with heterogeneous catalysis. Because of an increase of population which causes an increase of demand in diesel fuels, the quest for alternative fuels is widely focused. One possible alternative is biodiesel which consists of methyl esters from vegetable oil or animal fats that can be produced with the use of acid or base catalysts. Biodiesel production is effective by base catalysts such as NaOH, KOH and  $\text{CH}_3\text{COONa}$  but the separation of homogeneous catalyst from the esters is difficult (Ma and Hanna, 1999). This problem can be solved with the use of heterogeneous catalysts. The last part of this thesis involved the preparation of heterogeneous catalyst containing potassium oxide ( $\text{K}_2\text{O}$ ) on RH-MCM-41 to produce  $\text{K}_2\text{O}$  /RH-MCM-41. The RH-MCM-41 could improve dispersion of the active species,  $\text{K}_2\text{O}$  and provided available adsorption sites for the reagents, methyl alcohol and vegetable oil, before the conversion to methyl ester.

## **1.2 Research objectives**

1. To use rice husk silica as a silica source for the syntheses of mesoporous RH-MCM-41 and Ti-RH-MCM-41
2. To use the RH-MCM-41 as a support for  $\text{TiO}_2$ : grafted  $\text{TiO}_2$ /RH-MCM-41



prepared by grafting of titania precursor on the preformed RH-MCM-41 and dispersed TiO<sub>2</sub>/RH-MCM-41 prepared by dispersing titania nanoparticles on RH-MCM-41

3. To use the RH-MCM-41 as a support for K<sub>2</sub>O to produce K<sub>2</sub>O/RH-MCM-41.
4. To test Ti-RH-MCM-41 and grafted TiO<sub>2</sub>/RH-MCM-41 for photocatalytic degradation of methyl orange
5. To test dispersed TiO<sub>2</sub>/RH-MCM-41 for photocatalytic degradation ofalachlor and tetramethylammonium chloride.
6. To test K<sub>2</sub>O/RH-MCM-41 for the production of biodiesel from palm olein oil.
7. To understand factors affecting all the tested reactions as well as to investigate adsorption and kinetics.

### 1.3 References

- Burrows, H. D., Canle L, M., Santaballa, J. A., Steenken, S. (2002). Reaction pathways and mechanisms of photodegradation of pesticides, **Journal of Photochemistry and Photobiology B: Biology**. 67(2): 71-108.
- Carp, O., Huisman, C. L., Reller, A. (2004). Photoinduced reactivity of titanium dioxide. **Progress in Solid State Chemistry**. 32(1): 33-177.
- Chiarakorn, S., Areerob, T., Grisdanurak, N. (2007). Influence of functional silanes on hydrophobicity of MCM-41 synthesized from rice husk. **Science and Technology of Advanced Materials**. 8(1): 110-115.
- Chumee, J., Grisdanurak, N., Neramittagapong A., and Wittayakun, J. (2009).

Characterization of platinum-iron catalysts supported on MCM-41 synthesized with rice husk silica and their performance for phenol hydroxylation, **Science and Technology of Advanced Materials**. in press.

Conradt, R., Pimkhaohkam. P., Leela-Adisorn. (1992). Nano-structured silica from rice. **Journal of Non-Crystalline Solids**. 145(1): 75-79.

Della, V.P., Kuhn, I., Hotza, D. (2002). Rice husk ash as an alternate source for active silica production. **Materials Letters**. 57(4): 818-821.

Gridsdanurak, N., Chiarakorn, S., Wittayakun, J. (2003). Utilization of mesoporous molecular seive synthesis from natural source rice husk silica to chlorinated volatile organic compounds (CVOCs) adsorption, **Korean Journal of Chemical Engineering**. 20(5): 950-955.

Konstantinou, I. K., Albanis, T. A. (2004). TiO<sub>2</sub>-assisted photocatalytic degradation of azo dyes in aqueous solution: kinetic and mechanistic investigations: A review. **Applied Catalysis B: Environmental**. 49(1): 1-14.

Liou, T. -H. (2004). Preparation and characterization of nano-structured silica from rice husk. **Materials Science and Engineering A**. 364(2): 313-323.

Ma, F., Hanna, M. A. (1999). Biodiesel production: a review. **Bioresource Technology**. 70(1): 1-15.

Nur, H., Guan, L. C., Endud, S., Hamdan, H. (2004). Quantitative measurement of a mixture of mesophases cubic MCM-48 and hexagonal MCM-41 by <sup>13</sup>C CP/MAS NMR. **Materials Letters**. 58(12): 1971-1974.

Nur, H., Hamid, H., Endud, S., Hamdan, H., Ramli, Z. (2006). Iron-porphyrin encapsulated in poly(methacrylic acid) and mesoporous Al-MCM-41 as catalysts in the oxidation of benzene to phenol. **Materials Chemistry and**

**Physics.** 96(2): 337-342.

Poh, N. E., Nur, H., Muhid, M. N. M., Hamdan, H. (2006). Sulphated AlMCM-41: Mesoporous solid Brønsted acid catalyst for dibenzoylation of biphenyl.

**Catalysis Today.** 114(2): 257-262.

Ryu, C. S., Kim, M.-S., Kim, B.-W. (2003). Photodegradation of alachlor with the TiO<sub>2</sub> film immobilized on the grass tube in aqueous solution. **Chemosphere.**

53(7): 765-771.

Yalcin, N., Sevinc, V. (2001). Study on silica obtained from rice husk. **Ceramics**

**International.** 27(2): 219-224.

# **CHAPTER II**

## **LITERATURE REVIEW**

### **2.1 Introduction**

Rice husk is one of the major agricultural residues produced in Thailand. The Office of Agricultural Economics of Thailand estimates that about 21–26 million tons of rice is annually produced and about 6 million tons of rice husk is obtained as a by-product in rice mills (Ueda et al., 2007). The rice husk can be used mainly as fuel to produce energy for drying and boiling water (Kapur et al., 1998). However, a lot of rice husk may only be left as a solid waste and disposed by burning. The major constituents of rice husk are organic materials including celluloses and lignin. After burning in air, approximately 20 wt% of ash is produced and it contains 87-97 wt% of silica with small proportions of other elements (Chen and Chang, 1991).

The silica from rice husk could be utilized as a silica source for preparation of various adsorbents, for instance, mesoporous material MCM-41 (Grisdanurak et al., 2003; Chiarakorn et al., 2007; Nur et al., 2004 and 2006; Poh et al., 2006) which is regularly high specific surface area and provides in many applications including adsorption, molecular sieve and catalyst support (Maschmeyer et al., 1995; Koyano and Tatsum, 1997; Kruk et al., 1999).

The synthesis of MCM-41 in this work involved self-assembly and hydrothermal method in which silica precursor was mixed with a template, aged and crystallized under an autogenous pressure. We emphasize a utilization of the rice husk silica for the synthesis of mesoporous material, noted RH-MCM-41. This chapter

also includes a brief review about potential uses of RH-MCM-41 by other researchers.

Further study included modification of functionalized surface of RH-MCM-41 with various methods with Ti, TiO<sub>2</sub> and K<sub>2</sub>O including adding Ti precursor to the synthetic sol gel, grafting with Ti precursor, making composite with TiO<sub>2</sub> nanoparticles and impregnating to produce supported K<sub>2</sub>O. These prepared catalysts were applied for photodegradation of organic pollutants and transesterification for biodiesel production.

Photodegradations are the reactions that involve the break down the molecule upon the adsorption of photon particularly UV-visible range. These processes are very useful for removal organic pollutants in waste water including dye effluent and nitrogenously contaminated compounds. TiO<sub>2</sub> as a heterogeneous catalyst is mainly used incorporating with UV-light to generate active species such as OH radicals for oxidizing those degradable compounds. However, many drawbacks of photodegradation on TiO<sub>2</sub> have been concerned, for instance, electron-hole recombination, catalyst deactivation and difficulty in catalyst regeneration. To overcome these problems, RH-MCM-41 is considered as a support for TiO<sub>2</sub> because it can provide OH functionalized-surface to suppress electron-hole recombination and prevent particle agglomeration (Hoffmann et al., 1995; Carp et al., 2004; Ryu et al., 2003). Difficulty in catalyst regeneration can be diminished when RH-MCM-41 is used as catalyst support. Finally, the factors that affect photodegradative efficiency including initial organic pollutant concentration, TiO<sub>2</sub> loading, solution pH and light intensity and irradiation time should be studied.

With regards of the rapid increase of recently world population, fossil fuel as a major energy source will be run off. Consequently, it is important to find a renewable

energy sources. Biodiesel is one alternative that is known as a product from transesterification between alcohol and triglyceride in either oils or fats in the presence of basic or acidic homogeneous catalyst. However, the transesterification using homogeneous catalyst has some drawbacks such as competitive saponification, difficulty in separation of the catalysts from the products and catalyst regeneration. Consequently, heterogeneous catalysts such as  $K_2O$  supported RH-MCM-41 were used to overcome these problems.

## **2.2 Extraction of silica from rice husk ash**

Silica from rice husk can be obtained by acid-leaching and pyrolysis (Conradt et al., 1992; Real et al., 1996; Yalcin and Sevinc, 2001; Della et al., 2002; Liou, 2004). Specific surface area of the obtained silica was  $260 \text{ m}^2/\text{g}$  after burning at  $600 \text{ }^\circ\text{C}$  (Real et al., 1996). Della et al., (2002) developed active silica from rice husk silica with a high specific area to transform agricultural residual to useful raw materials. The relative purity of silica increased after burning out the carbonaceous material at different duration and temperatures. Silica powder could be produced after heat-treating at  $700 \text{ }^\circ\text{C}$  for 6 h. The specific surface area of particles was increased after wet milling from  $54$  to  $81 \text{ m}^2/\text{g}$ . The obtained rice husk silica can be used for many applications such as a support material for catalysts. For example, Tsay and Chang, (2000) extracted silica from rice husk ash to use as a support for nickel catalysts by ion exchange method. The results showed that nickel silicate with a layer structure formed after drying step and surface area of nickel with loading less than 17% was improved with the dispersion. The metal Ni phase was stabilized by silica without forming NiO at calcination temperature lower than  $300 \text{ }^\circ\text{C}$ . From the statement above,

silica extracted from rice ash promise the application in a field of catalysis. This work aimed to use rice husk silica to synthesize mesoporous material, MCM-41 which had surface area much higher than rice husk silica and more uniform pore sizes. The MCM-41 would be used as a support for  $\text{TiO}_2$  and  $\text{K}_2\text{O}$ .

### **2.3 Background of MCM- 41**

MCM-41, one of the most widely studied materials in the mesoporous M41s family is a micelle-templated mesoporous molecular sieve with regular mesopore diameter and large surface area possessed hexagonal rearrangement of mono-dimensional pore (Srinava et al., 2004; Koyano and Tatsum, 1997; Zhao et al., 1996; Eimer et al., 2006). With good aspects, MCM-41 has motivated researchers to investigate its chemical, physical and thermal properties. MCM-41 has a high potential to practical use as an adsorbent or a mesoporous support for active species. Interestingly, it is particularly useful in the synthesis of fine chemicals involving bulky molecules because the wide pore diameter makes these materials readily accessible to large molecules (Øye et al., 2001). The understanding in synthesis and forming mechanism of these materials has opened up a new area toward molecular tailor.

### **2.4 Synthesis of MCM- 41**

MCM-41 can be synthesized by self-assembly and hydrothermal method by mixing a silica source such as sodium silicate, fumed silica or tetraethylorthosilicate (TEOS) and a surfactant which serves as a template. The formation of the inorganic-organic composition is based on electrostatic interactions between the positively

charged surfactants and negatively charged silicate species which can be tuned by adjusting pH of the solution to base. Their interactions consequently form micellar rods under critical micelle concentration. The reactions continue when the micellar solution is hydrothermally kept at the temperature range of 100-150 °C for 24-124 h for crystallization (Selvam et al., 2001; Kumer et al., 2001). The product obtained after crystallization is filtered, washed with distilled water, dried at ambient temperature and calcined or extracted by a solvent to remove the template to result a mesoporous silicate/alumino silicate network.

Rice husk silica has been used for the synthesis of RH-MCM-41. Grisdanurak et al. (2003) synthesized the RH-MCM-41 from rice husk silica and cetyltrimethylammonium bromide (CTAB) as organic template with the molar ratio of 0.147 CTAB : 1.00 SiO<sub>2</sub> : 2.16 NH<sub>4</sub>OH : 148.94 H<sub>2</sub>O using an ambient condition. The obtained RH-MCM-41 with various aging time possessed high specific surface area in the range of 750-1100 m<sup>2</sup>/g and pore size distribution in the range of 20-35 Å. The efficiency of RH-MCM-41 in adsorption of chlorinated volatile organic compounds (CVOCs) was higher than a commercial mordenite and activated carbon. Nur et al. (2003) prepared mesoporous MCM-41 and MCM-48 from rice husk silica via a mixed cationic-natural templating route using CTAB and Trion x-100 (Tx-100) surfactants with the molar ration of 5 SiO<sub>2</sub> : (1-2) NaOH : 400 H<sub>2</sub>O : 0.85 CTAB : 0.15 Tx-100. The organization of the surfactants was affected by the concentration of NaOH. MCM-48 was formed when the concentration of NaOH was less than 1.5 M but MCM-41 was obtained when the concentration of NaOH was greater than 1.5 M. In order to obtain a pure phase of MCM-41 prepared with rice husk silica, the alkali concentration used to dissolve the silica should be controlled to avoid an undesired



mixed phase. A siliceous MCM-41 (sometimes referred to as Si-MCM-41) mesoporous material is electrically neutral, which limits its catalytic applications due to lack of cooperating between heteroatom. Thereby, it is necessary to increase the active site centers by adding other elements into the structure or dispersing them on the surface. Nur et al. (2006) synthesized Al-MCM-41 with Si/Al = 20 from rice husk silica with the gel weight ratio of 2.295 NaOH : 10.015 SiO<sub>2</sub> : 1.05 NH<sub>3</sub> : 9.1115 CTAB : 1.417 NaAlO<sub>2</sub>. Then, the product surface was modified by bulky iron (III)-5, 10, 15, 20-tetra-(4-pyridyl)porphyrin (Fe-TPyP), named Fe-TPyP-Al-MCM-41 and used as a catalyst for benzene oxidation to phenol. A performance of this catalyst was compared with poly(methacrylic acid) (PMAA) encapsulated Fe-TPyP, noted Fe-TPyP-PMAA. The Fe-TPyP-Al-MCM-41 gave a higher selectivity and regenerability than that of Fe-TPyP-PMAA. In addition, Poh et al. (2006) synthesized AlMCM-41 with SiO<sub>2</sub>/Al<sub>2</sub>O<sub>3</sub> = 15 and a gel molar composition of 6 SiO<sub>2</sub> : 1 CTAB : 1.5 Na<sub>2</sub>O : 0.15 (NH<sub>4</sub>)<sub>2</sub>O : 250 H<sub>2</sub>O. The product surface was modified by H<sub>2</sub>SO<sub>4</sub> with the ratio AlMCM-41/H<sub>2</sub>SO<sub>4</sub> = 0.5 g/30 μL to produce SO<sub>4</sub>-AlMCM-41 which was used as a catalyst for dibenzoylation of biphenyl. The SO<sub>4</sub>-AlMCM-41 gave a higher activity in the dibenzoylation of biphenyl with benzoyl chloride than that of sulfuric acid, AlMCM-41 and sulfated amorphous silica.

Moreover, Chiarakorn et al. (2007) prepared RH-MCM-41 from rice husk silica and rice husk ash with the gel molar composition of 1.0 SiO<sub>2</sub> : 1.1 NaOH : 0.13 CTAB : 0.12 H<sub>2</sub>O and further silylated by trimethylchlorosilane (TMCS) and phenyl-trimethylchlorosilane (PDMS) after calcination. The results exhibited that the structure of silylated RH-MCM-41 from both silica sources strongly influenced the degree of hydrophobicity. The surface polarity of silylated RH-MCM-41 was reduced

by less steric hindrance after grafting by TMCS and PDMS. These studies elucidated that RH-MCM-41 can be functionalized for adsorption of non-polar organic compounds and modified to increase active sites for chemical reactions.

## 2.5 Modification of MCM-41

There have been several attempts to impregnate some transition metals as active centers which can simultaneously improve chemical and thermal stability of MCM-41. A large number of functionalizing entities including both organic and inorganic ligands have been introduced in the MCM-41 channels to generate catalysts (Maschmeyer et al., 1995; Carvalho et al., 1999; Shephard et al., 1997; Badiei and Bonneviot, 1998; Van Der Voort et al., 1998; Ahn et al., 1999; Holland et al., 1998). All these modifications/functionalizations are achieved either by *in situ* synthesis or post-modification. The *in situ* synthesis is a method that active species and support are simultaneously mixed and crystallized to grow nanoparticle of active species on the support. On the other hand, the post-modification is a method that the preformed MCM-41 is impregnated with active species. This method allows one to sophisticatedly design and synthesize custom-tailored materials. Several researchers have focused on modification of MCM-41 by both methods.

The modifications of MCM-41 by active species from literatures particularly for photodegradation and transesterification are summarized. Anandan (2008) modified MCM-41 with Ti by *in situ* synthesis by adding titanium isopropoxide to the preparative gel. The products were designated TiMCM-41s and tested for photodegradation of methyl orange comparing with colloidal TiO<sub>2</sub> in the presence of electron acceptors including peroxomonosulphate (PMS), peroxodisulphate (PDS)

and hydrogenperoxide using visible light irradiation. The TiMCM-41 gave a triple higher photodegradation rate in the presence of PMS as well as double higher in the case of PDS than colloidal TiO<sub>2</sub>. Such method provided a good dispersion of TiO<sub>2</sub> and the particles or phase of TiO<sub>2</sub> could not be observed by XRD.

The degree of dispersion and catalytic performance depends on the precursor selection (Yuan et al., 2009). Two different TiO<sub>2</sub> precursors including TiF<sub>4</sub> and (NH<sub>4</sub>)<sub>2</sub>TiO(C<sub>2</sub>O<sub>4</sub>)<sub>2</sub> were selected for impregnation to MCM-41 powder. The average pore diameter of MCM-41 was reduced when the (NH<sub>4</sub>)<sub>2</sub>TiO(C<sub>2</sub>O<sub>4</sub>)<sub>2</sub> was used. Titanium oxides were highly dispersed on the pore wall of MCM-41 and the hexagonal mesostructures were not affected after the TiO<sub>2</sub> loading. The coordination of Ti examined by XAS technique, was four indicating that the Ti species mainly existed in a tetrahedral geometry. The transition process to grow TiO<sub>2</sub> supported MCM-41 included the replacement of Si-OH by Si-F on the surface of pore wall which increased the hydrophobic properties of MCM-41 and enhanced the adsorption of organic compounds on solid catalysts. With the same loading of TiO<sub>2</sub>, samples prepared from TiF<sub>4</sub> had a higher photocatalytic activity than that prepared from (NH<sub>4</sub>)<sub>2</sub>TiO(C<sub>2</sub>O<sub>4</sub>)<sub>2</sub>.

Another method to produce TiO<sub>2</sub> on MCM-41 was to form a composite between TiO<sub>2</sub> (Degussa P-25) and MCM-41. Bouazza et al. (2008) reported that the performance of pellets containing TiO<sub>2</sub> and MCM-41 with 70:30 weight ratio (prepared by pelletization of the mixture in water by a 5 mL plastic syringe) for the oxidation of propene was improved over the TiO<sub>2</sub> pellets probably due to the porosity of the MCM-41 additive. Phanikrishna Sharma et al. (2008) prepared a composite of TiO<sub>2</sub>/Al-MCM-41 by solid state dispersion method by mixing both components in

ethanol followed by evaporation and calcination. The composites were effective for photocatalytic degradation of isoturon herbicide in solar light. In this work the photocatalysts was prepared by slurring the  $\text{TiO}_2$  (Degussa P-25) and RH-MCM-41 in deionized water because it was convenient and the particle size of  $\text{TiO}_2$  was expected to be preserved. As mention above, the dispersion of  $\text{TiO}_2$  on RH-MCM-41 could prevent aggregation of titania particles.

The last modification method was to increase basicity of MCM-41 for transesterification. Xie et al. (2006) reported a modification of  $\text{Al}_2\text{O}_3$  to generate basic sites for transesterification of soybean oil with methanol by impregnation with potassium nitrate ( $\text{KNO}_3$ ) in an aqueous solution, followed by drying at  $120\text{ }^\circ\text{C}$  for 16 h and calcined at the range of  $300\text{-}700\text{ }^\circ\text{C}$ . The basic strength of the prepared catalysts was determined by titration with Hammett indicator-benzene carboxylic acid (0.02 mol/L anhydrous ethanol solution). Basic strengths of solid catalysts indicated by various Hammett indicators are shown in Table 2.1.

The basic strength of the  $\text{Al}_2\text{O}_3$  support was less than 3.3. After impregnation and calcination at  $500\text{ }^\circ\text{C}$  for 5 h, the basic strength of the  $35\%\text{KNO}_3/\text{Al}_2\text{O}_3$  was improved to 15.0. This material was ascribed as a strong base according to Tanabe's definition. Further increase of  $\text{KNO}_3$  content did not enhance the basic strength because excess amount of  $\text{KNO}_3$  would cover basic sites of the material. The XRD confirmed the existence of  $\text{K}_2\text{O}$  at  $2\theta$  of 31, 39, 51, 55 and 62 degree. Specific surface area of  $\text{Al}_2\text{O}_3$  decreased significantly with loading of  $\text{KNO}_3$ . The optimum condition for  $35\%\text{KNO}_3$  at reflux temperature of methanol, with a molar ratio of methanol to soybean oil of 15:1, a reaction time 7 h, and catalyst amount of 6.5% gave the highest biodiesel yield of 87.4%. The decomposition of the loaded  $\text{KNO}_3$  produced either  $\text{K}_2\text{O}$  species or

Al-O-K group in the composite which were probably the active basic sites.

**Table 2.1** Basic strength of solid catalysts indicated by Hammett indicators.

Hammett indicators	Hammett basic strength	Color change at end point
Dimethylaminoazobenzene	3.3	From yellow to red
Phenolphthalein	9.3	From colorless to red
2,4-dinitroaniline	15.0	From yellow to mauve
4-nitroaniline	18.4	From yellow to green

Xie et al. (2007) prepared soybean methyl esters using NaX zeolite loaded with KOH as a heterogeneous catalyst. The KOH/NaX was prepared by impregnation of KOH with different loadings, dried and heated in the oven at 120 °C for 3 h. The basic strength of NaX, also determined by Hammett indicators was improved from 9.3 to 15.0 after loading with KOH. The XRD spectra showed that the KOH loading between 4 and 14% had no apparent impact on the crystalline structure and the pore structure of zeolite, necessary for catalysis, was still maintained. For biodiesel production, the conversion increased with KOH loading and the highest conversion of 85.6% was obtained at the loading of 10%. However, the conversion decreased when the loaded KOH over 10% because the excess amount resulted in the agglomeration of KOH phase and/or the cover of basic sites. The best result was obtained on 10% KOH loading with the following condition: a molar ratio of methanol to soybean oil 10:1, a reaction time of 8 h and a catalyst amount of 3wt. %. However, catalyst

deactivation was reported that KOH was leached out from NaX after the separation of methyl esters. This phenomenon was not beneficial for the transesterification because the active sites of KOH was removed and consequently decreased biodiesel yield from 85.2% to 48.2%. This indicated that active species either  $K_2O$  or Al-O-K surface group should be permanently anchored onto the framework of the support by increase calcination temperature.

However, there were conflict results from the following experiment even though the catalyst was prepared in the same manner but on different solid support. Noiroj et al. (2009) prepared KOH/ $Al_2O_3$  and KOH/NaY catalysts for biodiesel production via transesterification of palm oil. After post-impregnation and heating at 110 °C for 2 h, KOH was well dispersed on  $Al_2O_3$  in the form of monolayer at the low loadings and  $K_2O$  was formed on the surface of alumina. In case of NaY, its peak intensity decreased significantly when high amount of KOH was introduced. For catalytic activity, the 25 wt% KOH/ $Al_2O_3$  and 10 wt% KOH/NaY catalysts were suggested to be the best due to their biodiesel yield of 91.07% at temperatures below 70 °C within 2–3 h at a 1:15 molar ratio of palm oil to methanol and a catalyst amount of 3–6 wt%. The 85% conversion of soybean was obtained on 10% KOH supported NaY. The leaching of any active species was not found from ICP results indicating that either  $K_2O$  or surface Al-O-K was established properly at low temperature.

Transesterification of soybean on alkyl guanidine immobilized MCM-41 was reported by Sercheli et al. (1999). The catalytic activity of unsupported methyl guanidine was compared with that encapsulated in MCM-41 and amorphous  $SiO_2$ . From the testing, methyl guanidine on MCM-41 showed highest activity because the diffusion was not affected in mesoporous system. However, enzyme immobilization

on solid support had a trouble from leaching out of the support. Because transesterification of palm olein on KOH supported MCM-41 was not yet reported, this study also paid attention to prepare  $K_2O/RH$ -MCM-41 to improve this reaction.

## **2.6 Catalysis on photocatalytic degradation**

Photodegradation is degradation of a molecule upon absorption of photons, particularly those wavelengths found in sunlight, such as infrared, visible and ultraviolet light. However, other forms of electromagnetic radiation can also cause photodegradation. The reaction includes photodissociation which involve a breakup of molecules into smaller units by photons and a change of molecular shape to make it irreversibly altered, such as denaturing of proteins and the addition of other atoms or molecules. A common photodegradation reaction is an oxidation which can be used to treat drinking water and wastewater facilities to eliminate organic pollutants.

### **2.6.1 Photodegradation of organic pollutants**

The European legislation places emphasis on the cleaning of wastewater effluents from industrial discharges or agrochemical products such as pesticides, textile, fungicides, fertilizers, and land filling domestic wastes. There is a growing demand for effective, economic and environmentally benign water treatment technologies where all materials (used or produced) in the mineralization process are completely harmless to the environment. In developing countries, water resources are limited and recycling of water in agriculture and industry is required. In most of these countries, solar energy is abundant and can be used as a source for photocatalytic degradation of organic pollutants in wastewater. Several studies have been conducted

on the issues of biological, physical and chemical treatment of organic pollutants in waste water. These methods can be summarized into 3 types. 1) Bio-treatment of organic pollutants is method that uses microbial or enzyme to break down organic pollutants. Many researchers reported that this method was ineffective due to the poison and resistance to aerobic degradation of pollutants. Furthermore, the organic pollutants that undergo reductive breakdown through anaerobic biological treatment potentially generate carcinogenic aromatic amines in the process (Chung and Cernilia, 1992). 2) Physical methods such as flocculation, reverse osmosis and adsorption on activated charcoal are non-destructive and merely transfer the pollutants to other media causing secondary pollution (Cooper, 1993). 3) Chemical destruction of organic pollutants may be accomplished using chlorine or ozone. The chemical treatments are interesting because they are effective for color and organics removal but the required dosages are often too high to be economically feasible (Davis et al., 1994).

In addition to those methods, advanced oxidation processes (AOPs) have been proposed as an alternative way of treating undesirable organic pollutants, such as dyestuffs (Fox and Dulay, 1993). These processes involve the generation and utilization of the high oxidizing potential of species like hydroxyl radicals to degrade organic pollutants. Among AOPs, heterogeneous photocatalysis by  $\text{TiO}_2$  seems to be an attractive method because it is effective for the degradation of various families of organic pollutants (Legrini et al., 1993; Hoffmann et al., 1995; Ollis and Al-Ekabi (Eds.), 1993; Turchi and Ollis, 1990). The reason for the increased interest in the photocatalytic method is that the process may use atmospheric oxygen as the oxidant. This allows the process to be carried out under ambient conditions and may lead to



total mineralization of organics to CO<sub>2</sub>, water and mineral acids. Furthermore, the methods that utilize environmentally benign photocatalysts, usually TiO<sub>2</sub>, are largely available, inexpensive, non-toxic and show relatively high chemical stability. Another necessary factor for photoreaction is UV light which acts as photoenergy source which cooperate with TiO<sub>2</sub> to generate active species, hydroxyl radicals ( $\bullet$ OH), for photodegradation process.

### 2.6.2 Photodegradation processes on TiO<sub>2</sub>

Heterogeneous photocatalysis is a process in which both light and catalyst are necessary to start a chemical reaction (Stylidi et al., 2003). The process is illustrated in Figure 2.1. Ultraviolet light interacts with a semiconductor, such as TiO<sub>2</sub>, to generate charge separation, pathway (a) in which electrons are excited from a valence band to a conduction band. The electrons in conduction band and holes in valence band can migrate to the surface of TiO<sub>2</sub> and react with chemisorbed O<sub>2</sub> and/or OH<sup>-</sup>/H<sub>2</sub>O molecules to generate reactive oxygen species, such as O<sub>2</sub><sup>•-</sup>, HOO<sup>•</sup> and  $\bullet$ OH radicals which can interact with organic pollutants leading to their degradation as demonstrated in pathway (b) and (c) (Stylidi et al., 2003). However, the generated hole and electron can recombine as shown in pathway (d) and (e) unless they react with organic pollutants (Carp et al., 2004). The recombination is a crucial problem that may retard photodegradation efficiency because the generated hole and electron are removed and cause the lack of precursor to generate hydroxyl radical or even highly efficient oxidizer to directly oxidize organic pollutants. This problem has been reported from many researchers and possible methods to solve it will be explained in the next section. Because TiO<sub>2</sub> is a well known photocatalyt, its characteristics will be

described in the next section as well.

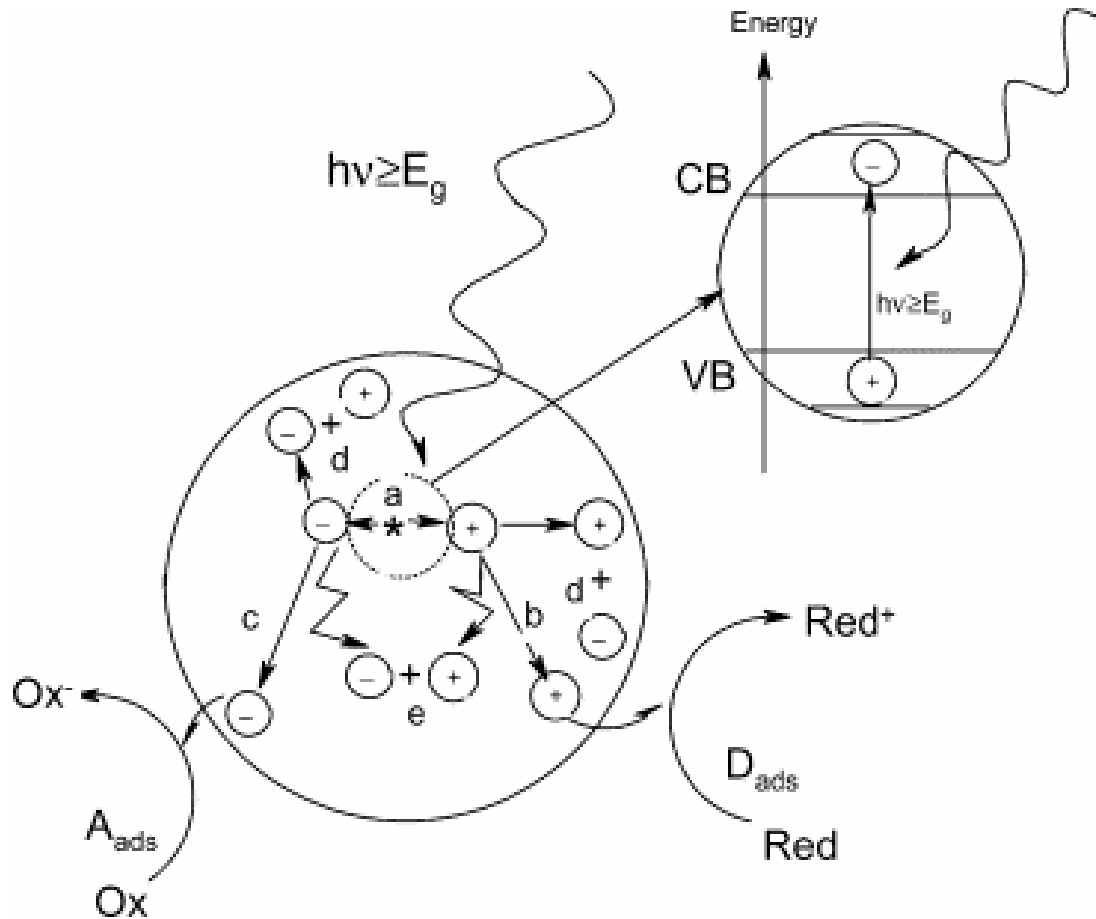


**Figure 2.1** Main processes described by Carp et al. (2004) in a semiconductor particle upon absorption of photon energy larger than band gap energy ( $E_g$ ) to excite electron from valence (VB) to conduction band (CB): (a) electron-hole generation; (b) oxidation of donor ( $D_{ads}$ ); (c) reduction of acceptor ( $A_{ads}$ ); (d) and (e) electron-hole recombination at surface and in bulk, respectively.

### 2.6.3 TiO<sub>2</sub> as a photocatalyst

Two kinds of titanium oxides are believed to be active for photo-degradation: rutile and anatase. Their structures are shown in Figure 2.2.

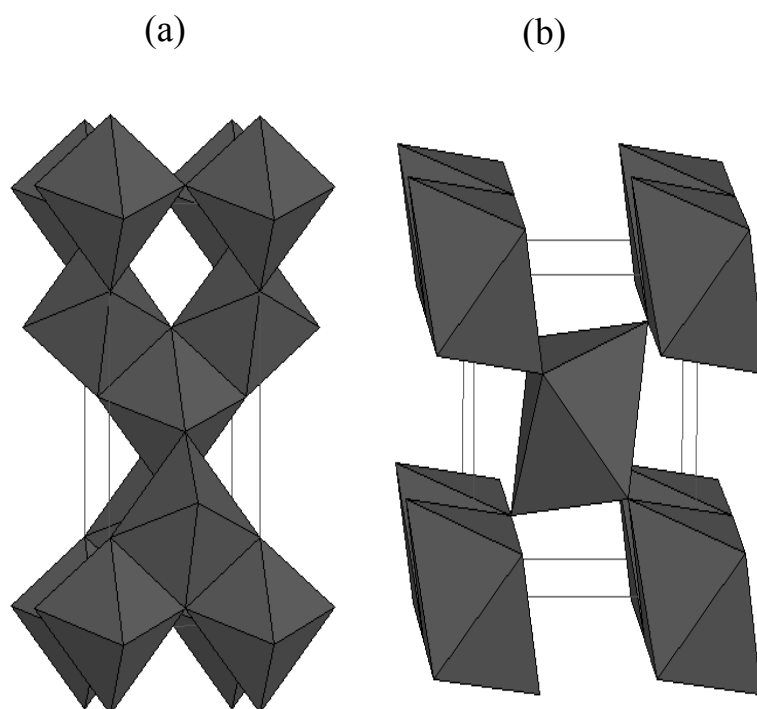


**Figure 2.2** Crystal structures of a) anatase and b) rutile, modified from Carp et al. (2004).

The structures of rutile and anatase compose of TiO<sub>2</sub><sup>6-</sup> octahedral units with edge sharing. The two crystal structures differ by the distortion of each octahedral and by the assembly patterns of the octahedral chains. Anatase is built-up from octahedra that are connected by their vertices but in rutile the edges are connected (Carp et al., 2004). Commercially available anatase typically contains particles with less than 50 nm in size. These particles have band gap energy of 3.2 eV

corresponding to a UV wavelength of 385 nm. In contrast, the thermodynamically stable rutile phase generally exists as particles larger than 200 nm (Yin et al., 2001). Rutile has a smaller band gap of 3.0 eV corresponding to wavelength of 410 nm. Both crystal structures, anatase and rutile, are commonly used as photocatalysts with anatase showing a greater photocatalytic activity for most reactions (Linsbigler et al., 1995; Tanaka et al., 1991). A higher photoreactivity of anatase is attributed to a slightly higher Fermi level than that of rutile which results in a lower capacity to adsorb oxygen, higher degree of hydroxylation (i.e., number of hydroxyl groups on the surface), higher adsorptive affinity of anatase for organic compounds and lower rates of recombination (10-fold greater rate of hole trapping of rutile) (Tanaka et al., 1991; Gerischer and Heller, 1992; Bickley et al., 1991). The agreement of the results may depend on the involved effects of various factors such as specific surface area, pore size distribution, crystal size and preparation methods or in the way the activity is expressed. Nevertheless, photoactivity of pure anatase is limited by visible absorption because of large band gap energy. There are attempts to mix rutile and anatase with several ratios to extend photoabsorptivity of anatase visible range. The most suitable ratios that give higher activity than pure anatase contain anatase about 70–75% and rutile about 30–25% (Basca and Kiwi, 1998; Muggli and Ding, 2001; Ohno et al., 2001). Furthermore, a commercial photocatalyst Degussa P25 containing nanoparticles  $\text{TiO}_2$  that consist of anatase and rutile with an approximate ratio of 80/20 is more active than both the pure crystalline phases (Bickley et al., 1991; Ohno et al., 2001; Zhang et al., 2000).

#### **2.6.4 Photodegradation of organic pollutants on TiO<sub>2</sub>**

Organic pollutants such as azo dye, nitrogenous compounds, herbicide and pesticide can contaminate water, aquatic life and harm human health. Under this circumstance, much attention has been paid on the removal of these compounds from an aqueous solution. Stylidi et al. (2003) investigated photocatalytic degradation of aqueous acid orange 7 by TiO<sub>2</sub> suspensions. The dye adsorbed on TiO<sub>2</sub> and underwent a series of oxidation steps which led to decolorization and formation of a number of intermediates, mainly aromatic and aliphatic acids. These molecules were further oxidized toward compounds of progressively lower molecular weight and eventually to CO<sub>2</sub> and inorganic ions such as sulfate, nitrate and ammonium ions. Kim and Choi (2002) carried out photodegradation of tetramethylammonium chloride on bare TiO<sub>2</sub>. The results indicated that the degradation was going well on both acid and base solution, however the reaction at a neutral pH (pH = 6.7), pH point of zero charge of TiO<sub>2</sub>, might cause particle aggregation and deactivate photoactivity of TiO<sub>2</sub>. Wong and Chu (2003) performed direct photocatalytic degradations of alachlor using three different monochromatic UV lamps and TiO<sub>2</sub> Degussa P25. The photocatalytic degradation rate of alachlor increased with the dosages of TiO<sub>2</sub> but an overdose of TiO<sub>2</sub> would retard the reaction due to light attenuation.

Those above results implied that photodegradation of organic dye and organic compound was effective but several researches still found limitations of the use of TiO<sub>2</sub> Degussa P25. There were two main problems in TiO<sub>2</sub> usage: the exponential decrease of the light availability due to the adsorbing of UV light by particles themselves and the difficulty in recycling photocatalysis (Ryu et al., 2003). Consequently, Ryu et al. (2003) carried out photodegradation of alachlor on TiO<sub>2</sub> film

prepared by sol-gel method. The thickness of TiO<sub>2</sub> film immobilized by 1-5 time-dip coating was 174 nm and the average diameter was 10-15 nm. The results showed that stability was established when 4% loading was used and photocatalytic activity was enhanced upon dip coating of TiO<sub>2</sub> film. Moreover, the system of TiO<sub>2</sub> particles immobilized on the supports was proposed to solve these problems. The system of TiO<sub>2</sub> particles immobilized on the supporters was proposed to solve these problems. Kuo and Lin (2000) immobilized TiO<sub>2</sub> at a film thickness of 1.5–2.0 μm on the blades of agitator, where the removal efficiency of an organic compound was improved with an increasing TiO<sub>2</sub> film area. Nevertheless, there was a different results that powders with a large surface area are usually associated with large amounts of crystalline defects which favor the recombination of electrons and holes leading to a poor photoactivity (Tanaka et al., 1991; Zhang et al., 1995). In order to overcome these problems, the supports that can suppress electron/hole recombination should be concerned.

Bhattacharyya et al. (2004) studied photocatalytic degradation of orange II by TiO<sub>2</sub> Degussa P25 and TiO<sub>2</sub> (10–80% of TiO<sub>2</sub> loading) catalysts supported on adsorbents (MCM-41, beta zeolite and montmorillonite). The results showed that all supported catalysts exhibited good photodegradation of orange II and their overall removal efficiency was always better than that of bare TiO<sub>2</sub> produced by the sol-gel method and commercial catalyst, Degussa-P25. This result implied that those catalysts had high hydroxyl surface groups which had played a key in the photodegradation process due to: 1) direct participation in the reaction mechanism by trapping of photogenerated holes that reach the catalyst surface producing very reactive surface •OH (Hoffmann et al., 1995); 2) a change in the adsorption of

reactant molecules both by acting itself as active sites for pollutant adsorption (Maira et al., 2000) and 3) by covering the sites (exposed titanium cations with unsaturated coordination) where electron trapping by adsorbed oxygen takes place (Maira et al., 2000). This process is not only important for producing oxygen radicals but also for hindering electron–hole recombination.

The achievement in photodegradation is involved not only proper photocatalyst but also factors influencing the reaction such as pH solution, substrate concentration, catalyst concentration and photoenergy of UV light. The following section gave overviews on those parameters.

## **2.6.5 Factors influencing the photocatalytic degradation**

### **2.6.5.1 Effect of initial concentration of organic pollutants**

It is important for both mechanism and application point of view to study the dependence of the photocatalytic reaction rate on the substrate concentration. In general, the degradation rate increases with an increase of substrate concentration to a certain level and a further increase in substrate concentration leads to decrease the degradation rate of the organic pollutants (Saqib and Muneer, 2003; Sakthivel et al., 2003). The rate of degradation relates to the probability of  $\bullet\text{OH}$  radicals formation on the catalyst surface and to the probability of  $\bullet\text{OH}$  radicals reacting with organic pollutant molecules (Konstantinou and Albanis, 2004). When the initial concentrations of the organic pollutants increase, the probability of reaction between organic molecules and  $\bullet\text{OH}$  radicals also increases, leading to an enhancement in the degradation rate. In contrast, the degradation efficiency of the organic pollutant decreases as the organic pollutant concentration increases further.

The presumed reason is that at high organic pollutant concentrations the generation of  $\bullet\text{OH}$  radicals on the surface of catalyst is reduced because the active sites of solid catalyst are covered by adsorbed organic pollutant. Another possibility is that adsorbed organic pollutant on solid catalyst might cause the UV-screening effect by itself (So et al., 2002; Grzechulska and Morawski, 2002). In addition, the major portion of degradation occurs in the region near to the irradiated side where the irradiation intensity is much higher than in the other side. Thus at higher dye concentration, degradation decreases at sufficiently long distances from the light source or the reaction zone due to the retardation in the penetration of light (Zhang et al., 1995).

#### 2.6.5.2 Effect of $\text{TiO}_2$ loading

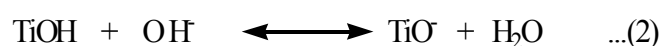
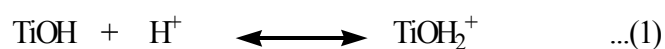
Among the static, slurry and dynamic reactor, the initial reaction rates are found to be directly proportional to catalyst concentration and certain level of concentration the reaction rate decreases and becomes independent of the catalyst concentration. Many studies reported that degradation rates were enhanced for catalyst loading up to 400–500 mg/l (Conçalves et al., 1999; Davis et al., 1994; Zielinska et al., 2001). Only a slight enhancement or decrease was observed when  $\text{TiO}_2$  concentration further increases up to 2000 mg/l. This can be rationalized in terms of availability of active sites on  $\text{TiO}_2$  surface and the light penetration into active site of the suspension. The existence of active sites increases with the suspension of catalyst loading, but the light penetration and the photoactivated volume of the suspension decreases. Moreover, the decrease in the percentage of degradation at higher catalyst loading may be due to deactivation of activated molecules by collision with ground state molecules (Neppolian et al., 2002).



Agglomeration and sedimentation of the TiO<sub>2</sub> particles were observed when 2000 mg/L of TiO<sub>2</sub> was added to the organic pollutant solution (So et al., 2002). The optimum amount of TiO<sub>2</sub> has to be added in order to avoid unnecessary excess catalyst and to ensure total absorption of light photons for efficient mineralization. The optimum loading of photocatalyst is dependent on the initial solute concentration (Hermann, 1999).

### 2.5.6.3 Effect of solution pH

The changes of pH always affect on the efficiency of organic pollutant degradation process because of the following reasons. First, pH change is related to functionalized-surface charge of solid catalyst according to the following reactions,



Corresponding to equation (1), when TiO<sub>2</sub> is suspended in an acidic solution (pH < 7) where the solution is rich of H<sup>+</sup>, the surface of TiO<sub>2</sub> will be protonated and its surface charge becomes positive. On the other hand, when TiO<sub>2</sub> is suspended in a basic solution (pH > 7) where the solution is rich of OH<sup>-</sup> (equation 2), the surface charge will be negative. The surface charge is important because it controls zeta potential. The point of zero charge (pzc) of the TiO<sub>2</sub> (Degussa P25) occurs at pH 6.8. Thus, the TiO<sub>2</sub> surface is positively charged in an acidic media (pH < 6.8), whereas it is negatively charged under alkaline conditions (pH > 6.8). Second, hydroxyl radicals can be formed by the reaction between hydroxide ions and positive holes. The positive holes are considered as the major oxidation species at low pH whereas

hydroxyl radicals are considered as the predominant species at neutral or high pH levels (Hermann, 1999; Tunesi and Anderson, 1991). In an alkaline, solution  $\bullet\text{OH}$  are easier to be generated by oxidizing more hydroxide ions available on  $\text{TiO}_2$  surface. However, there is a coulombic repulsion between the negative charged surface of photocatalyst and the hydroxide anions in this condition which could prevent the formation of  $\bullet\text{OH}$  and decrease the photooxidation. At low pH, a reduction by electrons in conduction band may in turn play a very important role in the degradation of organic pollutant due to the reductive cleavage of bonds. Third, the  $\text{TiO}_2$  particles tend to agglomerate under acidic condition and the surface area available for organic pollutants adsorption and photon absorption would be reduced (Fox and Dulay, 1993). Hence, pH plays an important role both in the characteristics of organic pollutants and in the reaction mechanisms that can contribute to organic pollutant degradation, namely, hydroxyl radical attack, direct oxidation by the positive hole and direct reduction by the electron in the conducting band.

#### 2.5.6.4 Effect of light intensity and irradiation time

Ollis et al. (1991) reviewed the studies about an effect of light intensity on the kinetics of the photocatalysis process and stated that 1) at low light intensities ( $0\text{--}20\text{ mW/cm}^2$ ), the rate would increase linearly with increasing light intensity (first order), 2) at intermediate light intensities beyond a certain value (approximately  $25\text{ mW/cm}^2$ ) (Hermann, 1999), the rate would depend on a square root of the light intensity (half order), and 3) at high intensities the rate is independent of light intensity. This is likely because reactions involving electron-hole formation are predominant at low light intensity and electron-hole recombination is negligible. However, electron-hole pair separation competes with recombination at increased

light intensity, thereby causing less effect on the reaction rate. In addition, it is evidenced that the percentage of decolorization and photodegradation increases with increase in irradiation time. The reaction rate decreases with irradiation time since it follows apparent first-order kinetics and additionally a competition for degradation may occur between the reactant and the intermediate products. The slow kinetics of dyes degradation after certain time limit is due to: 1) the difficulty in converting the N-atoms of dye into oxidized nitrogen compounds (Bandara et al., 1997), 2) the slow reaction of short chain aliphatics with  $\bullet\text{OH}$  radicals, and 3) the short life-time of photocatalyst because of active sites deactivation by strong by-products deposition (carbon etc.).

In summary, because conventional processes including biological treatment, physical adsorption and chemical treatment are not effective for removal of organic pollutants for wastewater, advanced oxidation processes (AOPs) or photocatalytic degradation could solve the problems. The processes need heterogeneous catalyst such as  $\text{TiO}_2$  and UV light cooperating to generate active species ( $\bullet\text{OH}$ ) for breaking organic pollutants. There are two kinds of  $\text{TiO}_2$ , anatase and rutile phases, known as active species of photodegradation. Most researches reported  $\text{TiO}_2$  anatase has higher photoactivity than that of  $\text{TiO}_2$  rutile because  $\text{TiO}_2$  anatase possesses higher specific surface area and slower electron hole recombination. Nevertheless, the use of pure anatase has been limited by photoabsorptivity of the light in visible range. The mixing of anatase to rutile with a molar ratio of 80:20 is believed to be the most active in photodegradation (Ohno et al., 2001). Unfortunately, the use of this material raises some problems including electron/hole recombination and catalyst regeneration. In order to overcome these problems, supports possessed high hydroxyl density on the

surface such as MCM-41 is introduced. During the reaction procedure in this work, there are many factors that need to be optimized, for instance, catalyst concentration, substrate concentration, irradiation time and pH solution and these parameters would be varied to find a suitable condition. Light intensity should be controlled to have sufficient photon energy to generate active species for photodegradation.

## **2.7 Catalysis on Transesterification**

### **2.7.1 General Background**

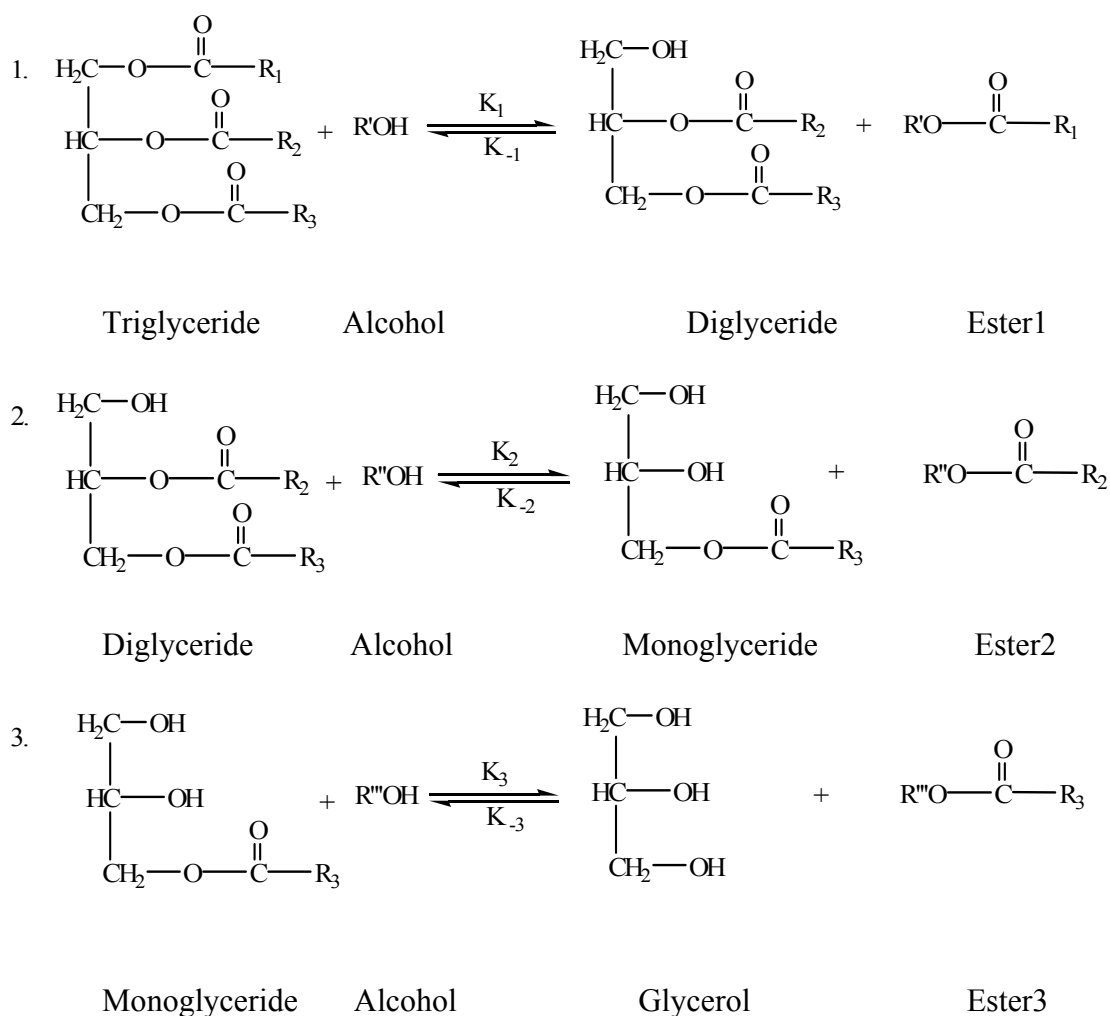
Because of a rapid growth of world population, diesel fuels are consumed in a very large scale per day and the fossil fuel will be depleted in the near future. Alternative renewable fuel sources are needed and biodiesel is among the best choices that can satisfy the desire for renewable energy sources. Biodiesel can be made from renewable biological sources such as vegetable oils and animal fats via transesterification reaction to produce alkyl esters. After processing, the main chemical substances compose of carbon 77%, hydrogen 12%, oxygen 11% and trace amount of nitrogen and sulfur (Encinar et al., 2005). Alkyl ester compositions depend on the kinds of alcohols and fats/oils used. Although C1-C8 alcohols are interesting in any biodiesel production process, methanol is the most favorite one because it has suitable physical and chemical properties than others. In the case of fats/oil, natural vegetable oils and animal fats usually contain glyceride (produced from fatty acid and glycerol), trace amount of fatty acid and water. Among several compositions, triglyceride is the main composition of vegetable oils or fats which possess >96 wt% of fats/oils. Actually, all types of triglycerides can be directly introduced to transesterification process using basic catalysts. An exception is made when there is a

large amount of fatty acid and water because they have significant effect on the conversion of triglyceride to alkyl ester (Ma and Hanna, 1999). As a result, it is necessary to pretreat oils/fats before running process of biodiesel production. In general, water can be removed by heat or drying with anhydrous substances such as magnesium or sodium sulfate anhydrous while free fatty acid can be removed by treating with NaOH and filtering out solid residuals. The appropriate free fatty acid content should be lower than 2.0 wt%.

The most common way to produce biodiesel is by transesterification using basic catalysts (NaOH, KOH and NaOCH<sub>3</sub>) because the reaction time is short (about 2 h) and the cost of raw materials is low. However, the use of base catalysts is versatile only for the well-refined vegetable oil with less than 2.0% free fatty acid (FFA) (Wang et al., 2006). Fortunately, acid catalyst process is favorable for either vegetable oils or animal fats contained with more than 2.0% FFA. This process requires excess of methanol, high pressure (170-180 kPa), high cost stainless steel equipment, and long reaction time for processing (Wang et al., 2006). Although the acidic process seems to have several disadvantages, the reaction can give a higher conversion and yields than that from basic process because there is no loss of raw material by soap formation in all esterification process. After pretreatment of the raw material, the most important process is triglyceride conversion to ester. In order to reach the maximum yield, the transesterification mechanism should be understood to control each processing step.

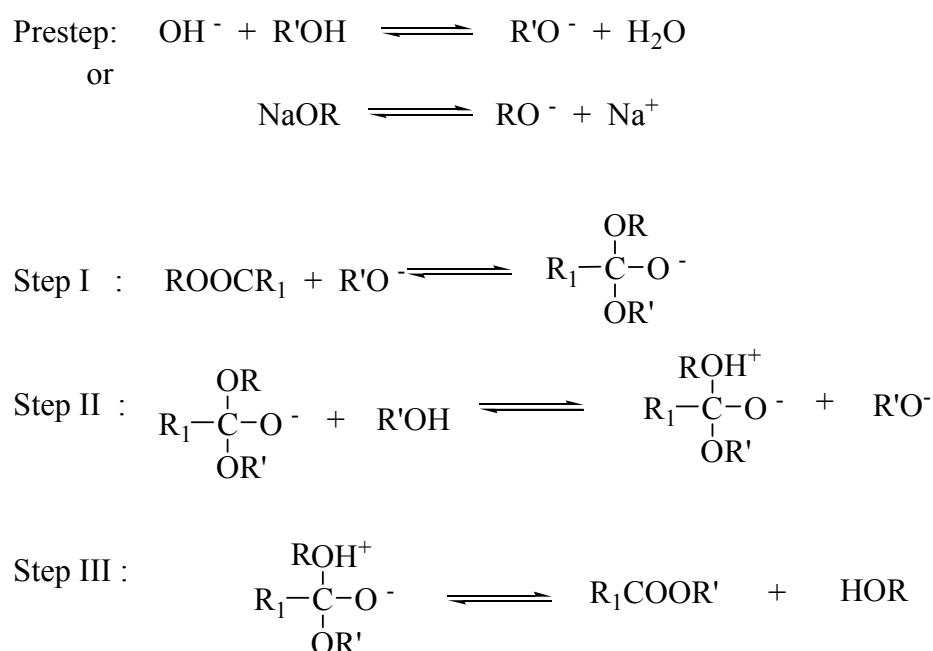
### 2.7.2 Mechanism of transesterification reaction using NaOH catalyst

Ma and Hanna, (1999) explained the transesterification mechanism of triglyceride using NaOH catalyst as shown in schematic 2.1 and 2.2. In the transesterification mechanism in scheme 2.1, triglyceride is converted stepwise to diglyceride, monoglyceride and finally glycerol. All reactions are reversible, although the equilibrium lies towards the production of fatty acid esters and glycerol. A mole of ester is liberated at each step.



**Scheme 2.1** Transesterification reaction of vegetable oil with alcohol to ester and glycerol.

However, if we take into account dynamic process of biodiesel production, there are three steps to convert triglyceride to alkyl ester. In this case, it is given example for only methanolysis. The first step in scheme 2.2 is an attack on the carbonyl carbon atom of the triglyceride molecule by the anion of the alcohol (methoxide ion) to form a tetrahedral intermediate. In the second step, the tetrahedral intermediate reacts with an alcohol (methanol) to regenerate the anion of the alcohol (methoxide ion). In the last step, rearrangement of the tetrahedral intermediate results in the formation of a fatty acid ester and a diglyceride. Methyl ester from this process is mixed with other compounds; H<sub>2</sub>O, glycerol, excess methanol and catalyst. In order to gain a pure biodiesel product, separation steps should be carried out.



**Scheme 2.2** The reaction mechanism of alkali-catalyzed transesterification of triglyceride with alcohol.

Where: R-OH = diglyceride, R<sub>1</sub> = long chain alkyl group, and R' = short alkyl group

### **2.7.3 Separation of mixed products from transesterification**

Products from alkali-catalyzed transesterification are mixed with the excess amounts of methanol. Thus, the first separation step is to distill methanol out from methyl ester and glycerol. The remaining mixed products exist in two layers. The upper layer contains methyl ester while the lower layer contains glycerol mixed with catalyst, soap and water. To neutralize the basic catalyst, appropriate amount of acid solution is dropped to the mixed solution. In the next step, water is used to separate organic compound (methyl ester) from glycerol and inorganic compound (water, soap, and salt). Because methyl ester may be contaminated with a trace amount of water, it is necessary to dry the product by mean of anhydrous extraction or evaporation. Finally, a purely yellow solution is obtained.

The production of biodiesel via homogeneous rout that the separation step is very difficult to operate and there are many undesired products which may affect environment. Recently, many researches focus on biodiesel production using heterogeneous catalysis to reduce production steps and enhance conversion and yields of the methyl ester.

### **2.7.4 Heterogeneous catalysts**

For the production of biodiesel fuels, the use of homogeneous catalyst (both basic and acidic catalyst) produces not only unfriendly environmental by-products but also involves difficulty in the product separation (Furuata et al., 2005; Gryglewicz, 1999; Peterson and Scarrach, 1984). New procedures should be invented to improve and develop steps of biodiesel production. Thus, several researchers have focused on utilizing heterogeneous catalysts to operate transesterification reaction.



Several efforts are based on the application of modified zeolite. Furuata et al. (2005) explored the use of  $\text{CaCO}_3$  as heterogeneous catalyst and got conversions above 95%. Ebiura et al. (2005) investigated transesterification of triolein (trioleoyl glycerol) with methanol using alumina loaded with potassium carbonate and obtained dioleoyl glycerol in 77% yield at 180 °C in 5 h. Xie et al. (2006) studied transesterification reaction of soybean oil and methanol with NaX Zeolite loaded with 10% KOH resulting conversion of soybean 85.6% at 65 °C for a reaction time of 8 h. Na/NaOH/ $\gamma$ - $\text{Al}_2\text{O}_3$  heterogeneous alkaline catalysts were applied for transesterification reaction of soybean oil with methanol using hexane as a co-solvent (Kim et al., 2004). The best result (> 90%) was obtained after 2 h with the molar ratio methanol: oil of 9:1 at 60 °C. There were some reports about the applications of modified MCM-41 to catalyze transesterification. Jaenicke et al. (2000) introduced alkyl guanidine to modify siliceous MCM-41. The catalysts prepared by immobilization of alkyl guanidines in microporous systems providing diffusion restrictions for the vegetable oil as well as the low stability of the inorganic framework. Monteiro and Cruz (2004) studied the transesterification of soybean oil using 10% $\text{La}_2\text{O}_3$ -MCM-41 as a catalyst. The reactions were carried out with a weight ratio of methanol: soybean: catalyst 4.5:6.0:0.3 at 70 °C for 8 h. The best results were obtained with conversion of 81%.

When compare between zeolite and MCM-41 modified inorganic functional group, conversion and yields were hardly different even MCM-41 modified possesses larger pore size than that of zeolite. In fact, triglyceride is bulk molecule that should diffuse through the pore of MCM-41 better than that of zeolite. That means the lack of active site center within pores of modified MCM-41. Taking into account with two steps in biodiesel production (Wang et al., 2006; Wang et al., 2007),

either vegetable oils or animal fats reached the maximum conversion by converting via both esterification (acid catalysis) and transesterification (base catalysis). These two steps gave the concepts that MCM-41 modified surface exhibits basic site of metal oxide so this reaction should be called transesterification. This study will establish basic site of RH-MCM-41 by adding potassium oxide to facilitate the separation of catalyst from methyl ester.

In summary, Biodiesel as renewable and sustainable energy source can be produced by the reaction between vegetable/fat oil and alcohol. Conventional production has focused on using basic and acidic catalysts and the use of basic catalyst was the most active and over 90% of biodiesel yielded within 2 h. However, basic catalysts has been limited by soap formation when oil possessed > 2% free fatty acid (FFA) was used. Consequently, the mixing among alkyl ester, glycerol and soap layers is very difficult to separate for each other. Utilization of acidic catalyst is proper for high FFA content because soap does not form under this condition. Nevertheless, strong condition to drive reaction forward is needed when acidic catalyst is used for biodiesel production. Furthermore, complete conversion of oil is slow and reaction is also costly. Thus, heterogeneous catalysis open up the way to accomplish biodiesel production effectively because the separation of solid catalyst from biodiesel product is much easier than that of homogeneous catalyst. In addition, the reaction under this circumstance is environmentally friendly and the waste from the biodiesel production can be dealt properly.

## References

- Ahn, W. S., Lee, D. H., Kim, T. J., Kim, J. H., Seo, G., Ryoo, R. (1999). Post-synthetic preparations of titanium-containing mesopore molecular sieves. **Applied Catalysis A: General**. 181(1): 39-49.
- Anandan, S. (2008). Photocatalytic effects of titania supported nanoporous MCM-41 on degradation of methyl orange in the presence of electron acceptors. **Dyes Pigments**. 76(2): 535-541.
- Badiei, A.-R., Bonneviot, L. (1998). Modification of mesoporous silica by direct template ion exchange using cobalt complexes. **Inorganic Chemistry**. 37(16): 4142-4145.
- Bandara, J., Nadtochenko, V., Kiwi, J., Pulgarin, C. (1997). Dynamics of oxidant addition as a parameter in the modeling of dye mineralization (Orange II) via advanced oxidation technologies. **Water Science and Technology**. 35(4): 87-93.
- Basca, R. R., Kiwi, J. (1998). Effect of rutile phase on the photocatalytic properties of nanocrystalline titania during the degradation of *p*-coumaric acid. **Applied Catalysis B: Environmental**. 16(1): 19-29.
- Bhattacharyya, A., Kawi, S., Ray, M.B. (2004). Photocatalytic degradation of orange II by TiO<sub>2</sub> catalysts supported on adsorbents. **Catalysis Today**. 98(3): 431-439.
- Bickley, R. I., Gonzales-Carreno, T., Lees, J. L., Palmisano, L., Tilley, R. J. D. (1991). A structural investigation of titanium dioxide photocatalysts. **Journal of Solid State Chemistry**. 92(1): 178-190.
- Bouazza, N., Lillo-Ródenas, M. A., Linares-Solano, A. (2008). Enhancement of the photocatalytic activity of pelletized TiO<sub>2</sub> for the oxidation of propene at low concentration. **Applied Catalysis B: Environmental**. 77(3): 284-293.

- Carp, O., Huisman, C. L., Reller, A. (2004). Photoinduced reactivity of titanium dioxide. **Progress in Solid State Chemistry**. 32(1): 33-177.
- Carvalho, W.A., Wallau, M., Schuchardt, U. (1999). Iron and copper immobilised on mesoporous MCM-41 molecular sieves as catalysts for the oxidation of cyclohexane. **Journal of Molecular Catalysis A: Chemical**. 144(1): 91-99.
- Chen, J. M., Chang, F. W. (1991). The chlorination kinetics of rice husk. **Industrial and Engineering Chemistry Research**. 30(10): 2241-2247.
- Chiarakorn, S., Areerob, T., Grisdanurak, N. (2007). Influence of functional silanes on hydrophobicity of MCM-41 synthesized from rice husk. **Science and Technology of Advanced Materials**. 8(1): 110-115.
- Chung, K.-T., Cerniglia, C. E. (1992). Mutagenicity of azo dyes: Structure-activity relationships. **Mutation Research-Genetic Toxicology and Environmental Mutagenesis**. 277(3): 201-220.
- Conçalves, M. S. T., Oliveira-Campos, A. M. F., Pinto, M. M. S., Plasencia, P. M. S., Queiroz, M. J. R. P. (1999). Photochemical treatment of solutions of azo dyes containing TiO<sub>2</sub>. **Chemosphere**. 39(5): 781-786.
- Conradt, R., Pimkhaohkam. P., Leela-Adisorn. (1992). Nano-structured silica from rice. **Journal of Non-Crystalline Solids**. 145(1): 75-79.
- Cooper, P. (1993). Removing colour from dyehouse wastewaters-a critical review of technology available. **Journal of the Society of Dyers and Colourists**. 109(3): 97-100.
- Davis, R. J., Gainer, J. L., O'Neal, G., Wu, I.-W. (1994). Photocatalytic decolorization of wastewater dyes. **Water Environment Research**. 66 (1): 50-53.

- Della, V.P., Kuhn, I., Hotza, D. (2002). Rice husk ash as an alternate source for active silica production. **Materials Letters**. 57(4): 818-821.
- Ebiura, T., Echizen, T., Ishikawa, A., Murai, K., Baba, T. (2005). Selective transesterification of triolein with methanol to methyl oleate and glycerol using alumina loaded with alkali metal salt as a solid-base catalyst. **Applied Catalysis A: General**. 283(1): 111-116.
- Eimer, G.A., Casuscelli, S.G., Ghione, G.E., Crivello, M.E., and Herrero, E.R. (2006). Synthesis, characterization and selective oxidation properties of Ti-containing mesoporous catalysts. **Applied Catalysis A: General**. 298(1): 232-242.
- Encinar, J. M., Gonzalez, J. F., Rodriguez-Renares, A. (2005). Biodiesel from used frying oil. variables affecting the yields and characteristics of the biodiesel. **Industrial and Engineering Chemistry Research**. 44(15): 5491-5499.
- Fox, M. A., Dulay, M. (1993). Heterogeneous photocatalysis. **Chemical Reviews**. 93(1): 341-357.
- Furuata S., Matsubishi H., and Arata, K. (2005). Biodiesel fuel production with solid amorphous-zirconia catalysis in fixed bed reactor. **Biomass and Bioenergy**. 30(10): 870-873.
- Gerischer, H., Heller A. (1992). Photocatalytic oxidation of organic molecules at TiO<sub>2</sub> particles by sunlight in aerated water. **Journal of the Electrochemical Society**. 139(1): 113-118.
- Gridsdanurak, N., Chiarakorn, S., Wittayakun, J. (2003). Utilization of mesoporous molecular sieve synthesis from natural source rice husk silica to chlorinated volatile organic compounds (CVOCs) adsorption, **Korean Journal of Chemical Engineering**. 20(5): 950-955.

- Gryglewicz, S. (1999). Rapeseed oil methyl esters preparation using heterogeneous catalysts. **Bioresource Technology**. 70(3): 249-253.
- Grzechulska, J., Morawski, A. W. (2002). Photocatalytic decomposition of azo-dye acid black 1 in water over modified titanium dioxide. **Applied Catalysis B: Environmental**. 36(1): 45-51.
- Hermann, J. M. (1999). Heterogeneous photocatalysis: fundamentals and applications to the removal of various types of aqueous pollutants. **Catalysis Today**. 53(1): 115-129.
- Hoffmann, M. R., Martin, S. T., Choi, W., Bahnemann, D. W. (1995). Environmental applications of semiconductor photocatalysis. **Chemical Reviews**. 95(1): 69-96.
- Holland, B. T., Walkup, C., Stein, A. (1998). Encapsulation, stabilization, and catalytic properties of flexible metal porphyrin complexes in MCM-41 with minimal electronic perturbation by the environment. **Journal of Physical Chemistry B**. 102(22): 4301-4309.
- Jaenicke, S., Chuah, G.C., Lin, X.H., Hu, X.C. (2000). Organic–inorganic hybrid catalysts for acid- and base-catalyzed reactions. **Microporous and Mesoporous Materials**. 35-36: 143-153.
- Kapur, T., Kandpal, T. C., Garo, H. P. (1998). Electricity generation from rice husk in Indian rice mills: potential and financial viability. **Biomass and Bioenergy**. 14(5): 573–583.
- Kim, H-J., Kang, B-S., Kim, M-J., Park, Y.M., Kim, D-K., Lee, J-S., and Lee, K-Y. (2004). Transesterification of vegetable oil to biodiesel using heterogeneous base catalyst. **Catalysis Today**. 93-95: 315-320.
- Kim, S., Choi, W. (2002). Kinetics and mechanisms of photocatalytic degradation of

$(\text{CH}_3)_n\text{NH}_{4-n}^+$  ( $0 \leq n \leq 4$ ) in  $\text{TiO}_2$  suspension: The role of OH radicals.

**Environmental Science and Technology**. 36(9): 2019-2025.

Konstantinou, I. K., Albanis, T. A. (2004).  $\text{TiO}_2$ -assisted photocatalytic degradation of azo dyes in aqueous solution: kinetic and mechanistic investigations: A review. **Applied Catalysis B: Environmental**. 49(1): 1–14.

Koyano, K.A., Tatsumi, T. (1997). Synthesis of titanium-containing MCM-41. **Microporous Materials**. 10(4): 259-271.

Kruk, M., Jaroniec, M., Ryoo, R., Kim, J. M. (1999). Characterization of high-quality MCM-48 and SBA-1 mesoporous silicas, **Chemistry of Materials**. 11(9): 2568-2572.

Kumer, D., Schumucher, K., de Fresne von Hoheneschen C. Grun, M. Unger, K. K. (2001). MCM-41, MCM-48, and related mesoporous adsorbents the synthesis and characterization. **Colloids and Surfaces A: Physicochemical and Engineering Aspects**. 187-188(1): 109-116.

Kuo, W. S., Lin, Y. T. (2000). Photocatalytic oxidation of xenobiotics in water with immobilized  $\text{TiO}_2$  on agitator. **Journal of Environmental Science and Health, Part B: Pesticides, Food Contaminants, and Agricultural Wastes**. 35(1): 61-75.

Legrini, O., Oliveros, E., Braun, A. M. (1993). Photochemical processes for water treatment. **Chemical Reviews**. 93(2): 671-698.

Linsbiger, A. L., Lu, G. Q., Yates Jr, J. T. (1995). Photocatalysis on  $\text{TiO}_2$  surfaces: principles, mechanisms, and selected results. **Chemical Reviews**. 95(3): 735-758.

Liou, T. -H. (2004). Preparation and characterization of nano-structured silica from

- rice husk. **Materials Science and Engineering A**. 364(2): 313-323.
- Ma, F., Hanna, M. A. (1999). Biodiesel production: a-review. **Bioresource Technology**. 70(1): 1-15.
- Maira, A. J., Yeung, K. L., Lee, C. Y., Yue, P. L., Chan C. K. (2000). Size effects in gas-phase photo-oxidation of trichloroethylene using nanometer-sized TiO<sub>2</sub> catalysts. **Journal of Catalysis**. 192(1): 185-196.
- Maschmeyer, T., Rey, F., Sankar, G., Thomas, J. M. (1995). Heterogeneous catalysts obtained by grafting metallocene complexes onto mesoporous silica. **Nature**. 378 (1): 159-162.
- Monteiro, R.S., Cruz, R.S. (2004). **Abstracts of the 27<sup>th</sup> reuniao annual da sociedade brasileira de quimica and XXVI congress latinoamericano de quimica**. Salvador, Brazil.
- Muggli, D. S., Ding, L. (2001). Photocatalytic performance of sulfated TiO<sub>2</sub> and Degussa P-25 TiO<sub>2</sub> during oxidation of organics. **Applied Catalysis B: Environmental**. 32(3): 181-194.
- Neppolian, B., Choi, H. C., Sakthivel, S., Arabindoo, B., Murugesan, V. (2002). Solar light induced and TiO<sub>2</sub> assisted degradation of textile dye reactive blue 4. **Chemosphere**. 46(8): 1173-1181.
- Noiroj, K., Intarapong, P., Luengnaruemitchai, A., Jai-In, S. (2009). A comparative study of KOH/Al<sub>2</sub>O<sub>3</sub> and KOH/NaY catalysts for biodiesel production via transesterification from palm oil. **Renewable Energy**. 34(4): 1145-1150.
- Nur, H., Guan, L. C., Endud, S., Hamdan, H. (2004). Quantitative measurement of a mixture of mesophases cubic MCM-48 and hexagonal MCM-41 by <sup>13</sup>C CP/MAS NMR. **Materials Letters**. 58(12): 1971-1974.



- Nur, H., Hamid, H., Endud, S., Hamdan, H., Ramli, Z. (2006). Iron-porphyrin encapsulated in poly(methacrylic acid) and mesoporous Al-MCM-41 as catalysts in the oxidation of benzene to phenol. **Materials Chemistry and Physics**. 96(2): 337-342.
- Ohno, T., Sarukawa, K., Tokieda, K., Matsumura, M. (2001). Morphology of a TiO<sub>2</sub> photocatalyst (Degussa, P-25) consisting of anatase and rutile crystalline phases. **Journal of Catalysis**. 203(1): 82-86.
- Ollis, D. F., Pelizzetti, E., Serpone, N. (1991). Destruction of water contaminants. **Environmental Science and Technology**. 25(9): 1523-1529.
- Ollis, D. F., Al-Ekabi (Eds.), H. (1993). Photocatalytic Purification and Treatment of Water and Air, **Elsevier Science Publishers**. Amsterdam, 1993.
- Øye, G., Sjöblom, J., Stöcker, M. (2001). Synthesis, characterization and potential applications of new materials in the mesoporous range, **Advances in Colloid and Interface Science**. 89-90: 439-466.
- Peterson, G.R., Scarrach, W. P. (1984). Rapeseed transesterification by heterogeneous catalysis. **Journal of the American Oil Chemists Society**. 61(10): 1593-1597.
- Phanikrishna Sharma, M.V., Durga Kumari, V., Subrahmanyam, M. (2008). Photocatalytic degradation of isoproturon herbicide over TiO<sub>2</sub>/Al-MCM-41 composite systems using solar light. **Chemosphere**. 72(4): 644-651.
- Poh, N. E., Nur, H., Muhid, M. N. M., Hamdan, H. (2006). Sulphated AlMCM-41: Mesoporous solid Brønsted acid catalyst for dibenzoylation of biphenyl. **Catalysis Today**. 114(2): 257-262.
- Real, C., Alcalá, M.D., Criado, J.M. (1996). Preparation of silica from rice husk. **Journal of the American Ceramic Society**. 79(8): 2012-2016.

- Ryu, C. S., Kim, M.-S., Kim, B.-W. (2003). Photodegradation of alachlor with the TiO<sub>2</sub> film immobilized on the glass tube in aqueous solution. **Chemosphere**. 53(7): 765-771.
- Sakthivel, S., Neppolian, B., Shankar, M.V., Arabindoo, B., Palanichamy, M., Murugesan, V. (2003). Solar photocatalytic degradation of azo dye: Comparison of photocatalytic efficiency of ZnO and TiO<sub>2</sub>. **Solar Energy Materials and Solar Cells**. 77(1): 65-82.
- Saquib, M., Muneer, M. (2003). TiO<sub>2</sub>/mediated photocatalytic degradation of a triphenylmethane dye (gentian violet), in aqueous suspensions. **Dyes Pigments**. 56(1): 37-49.
- Selvam, P., Bhatia, K.S., Sonwane, G.C. (2001). Recent Advances in Processing and Characterization of Periodic Mesoporous MCM-41 Silicate Molecular Sieves. **Industrial and Engineering Chemistry Research**. 40(15): 3237-3262.
- Sercheli, R., Vargas, R. M., Schuchardt, U. (1999). Alkylguanidine-catalyzed heterogeneous transesterification of soybean oil. **Journal of the American Oil Chemists Society**. 76(10): 1207-1210.
- Shephard, D. S., Maschmeyer, T., Johnson, B. F. G., Thomas, J. M., Sankar, G., Ozkaya, D., et al. (1997). Bimetallic Nanoparticle Catalysts Anchored Inside Mesoporous Silica. **Angewandte Chemie International Edition**. 36(20): 2242-2245.
- So, C. M., Cheng, M. Y., Yu, J. C., Wong, P. K. (2002). Degradation of azo dye Procion Red MX-5B by photocatalytic oxidation. **Chemosphere**. 46(6): 905-912.
- Srinivas, D., Srivastava, R., Ratnasamy, P. (2004). Transesterifications over

- titanosilicate molecular sieves. **Catalysis Today**. 96(3): 127-133.
- Stylidi, M., Kondarides, D. I., Verykios, X. E. (2003). Pathways of solar light-induced photocatalytic degradation of azo dyes in aqueous TiO<sub>2</sub> suspensions. **Applied Catalysis B : Environmental**. 40(4): 271-286.
- Tanaka, K., Capule, M. F. V., Hisanaga, T. (1991). Effect of crystallinity of TiO<sub>2</sub> on its photocatalytic action. **Chemical Physics Letters**. 187(1): 73-76.
- Tsay, M-T., Chang, F-W. (2000). Characterization of rice husk ash-supported nickel catalysts prepared by ion exchange. **Applied Catalysis A: General**. 203(1): 15-22.
- Tunesi, S., Anderson, M. (1991). Influence of chemisorption on the photodecomposition of salicylic acid and related compounds using suspended TiO<sub>2</sub> ceramic membranes. **Journal of Physical Chemistry**. 95(8): 3399-3405.
- Turchi, C. S., Ollis, D. F. (1990). Photocatalytic degradation of organic water contaminants: Mechanisms involving hydroxyl radical attack. **Journal of Catalysis**. 122(1): 178-192.
- Ueda, T., Kunimitsu, Y., Shinogi, Y. (2007). Potential conflicts for the reuse of rice husk in Thailand. **Paddy and Water Environment**. 5(2): 123-129.
- Van Der Voort, P., Morey, M., Stucky, G. D., Mathieu, M., Vansant, E. F. (1998). Creation of VO<sub>x</sub> surface species on pure silica MCM-48 using gas-phase modification with VO(acac)<sub>2</sub>. **Journal of Physical Chemistry B**. 102(3): 585-590.
- Wang, Y., Ou, S., Lui, P., Xue, F., Tang, S. (2006). Comparison of two different processes to synthesize biodiesel by waste cooking oil. **Journal of Molecular Catalysis A: Chemical**. 252(1): 107-112.

- Wang, Y., Ou, S., Lui, P., Zhang, Z. (2007). Preparation of biodiesel from waste cooking oil via two step catalyzed process. **Energy Conversion and Management**. 48(1): 184-188.
- Wong, C. C., Chu, W. (2003). The direct photolysis and photocatalytic degradation ofalachlor at different TiO<sub>2</sub> and UV sources. **Chemosphere**. 50(8): 981-987.
- Xie, W., Hong, P., Chen, L. (2006). Transesterification of soybean oil catalyzed by potassium loaded on alumina as a solid-base catalyst. **Applied Catalysis A: General**. 300(1): 67-74.
- Xie, W., Huang, X., Li, H. (2007). Soybean oil methyl esters preparation using NaX zeolites loaded with KOH as a heterogeneous catalyst. **Bioresource Technology**. 98(4): 936-939.
- Yalcin, N., Sevinc, V. (2001). Study on silica obtained from rice husk. **Ceramics International**. 27(2): 219-224.
- Yin, H., Wada, Y., Kitamura, T., Kambe, S., Murasawa, S., Mori, H., Sakata T., Yanagida. (2001). Hydrothermal synthesis of nanosized anatase and rutile TiO<sub>2</sub> using amorphous phase TiO<sub>2</sub>. **Journal of Materials Chemistry**. 11(10): 1694-1703.
- Yuan, S., Shi, L., Mori, K., Yamashita, H. (2009). Preparation of highly dispersed TiO<sub>2</sub> in hydrophobic mesopores by simultaneous grafting and fluorinating. **Microporous Mesoporous Materials**. 117(1): 356-361.
- Zhang, L., Liu, C. Y., Ren, X. M. (1995). Photochemistry of semiconductor particles 3. Effects of surface charge on reduction rate of methyl orange photosensitized by ZnS sols. **Journal of Photochemistry and Photobiology A: Chemistry**. 85(3): 239-245.

- Zhang, Q., Gao, L., Guo, J. (2000). Effects of calcination on the photocatalytic properties of nanosized TiO<sub>2</sub> powders prepared by TiCl<sub>4</sub> hydrolysis. **Applied Catalysis B: Environmental**. 26(3): 207-215.
- Zhao, X.S., (Max) Lu, G.Q., Millar, G.J. (1996). Advances in mesoporous molecular sieve MCM-41. **Industrial and Engineering Chemistry Research**. 35(7): 2075-2090.
- Zielinska, B., Grzechulska, J., Grzmil, B., Morawski, A. W. (2001). Photocatalytic degradation of reactive black 5. A comparison between TiO<sub>2</sub>-Tytanpol A11 and TiO<sub>2</sub>-Degussa P25 photocatalysts. **Applied Catalysis B: Environmental**. 35(1): L1-L7.

## CHAPTER III

# PHOTOCATALYTIC DEGRADATION OF METHYL ORANGE ON Ti-RH-MCM-41 AND TiO<sub>2</sub>/RH-MCM-41

### 3.1 Abstract

Photocatalytic degradation of methyl orange was tested on two catalysts containing 10wt% titanium supported on mesoporous MCM-41 synthesized with rice husk silica. The first catalyst was Ti-RH-MCM-41 prepared by adding tetrabutyl orthotitanate (TBOT) in a synthetic gel of RH-MCM-41 and the second catalyst was TiO<sub>2</sub>/RH-MCM-41 prepared by grafting TBOT on preformed RH-MCM-41. From X-ray diffraction, the mesoporous structures in both catalysts were preserved upon the addition of TBOT but anatase phase of titania was only observed in TiO<sub>2</sub>/RH-MCM-41. From X-ray absorption spectroscopy, the titanium in Ti-RH-MCM-41 had oxidation state of +4 and tetrahedrally coordinated to four oxygen atoms. From nitrogen adsorption, the surface area of both catalysts decreased slightly from the parent RH-MCM-41, i.e., from 1231 m<sup>2</sup>/g to 1074 and 1006 m<sup>2</sup>/g in Ti-RH-MCM-41 and TiO<sub>2</sub>/RH-MCM-41, respectively. In the catalytic testing, the TiO<sub>2</sub>/RH-MCM-41 was more active than Ti-RH-MCM-41 with the same Ti loading because of the presence of active anatase phase. The TiO<sub>2</sub>/RH-MCM-41 had optimum catalyst weight to methyl orange volume ratio of 5 g/L and the optimum initial concentration of the dye was 2.0 ppm. The degradation obeyed pseudo first order and the adsorption obeyed Langmuir isotherm.

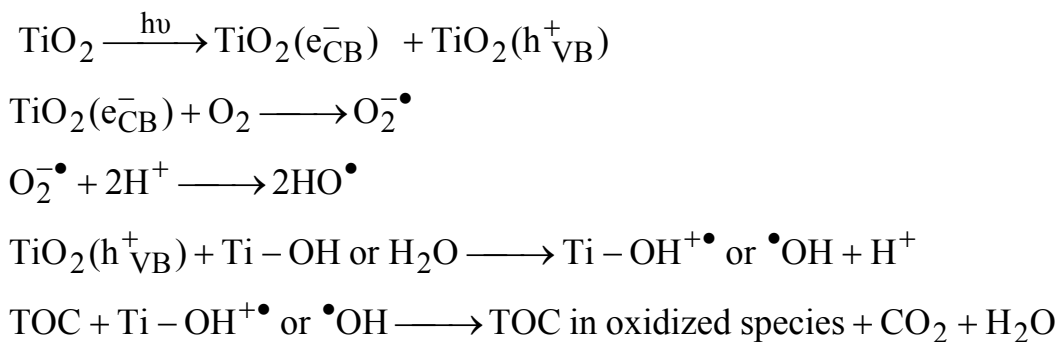
### 3.2 Introduction

Dye stuff is routinely applied in dyeing processes of various products such as textile, paper, leather, ceramic, cosmetics, and ink. It can be hazardous to human health and environment due to the fact that 15% of the dye produced is lost during production and application (Wang et al., 2008). Furthermore, the release of dye effluents causes water contamination which leads to pollution or originates dangerous by-products from reactions such as hydrolysis or oxidation in wastewater. Treatment processes are required to remove the undesired effluents.

Conventional processes such as biological, physical and chemical treatments have some disadvantages. For example, biological method by immobilizing enzyme on supports is not effective because most organic dyes are recalcitrant against enzyme. Physical treatment by adsorption can just transfer the organic pollutants to another source without decomposing them. Finally, chemical treatments including chlorination and ozonation are usually working for organic dye cracking but the complete decomposition is time consuming and costly. These problems can be overcome by using advanced oxidation processes (AOPs) which can effectively remove hazardous dyestuffs by photogeneration of active species for instance,  $\bullet\text{OH}$ ,  $\bullet\text{O}_2$  and  $\bullet\text{O}_2\text{H}$  to oxidize organic compound under UV light.

For, this photocatalyst  $\text{TiO}_2$  seems to have the most interesting utilization for AOPs because it is high stability, good performance and inexpensive. This  $\text{TiO}_2$  can generate electron on conduction band ( $e^-_{\text{CB}}$ ) and hole is left behind in valence band ( $h^+_{\text{VB}}$ ) upon irradiation with UV-vis light. The  $e^-_{\text{CB}}$  reduces  $\text{O}_2$  or electron acceptor and  $h^+_{\text{VB}}$  oxidizes titanol groups ( $\text{Ti-OH}$ ) or donator to generate hydroxyl radical ( $\bullet\text{OH}$ ). Finally, The  $\bullet\text{OH}$  can oxidize Total Organic Compounds (TOC) to from TOC

in oxidized species, H<sub>2</sub>O and CO<sub>2</sub>. The processes to generate <sup>•</sup>OH on TiO<sub>2</sub> are shown in Scheme 3.1.



**Scheme 3.1** Photodegradation process of organic carbon on TiO<sub>2</sub>.

These reactions are crucial important in photodegradation processes. There was a study of photodegradation of azo dye on bare TiO<sub>2</sub>. Konstantinou and Albanis, (2004) investigated photodegradation of azo dye on bare TiO<sub>2</sub> containing various functionalities in aqueous solution under UV irradiation. The process was mainly monitored by formation of intermediates including oxygenates and acid compounds and consecutively mineralized to downstream products. Kinetics analysis was approximated to be pseudo-first order, according to Langmuir model. Several variables had been affected the photodegradation of azo dye for instance, solution pH, catalyst concentration, substrate concentration and the present of electron acceptors. However, a significant part of electron hole recombination has been occurs to reduce photoactivity on TiO<sub>2</sub>. Furthermore, application of TiO<sub>2</sub> for photodegradation is also limited by regeneration of catalyst and particle aggregation. Kim and Choi (2002) performed photodegradation of tetramethylammonium chloride on bare TiO<sub>2</sub> under ambient circumstance. The result showed a great deactivity of TiO<sub>2</sub> when pH equal



pH point of zero charge ( $\text{pH}_{\text{PZC}}$ ) and particle aggregation was also reported. Consequently, many researches attempted to solve this problem by using  $\text{TiO}_2$  on several supports. Bhattacharyya et al. (2004) studied photodegradation of acid orange II on bare and supported  $\text{TiO}_2$  on MCM-41, montmorillonite, MCM-41 and zeolite beta under UV light. The catalysts were prepared by a so-gel method or impregnation on various supports with the loading of 10-80 wt% of  $\text{TiO}_2$ . The photocatalytic efficiencies on supported catalysts were greater than that on bare  $\text{TiO}_2$ . Li et al. (2007) used the same catalysts from Bhattacharyya's preparation to study the circumstantial dependence by varying solution pH. The results were found that the maximum photodegradation rate was achieved at the pH range of 4-5 for supported catalysts and 2.5 time as compared with unsupported  $\text{TiO}_2$  (Degussa P25). The supported  $\text{TiO}_2$  has a higher degradation rate and needed shorter in reaction time because the active sites are increased by the dispersion. The improvement was resonated by better adsorption of acid orange II molecule on supported mesoporous MCM-41 which possesses high surface area ( $1000\text{-}1400\text{ cm}^3/\text{g}$ ) and narrow pore size distribution ( $2\text{-}50\text{ \AA}$ ) where provides accessibility of bulky molecules. Moreover, OH radicals on MCM-41 were said to protect electron hole recombination by tapping generated hole that react catalyst surface  $\bullet\text{OH}$  (Carp et al., 2004). Those previous reasons promised the use of  $\text{TiO}_2$  supported on MCM-41 for photodegradation of azo dye but MCM-41 was prepared from commercial sources. The enhancement of photodegradation on  $\text{TiO}_2$  supported MCM-41 which prepared from natural source such as rice husk silica did not mention before. In addition, reactions to remove the waste or byproducts were set in glass swirl-rector that was costly and complicate for industrial. This work showed a simple method to remove methyl orange by using Ti and  $\text{TiO}_2$  dispersed on

mesoporous RH-MCM-41 prepared from rice husk silica. The prepared catalysts were used to test activity for photodegradation of methyl orange. Kinetics and adsorption of methyl orange were also investigated in this research.

### 3.3 Experimental

#### 3.3.1 Chemicals and materials

Chemical for silica extraction from rice husk was hydrochloric acid (97% HCl, Calo Erba). Chemicals for the syntheses of RH-MCM-41 and Ti-RH-MCM-41 were tetrabutyl orthotitanate (TBOT, 99%  $C_{16}H_{36}O_4Ti$ , Acros), cetyltrimethylammonium bromide or CTAB (96%  $C_{19}H_{42}NBr$ , Fluka), rice husk silica ( $SiO_2$ ), sodium hydroxide (97% NaOH, Carlo Erba) and sulfuric acid (96%  $H_2SO_4$ , Carlo Erba).

Chemicals for  $TiO_2$ /RH-MCM-41 preparation and photocatalytic degradation were RH-MCM-41, TBOT, nitric acid (65%  $HNO_3$ , Carlo Erba), NaOH and methyl orange (Riedel-de Haen).

#### 3.3.2 Apparatus and instruments

Apparatus for silica extraction; syntheses of RH-MCM-41, Ti-RH-MCM-41 and preparation of  $TiO_2$ /RH-MCM-41 included round bottle flask, condenser, heating mantle, beakers, magnetic stirrer, suction funnel, centrifuger, propylene bottle, teflon cylinder and teflon-lined autoclave, hot-air oven, muffle furnace, micropipette and pH meter.

Apparatus and equipments for photodegradation of methyl orange included glasswares, magnetic stirrer, balance, pH meter, UV lamp (Shimazu, UV 1201), timer, micropipette and UV-Vis spectrometer (Shimazu, UV 1201)

### 3.3.3 Preparation of rice husk silica

Rice husk was obtained from a local rice milling and silica preparation was via acid-leaching method modified from Chakraverty et al., (1991). The rice husk was thoroughly washed with water to remove the adhering soil and dust and dried at 100 °C overnight. It was refluxed with 3 M HCl for 6 h, filtered and washed several times with water until the filtrate is neutral and dried at 60 °C overnight. The black solid product was pyrolyzed in a muffle furnace at 550 °C for 6 h to remove the hydrocarbon and volatile organic compounds.

### 3.3.4 Synthesis of RH-MCM-41

RH-MCM-41 synthesis was modified the procedure described by srinivas et al. (2004) with the gel molar ratio of  $1.0\text{SiO}_2 : 0.25\text{CTABr} : 180\text{H}_2\text{O}$ . First, CTAB (1.45 g) was dissolved in deionized water (30.00 mL), stirred for 4 h to obtained a clear solution, denoted as solution A. Then solution B was simultaneously prepared by dissolving silica (1.00 g) and NaOH (2.00 g) deionized water (15 mL) with a constant stirring for 4 h to obtain a clear solution. Then Solution A was poured into a 100-mL teflon container and solution B was gradually added dropwise within 20 min. The mixture pH was adjusted to 11.5 by slowly dropping 5 N  $\text{H}_2\text{SO}_4$  until small particles agglomerate started to form. The gel mixture was then transferred into a teflon-lined autoclave and annealed hydrothermally in an oven at 100 °C for 72 h. The product mixture was filtered, dried at 100 °C, ground and calcined at 540 °C to remove the template. The products denoted as RH-MCM-41 were characterized by X-ray diffraction (XRD), nitrogen adsorption-desorption, Fourier transform infrared spectroscopy (FTIR).

### 3.3.5 Synthesis of Ti-RH-MCM-41

The Ti-RH-MCM-41 was synthesized from CTAB, TBOT and RHS dissolved in 3.33M NaOH solution with a gel molar ratio of  $1.0\text{SiO}_2 : 0.05\text{TBOT} : 3.0\text{NaOH} : 0.25\text{CTABr} : 180\text{H}_2\text{O}$  (Srinivas et al., 2004). The pH was adjusted to 11.5 and the mixture was crystallized at 100 °C for 72 h in a Teflon-lined autoclave. Then the as-prepared Ti-RH-MCM-41 was filtered, dried by deionized water several times, aged overnight and calcined at 540 °C for 6 h. The obtained white powder 10% Ti-RH-MCM-41s were characterized by X-Ray diffraction spectroscopy (XRD), nitrogen adsorption-desorption, X-ray absorption spectroscopy (XAS) and Fourier transform infrared spectroscopy (FTIR).

### 3.3.6 Preparation of $\text{TiO}_2/\text{RH-MCM-41}$

The preparation of  $\text{TiO}_2$  sol was by an acid catalyzed sol-gel formation method modified from Bhattacharyya et al. (2004). First, an aqueous solution of 1 M  $\text{HNO}_3$  acid (40 mL) was prepared and an appropriate amount of TBOT was added gradually under continuous stirring for 1.5–2 h to produce a transparent sol. Subsequently, the mixture was diluted with de-ionized water and the pH was adjusted to 3 with 1 M NaOH resulting a turbid colloid. A required amount of RH-MCM-41 to produce 10% $\text{TiO}_2/\text{RH-MCM-41}$  was added to the turbid colloid suspension. The resulting mixed suspension was agitated by a magnetic stirrer for another 2 h at room temperature, separated by centrifugations and washed several times with deionized water until the pH of the filtrate was about 6. The resulting 10% $\text{TiO}_2/\text{RH-MCM-41}$  was dried overnight in an oven and calcined in furnace at 300 °C for 1h.

### 3.3.7 Catalysts characterization

The crystalline phase of RH-MCM-41, TiO<sub>2</sub>/RH-MCM-41 and Ti-RH-MCM-41 were analyzed using powder XRD (Rigaku Model D/Max III and Bruker axis D5005 diffractometer) with CuK<sub>α</sub> radiation. The X-ray was generated with a current of 40 mA and a potential of 40 kV. The catalyst powder (0.20 g) was pressed in a sample holder and scanned from 1.5 to 80 degrees (2θ) in steps of 0.05 degrees per min.

X-ray absorption spectra of Ti-RH-MCM-41 and references compounds were measured in the energy region of the titanium K-edge in transmission mode at the beamline BL-8 of Synchrotron Light Research Institute (Public Organization). The X-ray beam 2s emitted by a storage ring running at 1.2 GeV. X-rays were monochromatized using a Si(111) two-crystal monochromator with energy resolution of  $1.0 \times 10^{-4}$ - $5.0 \times 10^{-4}$ . The monochromator covers the photon range 1830–8000 eV. Each sample (0.3 g) was pressed into a self-supporting wafer with an approximate thickness of 0.3 mm, placed in a holder, and mounted in a cell. The cell was evacuated and installed at the beamline.

XANES spectra were scanned at Ti K<sub>α</sub> edge (4966) with integration for 0.2 at each energy step in the range from 50 eV below the absorption edge to 150 eV beyond the edge. The pre-edge in the XANES region were normalized with the software ATHENA. The edge shifts were corrected to standard reference compounds to figure out characteristics of the sample.

EXAFS was also scanned at the Ti K<sub>α</sub> edge (4966 eV) in transmission mode with integration for 1 s at each energy step in the range from 50 eV below the absorption edge to 1000 eV beyond the edge. The Fourier transformation was

performed on  $k^3$ -weighted in the range of 2-10  $\text{\AA}^{-1}$ . The EXAFS data fitting was carried out with EXAFSPAK with single scattering paths calculated with FEFF7.0. Fitting was done both in  $r$  space ( $r$  is the distance from the absorber atom, Ti, O or Si) and  $k$  space ( $k$  is the wave vector) with application of  $k^1$ ,  $k^2$  and  $k^3$  weightings until excellent agreement between the fit for each of the  $k$  weightings.

Nitrogen adsorption-desorption isotherms were measured at  $-196\text{ }^\circ\text{C}$  from a relative pressure of 0.01 to 0.99 on a microporemetrics analyzer (ASAP 2010). Before measurement, each sample was degassed at  $250\text{ }^\circ\text{C}$  for 3 h. The BET surface area was obtained from the adsorption data in the relative pressure range of 0.02-0.2. The pore size and pore volumes were calculated from the desorption branches of the isotherm using Barrett-Joyner-Halenda (BJH) method.

The infrared spectra were recorded on a Bruker IFS 28 FTIR spectrometer equipped with an MCT detector in the range of  $400\text{-}4000\text{ cm}^{-1}$  with a resolution of  $4\text{ cm}^{-1}$  by KBr pellet technique. The solid sample and KBr were dried at  $120\text{ }^\circ\text{C}$  for 1 h before the preparation. Then 0.5 mg of sample and 30 mg of KBr were mixed and ground to form a homogeneous powder and pressed with 13 tons force for 1 min to form a pellet and put on a V-mount cell. The FTIR spectrum is recorded.

### **3.3.8 Catalytic testing for photocatalytic degradation of methyl orange**

The test was conducted in a photochemical reactor at room temperature. The weight to volume ratio of Ti-RH-MCM-41 and  $\text{TiO}_2/\text{RH-MCM-41}$  to methyl orange solution was 1.0, 2.5, 5.0, and 7.5 g/L and the concentration of methyl orange was 2.0 ppm in all mixtures. 30% w/v  $\text{H}_2\text{O}_2$  was added the mixture until obtaining 0.01M  $\text{H}_2\text{O}_2$  in the solution and stirred in a dark chamber for 30 min prior to

illumination with a UV lamp (10W). In order to investigate the changes of reaction, degraded products were withdrawn at regular interval (0, 5, 10, 15, 20 and 30 min.). Then the decrease of methyl orange concentration in the solution was determined by a UV-VIS (Shimazu, UV 1201) spectrometer. The catalyst with the highest conversion was tested further with various methyl orange concentrations (2.0, 4.0, 6.0, and 8.0 ppm).

### **3.3.9 Adsorption of methyl orange on TiO<sub>2</sub>/RH-MCM-41**

In order to study adsorption of methyl orange on TiO<sub>2</sub>/RH-MCM-41, various methyl orange concentrations, 2.0, 4.0, 6.0, 8.0 ppm, were prepared and mixed with TiO<sub>2</sub>/RH-MCM-41 in an erlenmeyer flask to give catalyst weight to methyl orange volume ratio of 5.0 g/L. The mixture was stirred vigorously in the dark for 30 min to establish equilibrium adsorption. Then, the liquid product was sampled for 1 mL to analyze by UV-Vis spectrometer. The decreases of methyl orange concentrations were plotted versus absorbance to reveal adsorption isotherm of methyl orange on the solid catalyst.

## **3.4 Results and Discussion**

### **3.4.1 Catalyst Characterization**

The purity of rice husk silica (RH-SiO<sub>2</sub>) analyzed by X-ray fluorescence was 98% with traces of alumina, potassium oxide and calcium oxide (Khemthong et al., 2007). The XRD of RH-SiO<sub>2</sub> is shown in Figure 3.1 containing a broad peak at the 2θ of 22.5 degree which is a characteristic of amorphous silica.

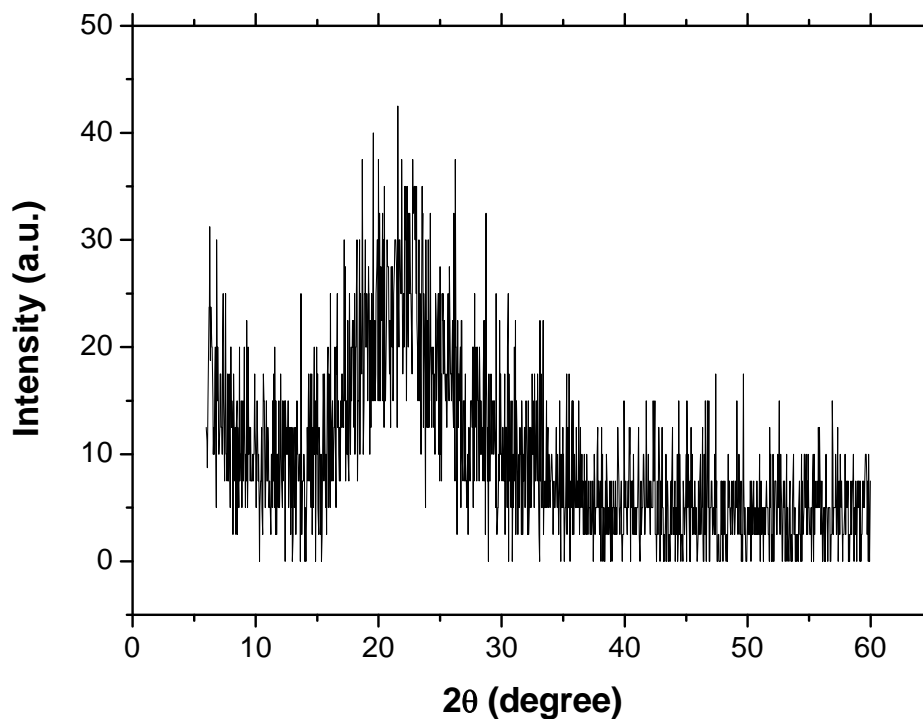


**Figure 3.1** XRD of spectrum of RH-SiO<sub>2</sub>.

XRD patterns of 10%TiO<sub>2</sub>/RH-MCM-41 and 10%Ti-RH-MCM-41 are shown in Figure 3.2A. Although they were prepared differently, they gave similar XRD patterns with four well-resolved peak of (100), (110), (200) and (211) planes. The diffraction patterns confirmed an ordered structure as in the parent MCM-41 (Schacht et al., 2004). The positions of the first peak of both samples were slightly different as shown in Table 3.1 resulting from a slight difference in d spacing of 10%Ti-RH-MCM-41 from the parent RH-MCM-41. Thus, incorporating Ti into the structure of RH-MCM-41 by adding TBOT into the synthetic gel caused an increase of d spacing while grafting TBOT on the preformed RH-MCM-41 did not cause much change.



**Table 3.1** Textural properties of RH-MCM-41, 10%TiO<sub>2</sub>/RH-MCM-41 and 10%Ti-RH-MCM-41.

Materials	2θ	a (Å)*	d <sub>100</sub> (Å)	S <sub>BET</sub> (m <sup>2</sup> /g)	V <sub>p</sub> (cm <sup>3</sup> /g)
RH-MCM-41	2.33	43.6	37.8	1231	0.73
10%Ti-RH-MCM-41	2.25	45.1	39.1	1074	0.63
10%TiO <sub>2</sub> /RH-MCM-41	2.37	44.1	38.2	1006	0.53

\* Unit cell parameter of RH-MCM-41, 10%Ti-RH-MCM-41 and 10%TiO<sub>2</sub>/RH-MCM-41 of d<sub>100</sub>, calculated from  $a = \frac{2}{\sqrt{3}}d_{100}$

Table 3.1 also shows surface areas and pore volumes of RH-MCM-41, 10%Ti-RH-MCM-41 and 10%TiO<sub>2</sub>/RH-MCM-41 calculated from nitrogen adsorption-desorption isotherms (see page 61).

In 10%Ti-RH-MCM-41, the characteristic peaks of either rutile or anatase phase of TiO<sub>2</sub> were not observed after calcination. The nature of Ti in this sample was investigated further by XANES and EXAFS (see page 64-66). In contrast, anatase phase was observed in 10%TiO<sub>2</sub>/RH-MCM-41 at 2θ of 25.3 degree (Figure 3.2B).

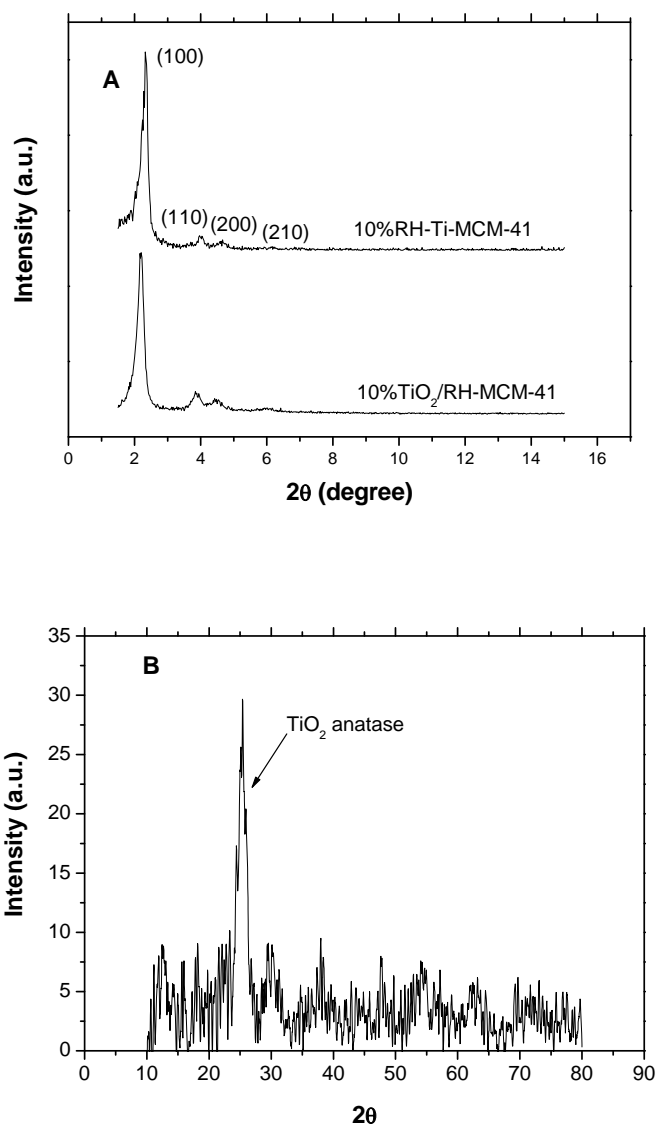


**Figure 3.2** A) low angle XRD patterns of Ti-RH-MCM-41 and TiO<sub>2</sub>/RH-MCM-41 and B) high angle XRD pattern of TiO<sub>2</sub>/RH-MCM-41.

Normalized Ti K-edge XANES spectrum of 10%Ti-RH-MCM-41 along with TiO<sub>2</sub> anatase and Ti foil references are shown in Figure 3.3. According to the concept, Ti (IV) is in a  $d^0$  configuration corresponding to  $A_{1g}$  or  $A_1$  state in octahedral or tetrahedral symmetry, respectively. The first aspect in the adsorption

spectra (pre-edge) is occurred from the excitation of electron from 1s electron to empty bound state, derived from Ti and O d and p state (Bordiga et al., 1994). From the results, titanium foil showed only one strong inflection of the zero energy (pre-edge) near 4967.9 eV. This is characteristics of tetrahedral symmetry which the final states are  $T_2$  and E ( $A_1 \rightarrow T_2$  and  $A_1 \rightarrow E$ ). As in  $T_2$  state, a significant mixing between 3d and 4p occurs and  $A_1 \rightarrow T_2$  transition is Laporte allowed. This is the reason why the prominently single peak emerges and overwhelms the transition peak from  $A_1 \rightarrow E$ . The XANES spectra of  $TiO_2$  anatase showed three low intensity pre-edge peaks bearing maximum (4968.1 eV) and very small peaks at 4964.6 and 4970.4 eV, the characteristic of octahedrally coordinated titanium atoms. These three states associate with the  $A_{1g} \rightarrow T_{2g}$  and  $A_{1g} \rightarrow T_{2g}$  transitions which are Laporte forbidden (Shul et al., 1997). Consequently, the pre-edge absorption of Ti (octahedral) is expected to be rather weak but the distorted octahedral symmetry let progressive relaxation occurs and the peaks are able to observed. The Ti XANES spectrum of 10%Ti-RH-MCM-41 sample exhibited the single pre-edge peak at the energy characteristic of the tetrahedrally coordinated titanium (IV) corresponding to a Laporte-allowed transition from  $A_1 \rightarrow T_2$  molecular levels built from 3d and 4p metal orbital (Kitano et al., 2007) and pre-edge energy of 4977.8 eV, with a shift of 4 eV comparing with Ti foil (4973.9). The data of pre-edge, edge and shift energy are shown in Table 3.2.

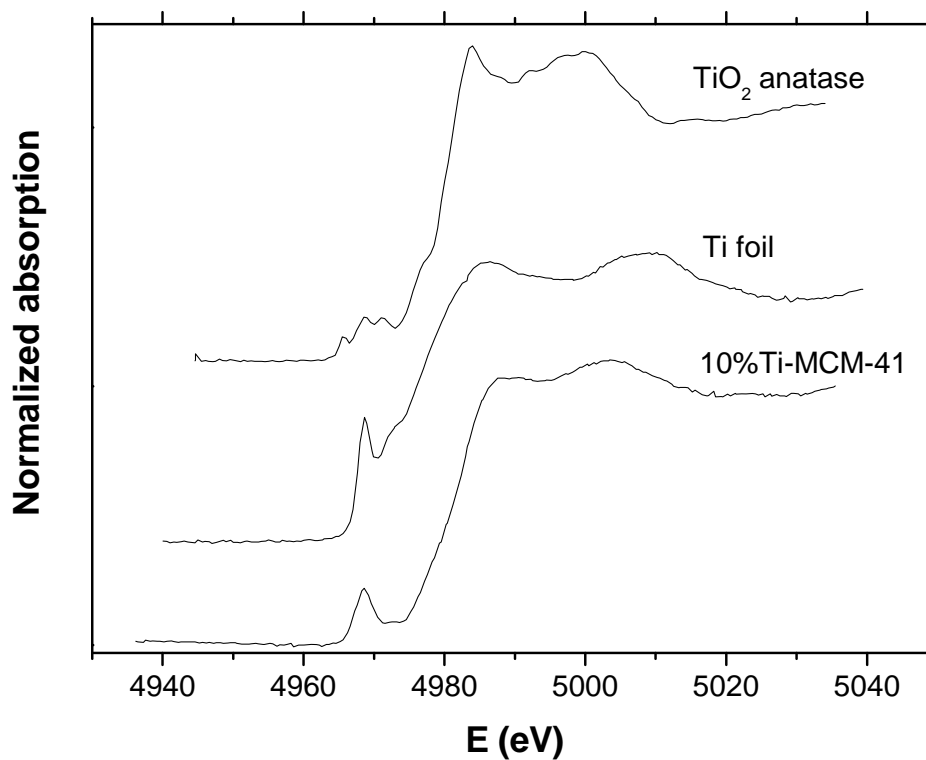


**Figure 3.3** Ti K-edge XANES spectra of 10%Ti-RH-MCM-41, Ti foil and TiO<sub>2</sub> anatase references.

For EXAFS, The Fourier transform of  $k^3$ -weighted Ti spectrum of Ti-RH-MCM-41 calculated in  $k$  and  $R$  range of  $2.30 < k < 9.55 \text{ \AA}^{-1}$  and  $0.0 < R < 4.0 \text{ \AA}$ , respectively. A good fitting curve confirmed that Ti was surrounded by four oxygen atoms in the first coordination shell with distances of 1.90 and 2.09  $\text{\AA}$  (Figure 3.4A-B). In the second coordination shell, one silicon atom was found at distance of 2.34  $\text{\AA}$  (Mrak et al., 2006). Other parameters were shown in the Table 3.3.

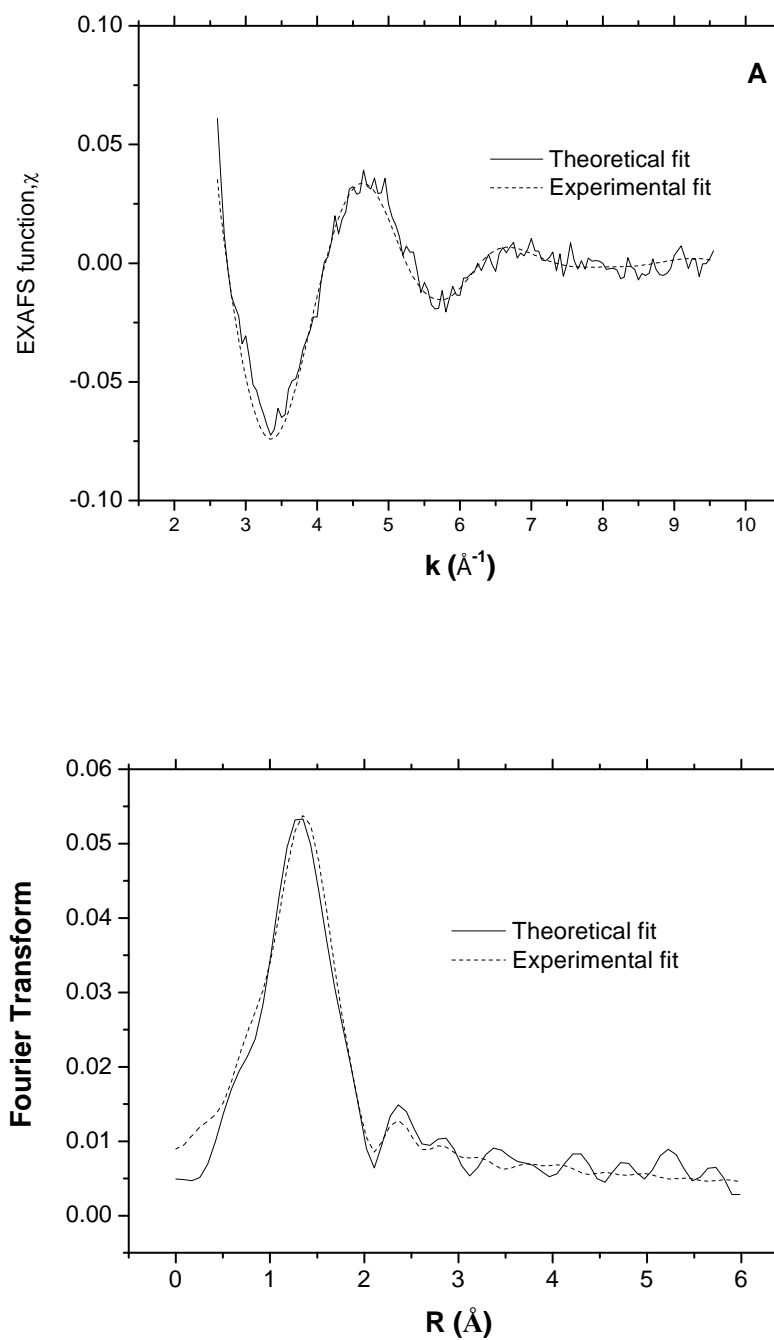


**Figure 3.4** Fourier-transform magnitude of the  $k^3$ -weighted Ti EXAFS spectrum of 10%Ti-RH-MCM-41, calculated in the  $k$  range of  $2.3$ - $9.55$   $\text{\AA}^{-1}$  (dotted line-experimental curve, solid line-theoretical curve): **A**)  $k$  space and **B**)  $R$  space.

**Table 3.2** Pre-edge and edge energy of 10%Ti-RH-MCM-41 from normalized absorption of XANES.

Materials	Pre-edge (eV)	Edge (eV)	Energy Shift
			(eV)
Ti foil	4967.9	4971.0	0
TiO <sub>2</sub> anatase	4964.6-4970.2	4975.2	+4.2
<b>10%Ti-RH-MCM-41</b>	4968.1	4977.5	+6.5

**Table 3.3** Structure parameters of the nearest coordination shell around Ti atom in 10%Ti-RH-MCM-41 with the amplitude reduction factor ( $S^2_0$ ) = 0.42.

Neighbors	N	R (Å)	$\sigma^2(\text{Å}^2)$	E <sub>0</sub> (eV)
Ti-O	1.79 ± 0.05	1.90 ± 0.09	0.0029 ± 0.00013	10.12 ± 0.08
Ti-O	1.57 ± 0.07	2.09 ± 0.06	0.0141 ± 0.00117	10.12 ± 0.08
Ti-Si	0.89 ± 0.01	2.34 ± 0.08	0.0059 ± 0.00014	10.12 ± 0.08

The nitrogen adsorption-desorption isotherms of RH-MCM-41, 10%Ti-RH-MCM-41 and 10%TiO<sub>2</sub>/RH-MCM-41 are compared in Figure 3.5A. They all gave Type-IV isotherm with three well-defined stages. The adsorption, in the first step at relative pressure around 0.0-0.2, concaved to the P/P<sub>0</sub> axis due to monolayer adsorption on external surface which were large pores. The lower adsorption volume

on 10%Ti-RH-MCM-41 and 10%TiO<sub>2</sub>/RH-MCM-41 indicated lower surface area. The adsorption at relative pressure of 0.2-0.4 was from adsorption in mesopores. The difference adsorbed volume on 10%TiO<sub>2</sub>/RH-MCM-41 from the parent RH-MCM-41 in this range indicated that some mesopores were blocked by TiO<sub>2</sub> particles.

The specific surface area and total pore volume of RH-MCM-41, 10%Ti-RH-MCM-41 and 10%TiO<sub>2</sub>/RH-MCM-41 are presented in Table 3.1. The surface area and pore size decreased with the addition of Ti or TiO<sub>2</sub> to RH-MCM-41. The mesopore volume was in the order of RH-MCM-41 > 10%Ti-RH-MCM-41 > 10%TiO<sub>2</sub>/RH-MCM-41, proportional to their hysteresis volume.

The pore size distribution in RH-MCM-41, 10%Ti-RH-MCM-41 and 10%TiO<sub>2</sub>/RH-MCM-41 are presented in Figure 3.4B showing both micropores and mesopores. The plot showed relationship between volume adsorbed and pore diameter (D) ratio in the pattern of differentiate operator (d). Large portion of mesopores were presented in all samples with diameter of 28.2, 27.4 and 24.9 Å in RH-MCM-41, 10%Ti-RH-MCM-41 and 10%TiO<sub>2</sub>/RH-MCM-41, respectively.

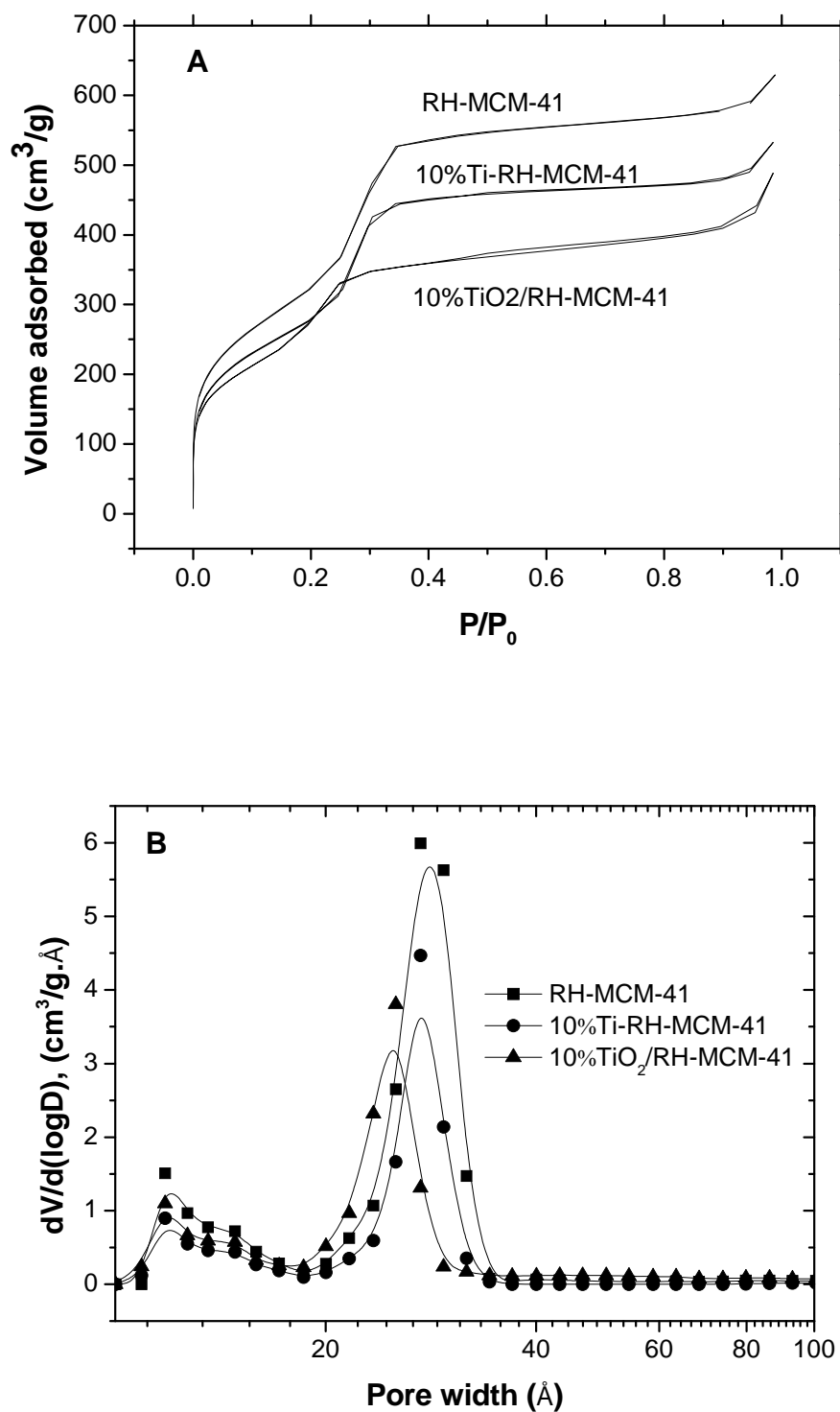


**Figure 3.5** A) N<sub>2</sub> adsorption-desorption isotherm and B) pore size distribution of RH-MCM-41 and 10%Ti-RH-MCM-41.



The FTIR spectra of RH-MCM-41 and 10%Ti-MCM-41 are shown in Figure 3.6. Both samples gave a weak peak at  $3739\text{ cm}^{-1}$  arising from isolate silanol groups. In addition, broad band at  $3600\text{-}3325\text{ cm}^{-1}$  was attributed to water and/or bonded silanol groups. The band at  $1630\text{ cm}^{-1}$  was assigned as bending mode of  $\text{H}_2\text{O}$ . The broad bands at  $1061\text{ cm}^{-1}$  with a shoulder at  $1220\text{ cm}^{-1}$  were all characteristic of  $\text{SiO}_2$  and corresponded to asymmetric and symmetric Si-O stretching and Si-O-Si bending, respectively (Romero et al., 1998). Furthermore, the band at  $980\text{ cm}^{-1}$  was observed on 10%Ti-RH-MCM-41 only which represented Si-O-Ti stretching (Balu et al., 2008). This evidence also confirmed the presence of Ti in the framework of 10%Ti-RH-MCM-41.

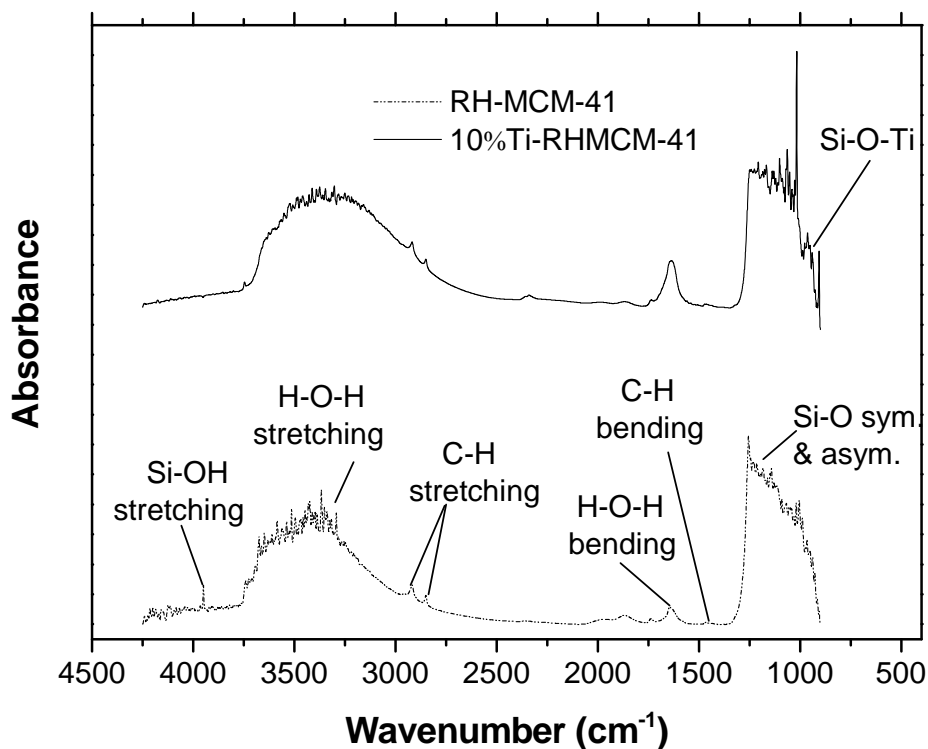
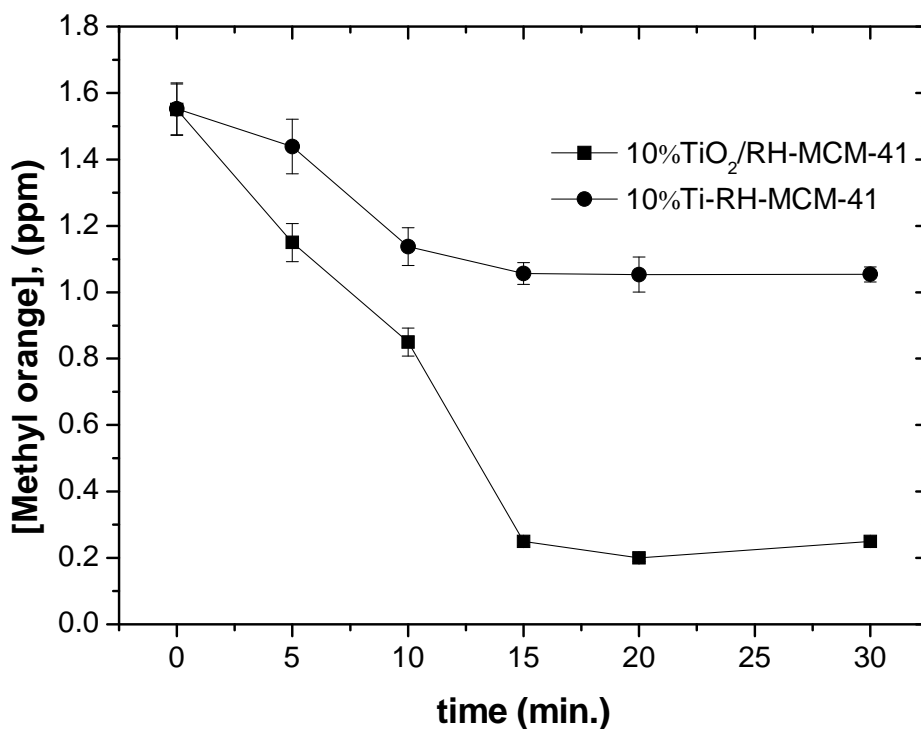


Figure 3.6 FTIR of RH-MCM-41 and Ti-MCM-41.

### **3.4.2 Photodegradation of methyl orange on 10%TiO<sub>2</sub>/RH-MCM-41 and 10%Ti-RH-MCM-41**

#### **3.4.2.1 Catalytic performance of solid catalysts**

The decreases of methyl orange concentration from photocatalytic degradation on 10%TiO<sub>2</sub>/RH-MCM-41 and 10%Ti-RH-MCM-41 are shown in Figure 3.7. The photoactivity on 10%TiO<sub>2</sub>/RH-MCM-41 was better than that on 10%Ti-RH-MCM-41 at every sampling time. The conversions of 87.10% and 32.26% were achieved after 20 min. from 10%TiO<sub>2</sub>/RH-MCM-41 and 10%Ti-RH-MCM-41, respectively. Because the XRD results indicated that the 10%TiO<sub>2</sub>/RH-MCM-41 possessed TiO<sub>2</sub> anatase in a larger extent than the 10%Ti-MCM-41. Thus, anatase phase was responsible for the photocatalytic activity because it could provide hydroxyl radicals for photooxidation of organic pollutants (Carp et al., 2004). From this point forward, only TiO<sub>2</sub>/RH-MCM-41 was studied to understand role of parameters and nature of the dye adsorption.



**Figure 3.7** Catalytic activity of 10%Ti-RH-MCM-41 and 10%Ti-MCM-41: cat = 2.5 g/L,  $C_0 = 2$  ppm, pH = 4.5,  $[H_2O_2] = 0.01$  M.

#### 3.4.2.2 Influence of added amount of catalysts

Various weights of catalyst was added to a solution containing 2.0 ppm of methyl orange to produce concentrations of 1.0, 2.5, 5.0 and 7.5 g/L for the determination of the optimum catalyst concentration. The results are shown in Figure 3.8. At the beginning, the initial concentrations were different because methyl orange adsorbed on the catalyst surface. The amount adsorbed increased with the catalyst concentration. The concentration of methyl orange in each test decreased linearly with time and became constant after 17 min. The degradation ratio increased with increasing of catalyst concentration along with reaction time until the

concentration reaches 5.0 g/L. Further increasing catalyst concentration, degradation ratio was not significantly different due to the fact that larger suspension catalysts may block UV light and sequentially decrease hydroxyl radical that acts as active species for photodegradation (Konstantinou and Albanis, 2004). Moreover, the decrease in the percentage of degradation at higher catalyst loading may due to deactivation of activated molecules by collision with ground state molecules (Neppolian et al., 2002). Thus, results suggested an optimal 5.0 g/L of 10%TiO<sub>2</sub>/RH-MCM-41 to achieve most effective degradation of methyl orange. In this study, we will use catalyst at the concentration of 5.0 g/L for further experiment.

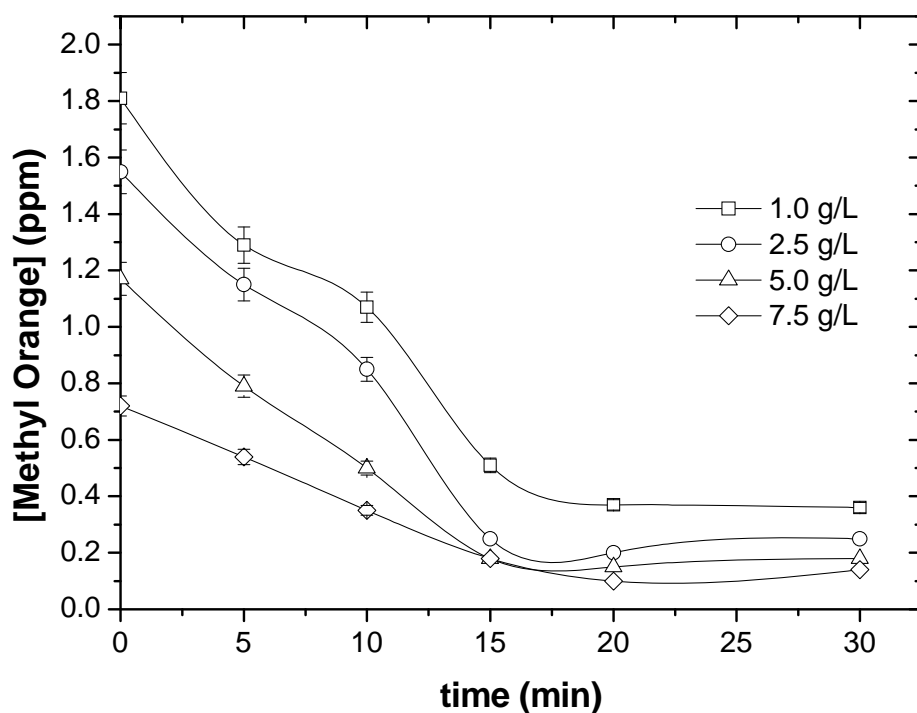


**Figure 3.8** Effect of catalyst concentration on photocatalytic degradation of methyl orange on 10%TiO<sub>2</sub>/RH-MCM-41: C<sub>0</sub> = 2 ppm, pH = 4.5, [H<sub>2</sub>O<sub>2</sub>] = 0.01 M.

### 3.4.2.3 Influence of initial concentration of methyl orange

Different initial concentrations (2, 4, 6, and 8 ppm) were used to study the influence of degradation ratio. The plot between  $C/C_0$  (Where  $C$  and  $C_0$  stand for the concentration of methyl orange at any and initial time, respectively) with time in Figure 3.9 showed that the lower initial concentration gave higher degradation efficiency. There are two reasons possible explanations. First, the certain amount of 10%TiO<sub>2</sub>/RH-MCM-41 produces certain amount of hydroxyl radical. No more hydroxyl radical, no more active species to initiate reaction. Second, higher concentration of methyl orange will adsorb and cover on the surface of catalyst cause deactivates catalyst activity (Wang et al., 2008). In the next experiment, the initial concentration of 2 ppm was used for rate law determination of reaction order because the equilibrium could be obtained in short time.

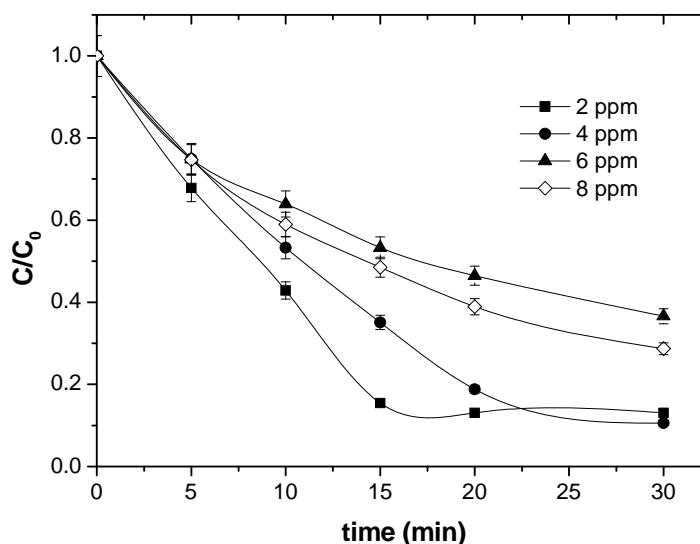


**Figure 3.9** Effect of methyl orange concentration to photocatalytic degradation on 10%TiO<sub>2</sub>/RH-MCM-41: [cat.] = 5.0 g/L,  $C_0 = 2$  ppm, pH = 4.5, [H<sub>2</sub>O<sub>2</sub>] = 0.01 M.

#### 3.4.2.4 Initial degradation rate

Rate of reaction was assumed to be proportional to concentration of reactant. The plot between  $-R_{CA}$  and  $C_A$  (Figure 3.10) demonstrated that rate of reaction increased exponentially with methyl orange concentration. At the beginning of reaction, there are a lot of active species to propagate reaction including hydroxyl radicals and adsorbed methyl orange. Thus, degradation rate of methyl orange rapidly increased. After  $\cdot\text{OH}$  was exhausted, the maintaining of methyl orange only adsorbed on the catalyst. Consequently, degradation rate decreased.

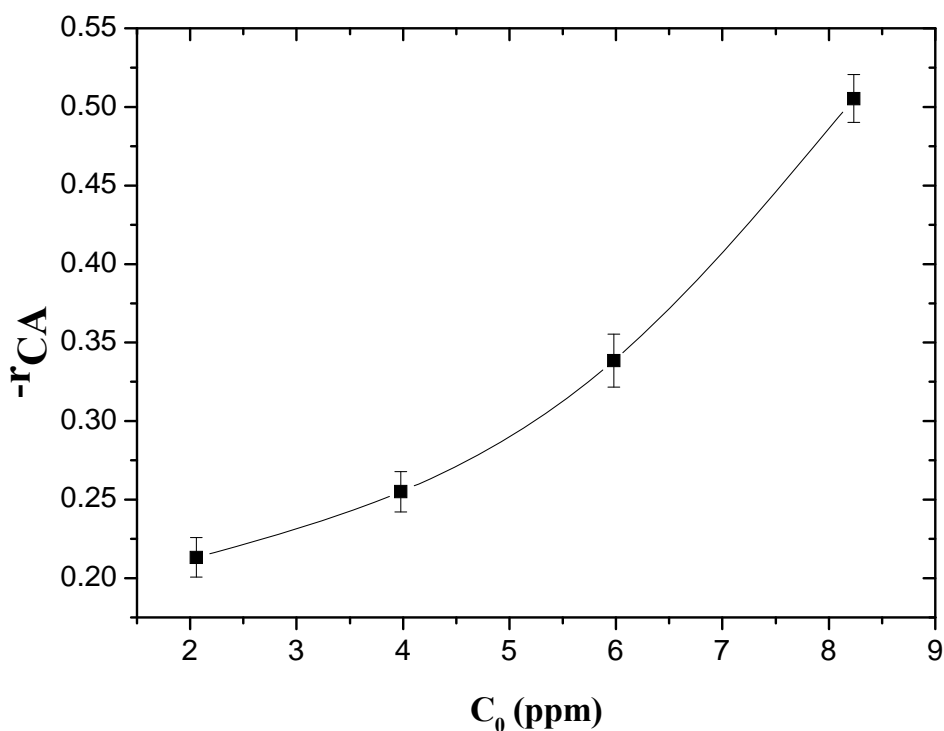


**Figure 3.10** Initial degradation rate of methyl orange degradation.

In addition, the reaction rate was determined equation (1) which showed relationship between  $\ln C_A$  and reaction time.

$$\ln(C_A) = -kt + \ln C_0 \quad \dots(1)$$

From Figure 3.11, the fit gave straight line with  $R^2 > 0.996$ . The slope of the linear relationship was rate of reaction ( $k$ ) which was  $0.17 \text{ min}^{-1}$ . This result indicated that the photocatalytic degradation methyl orange obeyed the pseudo-first order.

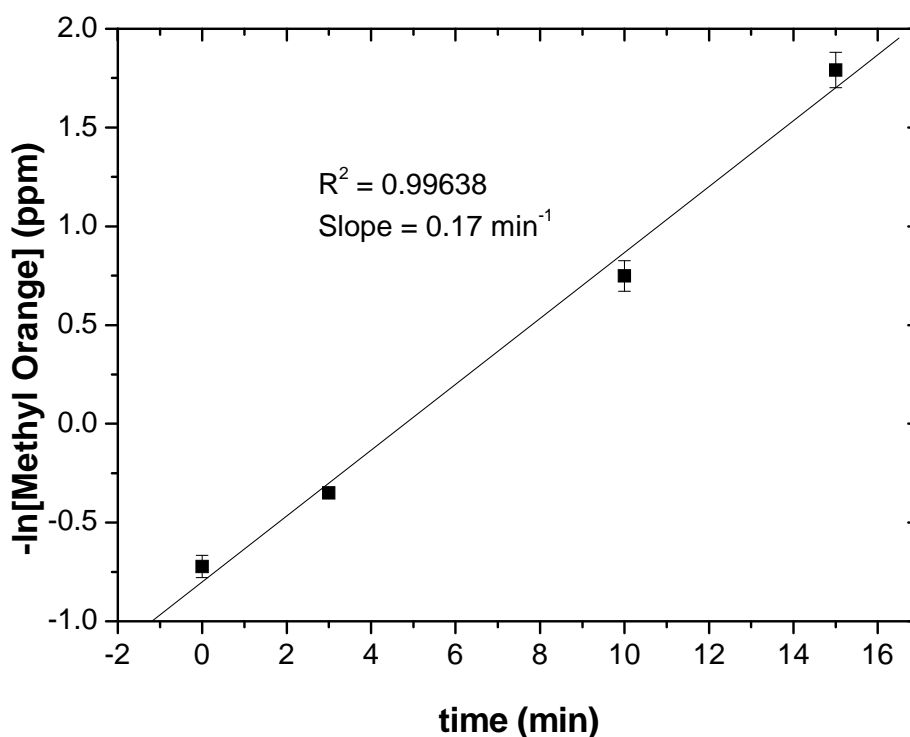


**Figure 3.11** Pseudo-first order plot of photocatalytic degradation of methyl orange on  $\text{TiO}_2/\text{RH-MCM-41}$ .

### 3.4.3 Adsorption of methyl orange on 10%TiO<sub>2</sub>/RH-MCM-41

Adsorption of methyl orange on 10%TiO<sub>2</sub>/RH-MCM-41 was studied by stirring the mixture of methyl orange and catalyst in the dark and sampling clear solution after 0.5 h and the raw data were shown in Table 3.4.

**Table 3.4** Raw data from adsorption of methyl orange on 10%TiO<sub>2</sub>/RH-MCM-41.

<b>C<sub>0</sub> (mg/L)</b>	<b>C<sub>e</sub> (mg/L)</b>	<b>q<sub>e</sub> (mg/g)</b>	<b>C<sub>e</sub>/q<sub>e</sub> (g/L)</b>	<b>log q<sub>e</sub> (mg/L)</b>	<b>log C<sub>e</sub> (mg/g)</b>
2	1.16	0.16	7.02	-0.77	0.06
4	3.03	0.19	15.66	-0.71	0.48
6	5.09	0.18	27.98	-0.74	0.70
10	9.08	0.18	49.46	-0.73	0.95

The adsorption of methyl orange on bare TiO<sub>2</sub> was previously studied and it obeyed Langmuir isotherm (Kostantinou and Albanis, 2004). However, the adsorption isotherms were elucidated by extrapolating with both Langmuir and Freundlich isotherm in this experiment. It was postulated that if simple adsorption between methyl orange was found, chemical interaction with monolayer adsorption should be noted for this reaction and isotherm could be explained by Langmuir isotherm. Nevertheless, if the interaction was more complicated with both physical and chemical interaction, multilayer adsorption could be found in spite of simple interaction and the adsorption should be obeyed Freundlich isotherm. Sequent to



obtain data, both models was plotted and described equation (3) and (4);

$$\frac{C_e}{q_e} = \frac{C_e}{q_{\max}} + \frac{1}{K_{ad} \times q_{\max}} \quad \dots(2)$$

$$\log(q_e) = \log(K) + \frac{1}{n} \log(C_e) \quad \dots(3)$$

Where:

$C_e$  = The equilibrium concentration of methyl orange in solution (mg/L)

$q_e$  = The amount of adsorbed methyl orange on the catalyst at the equilibrium concentration (mg/g)

$q_{\max}$  = The maximum adsorption amount (mg/g)

$K_{ad}$  = The apparent adsorption equilibrium concentration (mg/L)<sup>-1</sup>

$K$  = The adsorption capacity constant (mg/L)<sup>-1</sup>

$n$  = The adsorption layer of methyl orange

Equation (2) belonged to Langmuir explanation while equation (3) was for Freundlich isotherm. As shown in Figure 3.12A-B, the plot between  $C_e/q_e$  and  $C_e$  in Figure 3.12A gave a straight line demonstrating that adsorption amount of methyl orange increased with initial concentration of methyl orange. The plot fit well with Langmuir isotherm indicated that adsorption of methyl orange on 10%TiO<sub>2</sub>/RH-MCM-41 was monolayer. There was no dependent interaction with surrounding molecule. In addition, the plot gave a linear fit with  $R^2 > 0.99$ . From equation (2), the maximum adsorption amount ( $q_{\max}$ ), calculated from the slope, was 0.18 mg/g. Furthermore, the adsorption constant ( $K_{ad}$ ), calculated from  $q_{\max}$  and Y-interception, was 44.75 (mg/L)<sup>-1</sup>. The adsorption could not be described by Freundlich isotherm (equation 3) because reagent molecule of methyl orange possessed negatively charged

species which would be preferable adsorption on solid catalyst with chemical interaction so that catalyst surface was covered by monolayer of methyl orange (see Figure 12B).

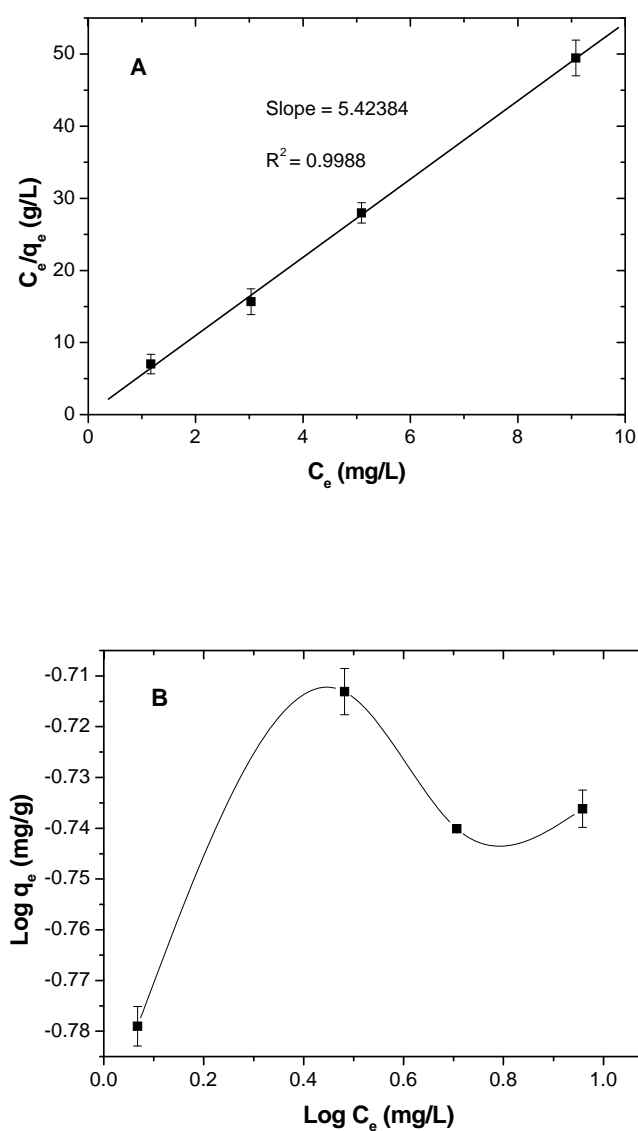


**Figure 3.12** Adsorption of methyl orange on TiO<sub>2</sub>/RH-MCM-41; cat = 5 g/L, C<sub>0</sub> = 2, 4, 6 and 10 ppm, pH = 4.5, [H<sub>2</sub>O<sub>2</sub>] = 0.01 M: **A)** Langmuir isotherm and **B)** Freundlich isotherm.

### 3.5 Conclusions

The 10%Ti-RH-MCM-41 was successfully synthesized with rice husk silica by adding TBOT into the synthetic gel while TiO<sub>2</sub>/RH-MCM-41 was successful by impregnating sol-gel TiO<sub>2</sub> on RH-MCM-41. The 10%Ti-MCM-41 had mesoporous structure and high surface area of 1006 m<sup>2</sup>/g which ensured good Ti dispersion. The Ti cations were in the form of tetrahedrally coordinated titanium (IV). TiO<sub>2</sub>/MCM-41 showed particular structure of RH-MCM-41 and TiO<sub>2</sub> anatase. TiO<sub>2</sub> did not affect the micropore structure of RH-MCM-41. 10%TiO<sub>2</sub>/RH-MCM-41 was more active for photodegradation of methyl orange than that 10%Ti-RH-MCM-41. The optimum weight to volume ratio of 10%TiO<sub>2</sub>/RH-MCM-41 to methyl orange solution was 5 g/L and the optimum concentration of methyl orange was 2.0 ppm. The photocatalytic degradation of methyl orange on TiO<sub>2</sub>/RH-MCM-41 obeyed pseudo-first order.

### 3.6 References

- Balu, A. M., Hidalgo, J. M., Campelo, J. M., Luna, D., Luque, R., Marinas, J. M., Romero, A. A. (2008). Microwave oxidation of alkenes and alcohols using highly active and stable mesoporous organotitanium silicates. **Journal of Molecular Catalysis A: Chemical**. 293(1): 17–24.
- Bhattacharyya, A., Kawi, S., Ray, M.B. (2004). Photocatalytic degradation of orange II by TiO<sub>2</sub> catalysts supported on adsorbents. **Catalysis Today**. 98(3): 431-439.
- Bordiga, S., Coluccia, S., Lamberti, C., Marchese, L., Zecchina, A., Boscherini, F., et al. (1994). XAFS study of Ti-Silicate: structure of framework Ti(IV) in the presence and absence of relative molecules (H<sub>2</sub>O, NH<sub>3</sub>) and comparison with

- ultraviolet and IR results. **Journal of Physical Chemistry**. 98(15): 4125-4132.
- Carp, O., Huisman, C. L., Reller, A. (2004). Photoinduced reactivity of titanium dioxide. **Progress in Solid State Chemistry**. 32(1): 33-177.
- Chakraverty, A., Kaleemullah, S. (1991). Conversion of rice husk into amorphous silica and combustible gas. **Energy Conversion and Management**. 32(6): 565-570.
- Khemthong, P., Prayoonpokarach, S., Wittayakun, J. (2007). Synthesis and characterization of zeolite LSX from rice husk silica, **Suranaree Journal of Science and Technology**. 14(4): 367-379.
- Kim, S., Choi, W. (2002). Kinetics and mechanisms of photocatalytic degradation of  $(\text{CH}_3)_n\text{NH}_{4-n}^+$  ( $0 \leq n \leq 4$ ) in  $\text{TiO}_2$  suspension: The role of OH radicals. **Environmental Science and Technology**. 36(9): 2019-2025.
- Kitano, M., Matsuoka, M., Ueshima, M., Anpo, M. (2007). Recent developments in titanium oxide-based photocatalysts. **Applied Catalysis A: General**. 3259(1): 1-14.
- Konstantinou, I. K., Albanis, T. A. (2004).  $\text{TiO}_2$ -assisted photocatalytic degradation of azo dyes in aqueous solution: kinetic and mechanistic investigations: A review. **Applied Catalysis B: Environmental**. 49(1): 1-14.
- Li, G., Zhao, X. S., Ray, M. B. (2007). Advanced oxidation of orange II using  $\text{TiO}_2$  supported on porous adsorbents: The role of pH,  $\text{H}_2\text{O}_2$  and  $\text{O}_3$ . **Separation and Purification Technology**. 55(1): 91-97.
- Mrak, M., Tusar, N. N., Logar, N. Z., Mali, G., Kljajic, A., Arcon, I., et al. (2006). Titanium containing microporous/mesoporous composite (Ti, Al)-Beta/MCM-41: synthesis and characterization. **Microporous Mesoporous Materials**. 95(1):

76–85.

- Neppolian, B., Choi, H.C., Sakthivel, S., Arabindoo, B., Murugesan, V. (2002). Solar light induced and TiO<sub>2</sub> assisted degradation of textile dye reactive blue 4. **Chemosphere**. 46(8): 1173-1181.
- Romero, A. A., Alba, M. D., Klinowski, J. (1998). Aluminosilicate mesoporous molecular sieve MCM-48. **Journal of Physical Chemistry B**. 102(1): 123-128.
- Schacht, P., Noreña-Franco, L., Ancheyta, J., Ramírez, S., Hernández-Pérez, I., García, L.A. (2004). Characterization of hydrothermally treated MCM-41 and Ti-MCM-41 molecular sieves. **Catalysis Today**. 98(1): 115-121.
- Shul, Y. G., OH, K. S., Yang, J. C. (1997). Effect of organic additive on the preparation of rutile TiO<sub>2</sub> by Steam Treatment. **Journal of Sol-Gel Science and Technology**. 8(1): 255-259.
- Srinivas, D., Srivastava, R., Ratnasamy, P. (2004). Transesterifications over titanosilicate molecular sieves. **Catalysis Today**. 96(3): 127-133.
- Wang, H., Nui, J., Long, X., He, Y. (2008). Sonophotocatalytic degradation of methyl orange by nano-sized Ag/TiO<sub>2</sub> particles in aqueous solutions. **Ultrasonics Sonochemistry**. 15(4): 386-392.

# CHAPTER IV

## PHOTOCATALYTIC DEGRADATION OF ALACHLOR ON TiO<sub>2</sub>/RH-MCM-41

### 4.1 Abstract

Photocatalytic degradation of alachlor, a herbicide, in water on unsupported and supported TiO<sub>2</sub> nanoparticles on mesoporous material RH-MCM-41 were studied. The RH-MCM-41 support was synthesized from rice husk silica and other reagents by hydrothermal method. The required amount of titania (TiO<sub>2</sub> P25 Degussa) to give 10-60% was mixed with RH-MCM-41 and calcined at 300 °C for 6 h. The catalytic activities of both TiO<sub>2</sub> and TiO<sub>2</sub>/RH-MCM-41 for alachlor degradation were performed under UV radiation with wavelength of 300 nm with the ratio of catalyst weight to volume of alachlor solution of 1 g/L. The reaction equilibrium was established in 30 min. in deionized water without adjusting the solution pH. The dispersion of TiO<sub>2</sub> on RH-MCM-41 improve alachlor adsorption from the bare TiO<sub>2</sub> (namely, 17% vs. 5%). The photocatalytic activity of alachlor degradation on all TiO<sub>2</sub>/RH-MCM-41s was higher than that on the bare TiO<sub>2</sub>. By comparison per weight of TiO<sub>2</sub>, the 10%TiO<sub>2</sub>/RH-MCM-41 gave the highest alachlor conversion of 100% after 20 minute while 1% bare TiO<sub>2</sub> showed conversion of 95%.

## 4.2 Introduction

Alachlor is one of variety of herbicides. Its full name is 2-chloro-2', 6'-diethyl-N-(methoxymethyl) acetanilide and the chemical structure is shown in Figure 4.1.

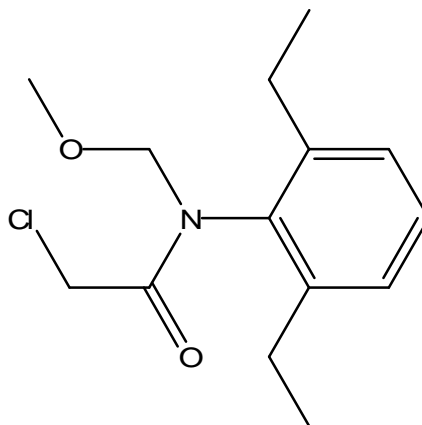


**Figure 4.1** chemical structure of alachlor

Usually, alachlor is used in agricultural lands and can contaminate water and raise various problems including carcinogenesis, neurotoxicity and effect on reproduction and cell development (Burrows et al., 2002). Because alachlor is stable-to-natural decomposition, its degradation either by conventional, biological or physical method is not effective (Bhattacharyya et al., 2004; Li et al., 2007). A recent method to decompose alachlor is by advanced oxidation processes (AOPs) which involve the generation of reactive species such as hydroxyl radical ( $\text{HO}^\bullet$ ) to break down organic compounds (Konstantinou and Albanis, 2004). Titania ( $\text{TiO}_2$ ) is a photocatalyst that can generate the  $\text{HO}^\bullet$  for such purpose but the use of  $\text{TiO}_2$  is limited by structure and morphological aspects, for example, the bare  $\text{TiO}_2$  can be deactivated by electron-hole recombination (Carp et al., 2004). Recent researches have been concerning on both degradation and adsorption of alachlor on many solid catalysts.

For example, Wong and Chu (2003) investigated photocatalytic degradation of alachlor by bare suspension of  $\text{TiO}_2$  with hydrogen peroxide ( $\text{H}_2\text{O}_2$ ). They showed the effect of UV light power, suitable dose of  $\text{H}_2\text{O}_2$  for reaction and product distribution. Adsorption of alachlor on montmorillonite and modified montmorillonite by cationic surfactant were also investigated by Sanchez-Martin et al. (2006). The results showed that octadecyltrimethylammonium bromide supported montmorillonite had a higher adsorptive activity than that of montmorillonite. The adsorptive isotherms were fit well with Freundlich model. Because kinetics and adsorption of alachlor on mesoporous materials were rarely concerned, this study investigated an improvement in catalytic activity of commercial nanoparticles  $\text{TiO}_2$  by dispersing them on RH-MCM-41 of which the surface composed of hydroxyl groups. Hole-electron recombination could be suppressed and active species could be easily transferred to degrade pollutants. This study aimed to use  $\text{TiO}_2/\text{RH-MCM-41}$  which was prepared differently from the previous chapter for photocatalytic degradation of alachlor. Factors that affect the reaction including  $\text{TiO}_2$  loading, catalyst concentration, alachlor concentration and solution pH were also investigated. Adsorption and kinetics were also studied in this research.

## **4.3 Experimental**

### **4.3.1 Chemicals and materials**

Chemicals for  $\text{TiO}_2/\text{RH-MCM-41}$  preparation were RH-MCM-41 which was prepared from the previous chapter, titanium dioxide ( $\text{TiO}_2$  Degussa P25) and deionized water.

Chemicals for photodegradation of alachlor on  $\text{TiO}_2/\text{RH-MCM-41}$  were



RH-MCM-41, TiO<sub>2</sub>/RH-MCM-41, TiO<sub>2</sub> Degussa P25 (Aldrich), CH<sub>3</sub>CN (Aldrich), HCl (S.P.C. GR Reagent, Japan), and LiOH (S.P.C. GR Reagent, Japan), alachlor (Aldrich) and deionized water.

#### **4.3.2 Apparatus and instruments**

Apparatus and equipments for TiO<sub>2</sub>/RH-MCM-41 preparation included graduated cylinder, erlenmeyer flask, magnetic stirrer, suction funnel, furnace and micropipette.

Apparatus and equipments for photodegradation of alachlor on TiO<sub>2</sub>/RH-MCM-41 included glassware, magnetic stirrer, balancer, sonicator, pyrex reactor, pH meter, Xe-arc lamp (300 W, Oriel), timer, micropipette, PTFE filters (Millipore), syringe and high performance liquid chromatograph (HPLC: Agilent 1100 series).

#### **4.3.3 Preparation of TiO<sub>2</sub>/RH-MCM-41**

RH-MCM-41 synthetic method was similar to the explanation in the previous chapter excepting for aging time, 24 h. TiO<sub>2</sub>/RH-MCM-41, prepared by sol-gel method from the previous chapter was also used to prepare activity with nanoparticles TiO<sub>2</sub>/RH-MCM-41. The nanoparticles TiO<sub>2</sub>/RH-MCM-41 was prepared by slurring a desired amount of TiO<sub>2</sub> Degussa P25 and RH-MCM-41. A desired amount of TiO<sub>2</sub> was added to slurry of RH-MCM-41 in deionized water under continuous stirring for 2 h. The mixture was washed several times with de-ionized water to remove Na<sup>+</sup> ions, dried and calcined at 300 °C for 6 h. The prepared nanoparticles TiO<sub>2</sub>/RH-MCM-41 catalysts contained 10, 20, 40 and 60% of TiO<sub>2</sub>. All

prepared catalysts were characterized by X-Ray diffraction spectrometry (XRD), Nitrogen adsorption-desorption, Scanning electron microscopy (SEM), Diffuse reflectance UV spectroscopy (DR-UV) and zeta potential analysis and further used to test adsorption of alachlor and photoactivity of alachlor degradation.

#### 4.3.4 Catalyst characterization

The crystalline phase of bare TiO<sub>2</sub>, RH-MCM-41 and TiO<sub>2</sub>/RH-MCM-41 were analyzed using powder X-ray diffraction (XRD: Rigaku Model D/Max III and Bruker axs D5005 diffractometer) with CuK<sub>α</sub> radiation. The X-ray was generated with a current of 40 mA and a potential of 40 kV. The catalyst powder (0.20 g) was pressed in a sample holder and scanned from 1.5 to 80 degrees (2θ) in steps of 0.05 degrees per min by Bruker axs D5005 diffractometer. The XRD patterns of anatase and rutile TiO<sub>2</sub> was scanned from 10-80 degrees (2θ) in steps of 0.05 degrees per min by Rigaku Model D/Max III. The powder patterns of the samples were recorded at the same day and with the same amount of material, so that the intensity of the peak height (100) could be compared.

Physical characteristics of the sample are determined by N<sub>2</sub> adsorption-desorption isotherm at -196 °C for relative pressure from 10<sup>-2</sup> to 0.99 on a microporemetrics analyzer (ASAP 2010 V4.00 H). Before measurement, sample was degassed with heat at 300 °C for 3 h. The BET surface area was obtained from the N<sub>2</sub> adsorption data in the relative pressure range of 0.02-0.2. The pore size and pore volumes were calculated from the desorption branches using Barrett-Joyner-Halenda (BJH) method.

The UV absorption spectra of bare  $\text{TiO}_2$  and  $\text{TiO}_2/\text{RH-MCM-41}$  powders were recorded using a Shimadzu UV–Vis spectrophotometer equipped with a diffuse reflectance attachment (Shimadzu ISR-2200). All sample powders were diluted with  $\text{BaSO}_4$  ( $\text{TiO}_2:\text{BaSO}_4 = 1:17$ ) and referenced to  $\text{BaSO}_4$ .

In order to understand electric potential in the interfacial double layer at the location of the slipping plane versus a point in the bulk fluid away from the interface of bare  $\text{TiO}_2$ , RH-MCM-41 and  $\text{TiO}_2/\text{RH-MCM-41}$ , the electrokinetic potential or zeta potential in colloidal systems of these materials was measured. In the procedure, the electrophoretic mobilities of bare  $\text{TiO}_2$ , RH-MCM-41 and  $\text{TiO}_2/\text{RH-MCM-41}$  particles were suspended in water with the concentration of 0.5 g/L and their zeta potentials as a function of pH were determined by using an electrophoretic light scattering spectrophotometer (ELS 8000, Otsuka) equipped with a He–Ne laser and a thermostatted flat board cell.

Morphologies of bare  $\text{TiO}_2$ , RH-MCM-41 and  $\text{TiO}_2/\text{RH-MCM-41}$  powders investigated with a high-resolution transmission electron micrographs (HRTEM) using a JEM-2100F microscope with Cs-corrected. Specimens for TEM studies were dispersed in absolute ethanol, sonicated to disperse particles and deposited on a carbon-only grid and dried in the air.

#### **4.3.5 Photocatalytic degradation ofalachlor**

All experiments were carried out in a pyrex reactor (33 mL) with a quartz window. The catalyst powder was well suspended at 1.0 g/L in 30 mlalachlor (100  $\mu\text{M}$ ) by sonicating for 30 s. The initial pH ( $\text{pH}_i$ ) of the suspension was adjusted with  $\text{HNO}_3$  or  $\text{LiOH}$  standard solutions. A Xe-arc lamp (300 W, Oriel) was used as

the illumination. Sample aliquots of 1 mL were collected at appropriate time intervals and filtered through 0.45- $\mu\text{m}$  PTFE filters (Millipore). Alachlor and its mineralized products were analyzed by High performance liquid chromatograph (HPLC: Agilent 1100 series) equipped with a diode array to determine alachlor adsorption. In order to compare activity between  $\text{TiO}_2/\text{RH-MCM-41}$  which prepared by sol-gel method from the previous chapter and nanoparticles  $\text{TiO}_2/\text{RH-MCM-41}$ , both were used to test photoactivity with alachlor with the same conditions. The better catalyst was used further in the rest of the chapter.

Effect of loading  $\text{TiO}_2$  on RH-MCM-41 was studied by varying  $\text{TiO}_2$  loading from 10 to 60 wt% as well as comparing with bare  $\text{TiO}_2$ . The synergistic effect of RH-MCM-41 support was performed and the catalytic activities in the dark and under UV irradiation were also compared. The catalytic performance of  $\text{TiO}_2/\text{RH-MCM-41}$  was studied at various concentrations of alachlor in the range of 70-100  $\mu\text{M}$ . In addition, the reaction rate was monitored with the decrease of alachlor concentration. Then reaction order was obtained from the plot between time and alachlor concentration. Finally, pH influencing reaction was carried out in the range of 2 to 8. The results were shown in the relationship between pH versus conversion and reaction rate.

#### **4.3.6 Adsorption isotherm of alachlor**

Adsorption isotherm of alachlor was determined by mixing each catalyst powder in 30 mL alachlor (70-100  $\mu\text{M}$ ) at weight per volume ratio of 1 g/L. The solution pH was adjusted to 4 by  $\text{HNO}_3$  and  $\text{LiOH}$  standard solutions before the mixture was sonicated for 30 s and stirred in the dark for 30 min. Sample aliquots of 1

mL were collected at appropriate time intervals, filtered through 0.45- $\mu\text{m}$  PTFE filters and analyzed by a high performance liquid chromatograph.

## 4.4 Results and Discussion

### 4.4.1 Characterization of catalysts by XRD

XRD patterns of RH-MCM-41 and  $\text{TiO}_2/\text{RH-MCM-41}$  are shown in Figure 4.2A. There are three MCM-41 characteristic peaks at 2.32, 4.05 and 4.69 degree, respectively. The diffraction pattern of the  $\text{TiO}_2/\text{RH-MCM-41}$  indicated the possession of an ordered structure of hexagonal pore array similar to that of RH-MCM-41 (Schacht et al., 2004). After  $\text{TiO}_2$  particles were dispersed on RH-MCM-41, peak intensities of all planes of the support decreased. This may be explained by reasoning: either a part of the pore structure is blocked with  $\text{TiO}_2$ , which can also be seen from the decrease of the BET surface area and the pore size (Sun et al., 2005) or the loss of scattering contrast between pore and wall, because the porosity of the material was preserved (Narkhede et al., 2008). Figure 4.2B shows XRD patterns of the bare and supported  $\text{TiO}_2$  on RH-MCM-41. The bare  $\text{TiO}_2$  particles which were used as purchased composed of anatase and rutile phases with 80:20 ratio. After dispersing on the support, characteristic peaks of anatase and rutile were still observed in all samples. The peak intensities decreased when the loading of  $\text{TiO}_2$  decreased. From the area ratio between anatase and rutile, there was no phase transformation of  $\text{TiO}_2$  because all the catalysts were calcined at 300  $^\circ\text{C}$ , lower than 625  $^\circ\text{C}$  at which the phase transformation occurs (Vohra et al., 2005).

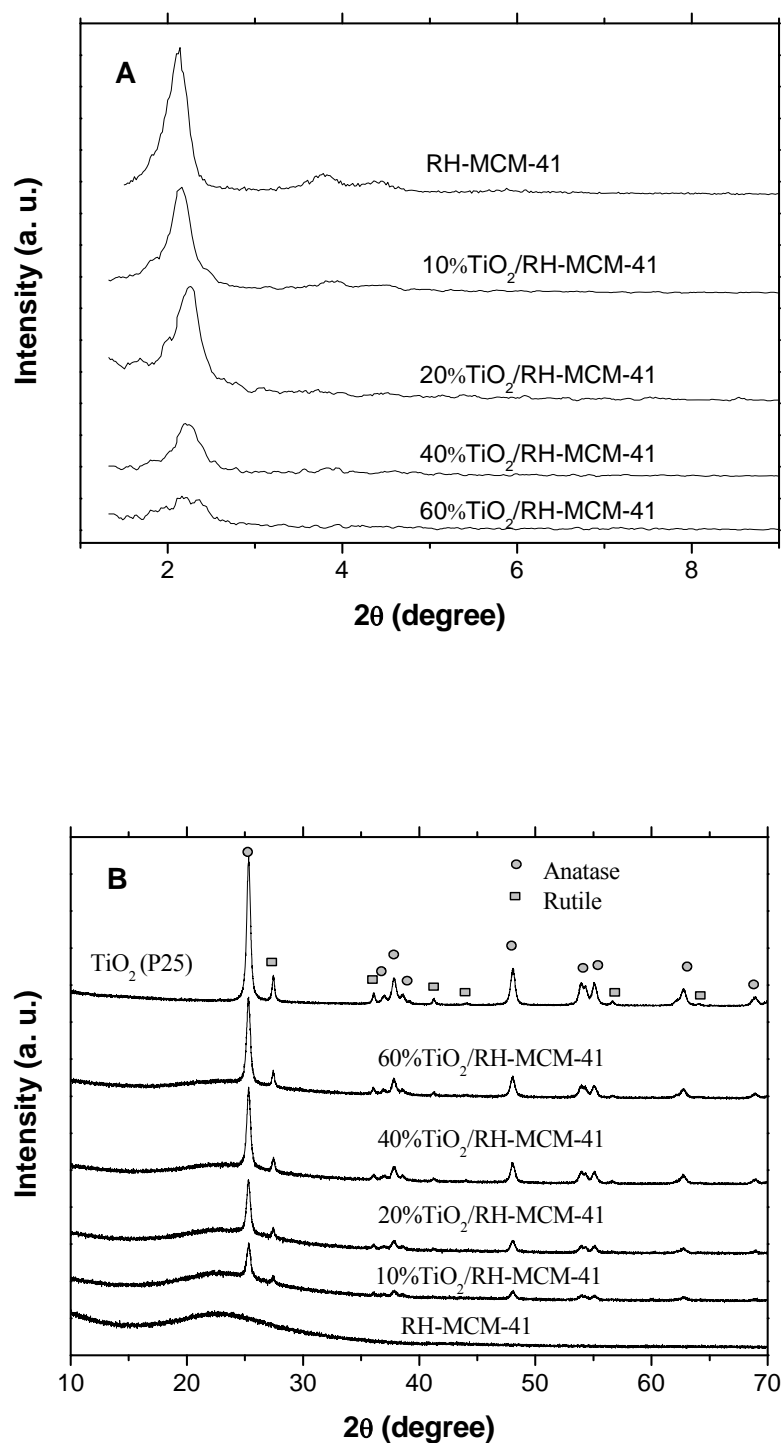


**Figure 4.2** XRD spectra; A) characteristic peaks of RH-MCM-41 and B) characteristic peaks of anatase and rutile phase of TiO<sub>2</sub>.

#### 4.4.2 Characterization by Nitrogen adsorption-desorption

The nitrogen adsorption-desorption isotherms of RH-MCM-41, TiO<sub>2</sub>/RH-MCM-41 samples and bare TiO<sub>2</sub> are shown in Figure 4.3A-B. The isotherms (Figure 4.3A) of RH-MCM-41 and TiO<sub>2</sub>/RH-MCM-41 corresponded to a mixture of type IV and type I which are typical isotherms of mesoporous materials. The adsorption at low relative pressure ( $P/P_0 < 0.2$ ) increased quickly due to monolayer adsorption on external surface. The lower adsorption volume on TiO<sub>2</sub>/RH-MCM-41 indicated lower surface areas. The N<sub>2</sub> adsorption increased again before reaching a nearly constant volume. At the relative pressure range of 0.2-0.4 corresponded to nitrogen adsorption in the mesopores. As the TiO<sub>2</sub> loading increased, the adsorption in this range decreased indicating the blocking of mesopores by the TiO<sub>2</sub> particles. For the bare TiO<sub>2</sub>, the adsorption was low at all pressure range indicating that it had low surface area. The specific surface areas and pore diameters of all catalysts were shown in Table 4.1. The surface area of TiO<sub>2</sub>/RH-MCM-41 decreased with the amount of TiO<sub>2</sub> loading indicated that TiO<sub>2</sub> covered outer surface area of RH-MCM-41. However, all catalysts still possessed significantly higher surface areas than the bare TiO<sub>2</sub> implied that the TiO<sub>2</sub> particles were well dispersed on RH-MCM-41. The dispersion could prevent agglomeration of particles that could suppress catalytic activity. In addition, pore diameter of all TiO<sub>2</sub>/RH-MCM-41s calculated from BJH equation (Brunauer et al., 1938), were in the same range of 25-35 Å (Figure 4.3B) implying that most of them only dispersed on the outer surface of RH-MCM-41. The TiO<sub>2</sub> particles also blocked some mesopores as indicated in the N<sub>2</sub>-isotherm mentioned earlier.

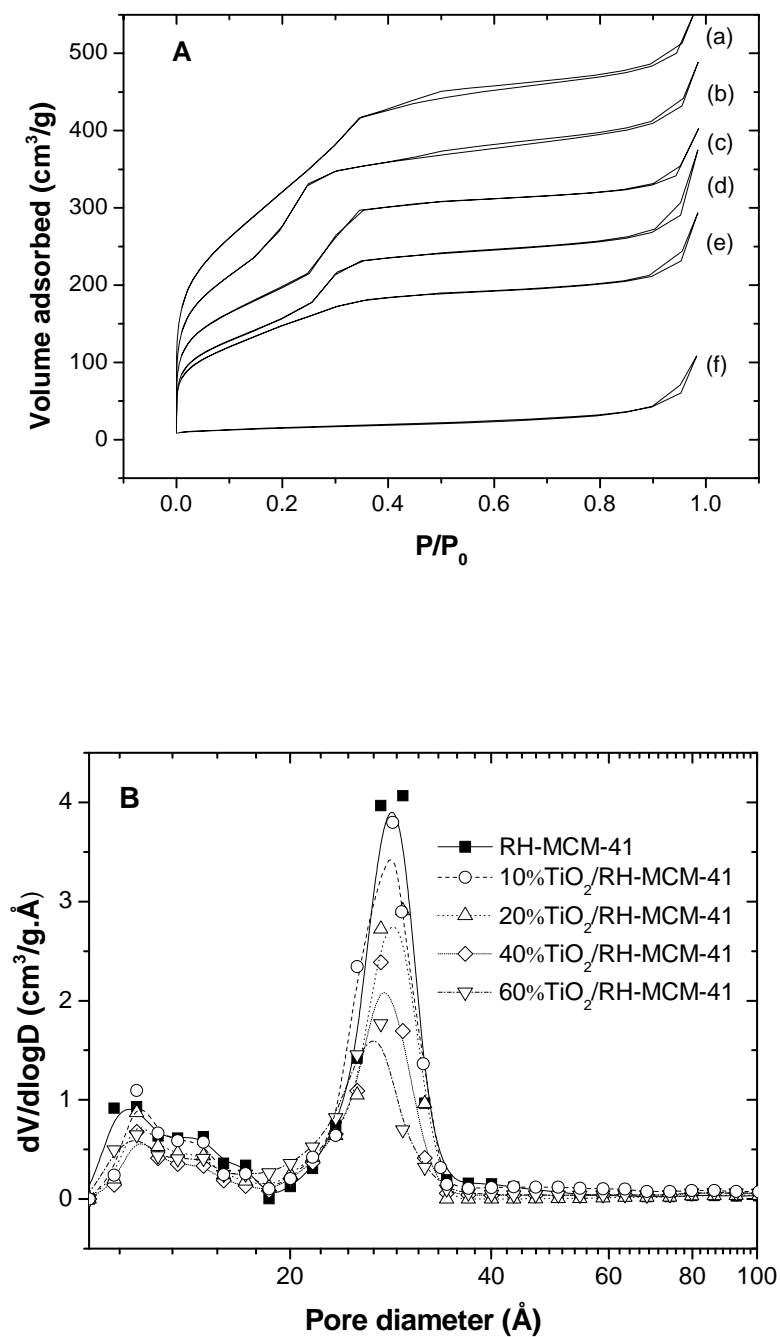


**Figure 4.3** A) N<sub>2</sub> adsorption-desorption isotherm; a) RH-MCM-41, b) 10%TiO<sub>2</sub>/RH-MCM-41, c) 20%TiO<sub>2</sub>/RH-MCM-41, d) 40%TiO<sub>2</sub>/RH-MCM-41, e) 60%TiO<sub>2</sub>/RH-MCM-41 and f) bare TiO<sub>2</sub>. B) Mesopore size distribution of RH-MCM-41 and 10%TiO<sub>2</sub>/RH-MCM-41.



These results agreed well with the results from alachlor adsorption that the volume adsorbed on TiO<sub>2</sub>/RH-MCM-41 was greater than that of bare TiO<sub>2</sub>. Because the catalytic activity depends strongly on surface area, the TiO<sub>2</sub>/RH-MCM-41 catalysts were expected to be more active than the bare TiO<sub>2</sub>.

**Table 4.1** BET surface area and average mesopore diameters of TiO<sub>2</sub>, RH-MCM-41 and TiO<sub>2</sub>/RH-MCM-41 at STP

Materials	S <sub>BET</sub> (m <sup>2</sup> /g)	Mean pore diameter (Å)	Crystallize size of TiO <sub>2</sub> (nm)
TiO <sub>2</sub> (P25)	53 ± 0.4	-	32.3
RH-MCM-41	943 ± 30	28.59 ± 0.03	-
10% TiO <sub>2</sub> /RH-MCM-41	760 ± 25	28.45 ± 0.03	37.1
20% TiO <sub>2</sub> /RH-MCM-41	729 ± 6	28.31 ± 0.02	46.0
40% TiO <sub>2</sub> /RH-MCM-41	623 ± 8	27.63 ± 0.02	63.3
60% TiO <sub>2</sub> /RH-MCM-41	590 ± 6	26.68 ± 0.01	101.2

#### 4.4.3 Characterization by TEM

The TEM morphologies of RH-MCM-41, bare TiO<sub>2</sub> and 10%TiO<sub>2</sub>/RH-MCM-41 are displayed in Figure 4.4A-D. The micrograph of RH-MCM-41 in Figure 4.4A confirmed the highly ordered hexagonal arrays and one-dimensional mesoporous parallel channels. Figure 4.4B showed nanoparticles of the bare TiO<sub>2</sub> (P25) with particle sizes in the 15-30 nm range. The particle sizes of TiO<sub>2</sub> on RH-MCM-41 were similar to those of bare TiO<sub>2</sub>. The image of TiO<sub>2</sub> nanoparticles

dispersed on RH-MCM-41 support is clearly seen in the high-resolution TEM image (Figure 4.4D).

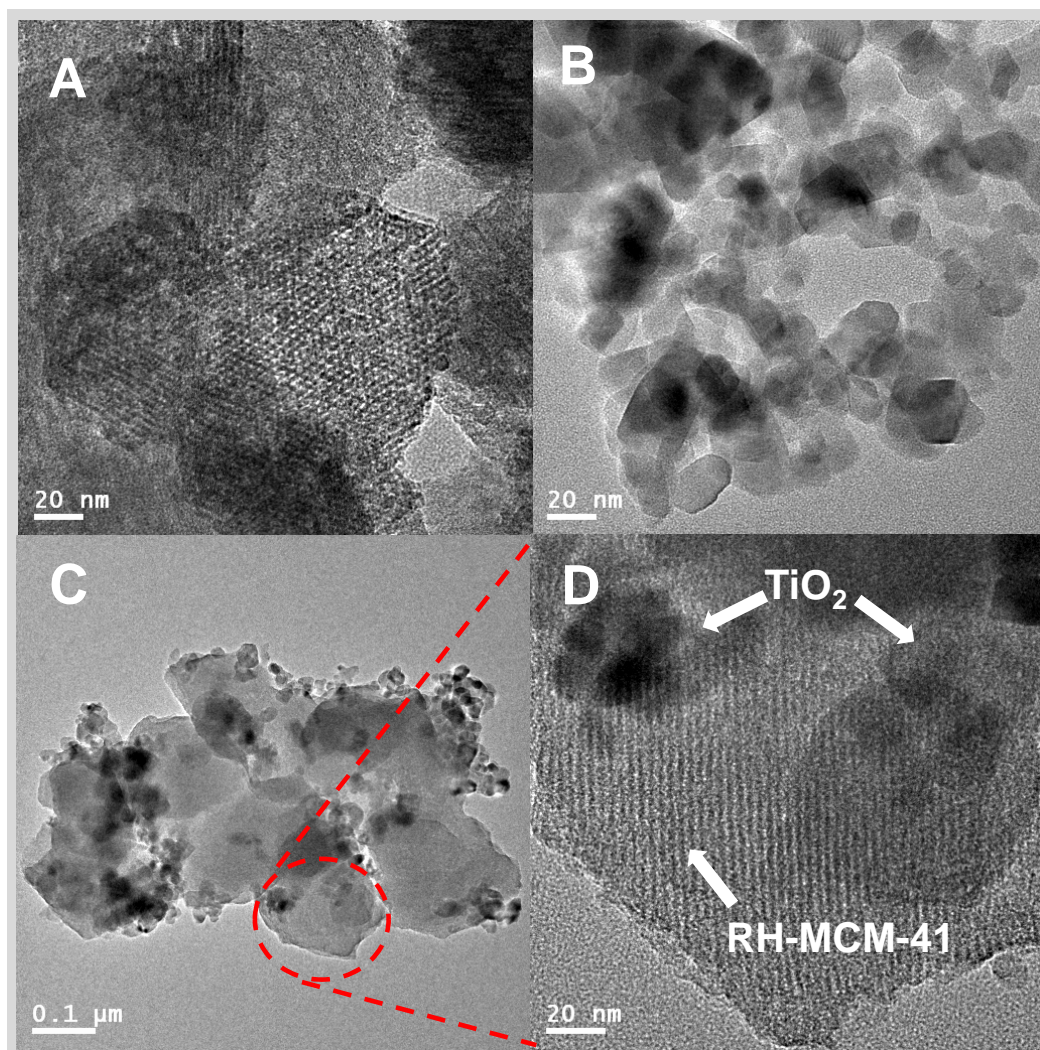


**Figure 4.4** High-resolution TEM images of RH-MCM-41,  $\text{TiO}_2$  and 10% $\text{TiO}_2$ /RH-MCM-41; A) Hexagonal structure of RH-MCM-41 (100k), B) unsupported bare  $\text{TiO}_2$  nanoparticles (25k), C) and D)  $\text{TiO}_2$  particles on RH-MCM-41 (25k).

#### 4.4.4 Characterization by DR-UV

The effect of RH-MCM-41 to UV light adsorption of alachlor of bare  $\text{TiO}_2$  was shown in Figure 4.5. In general, it was expected that modification of  $\text{TiO}_2$  would reduce its band gap energy, less than 3.2 eV. If this phenomenon occurred, electrons in valence band would be easily excited to conduction band and the hydroxyl radicals ( $\text{HO}^\bullet$ ) could be easily produced for photocatalytic degradation.

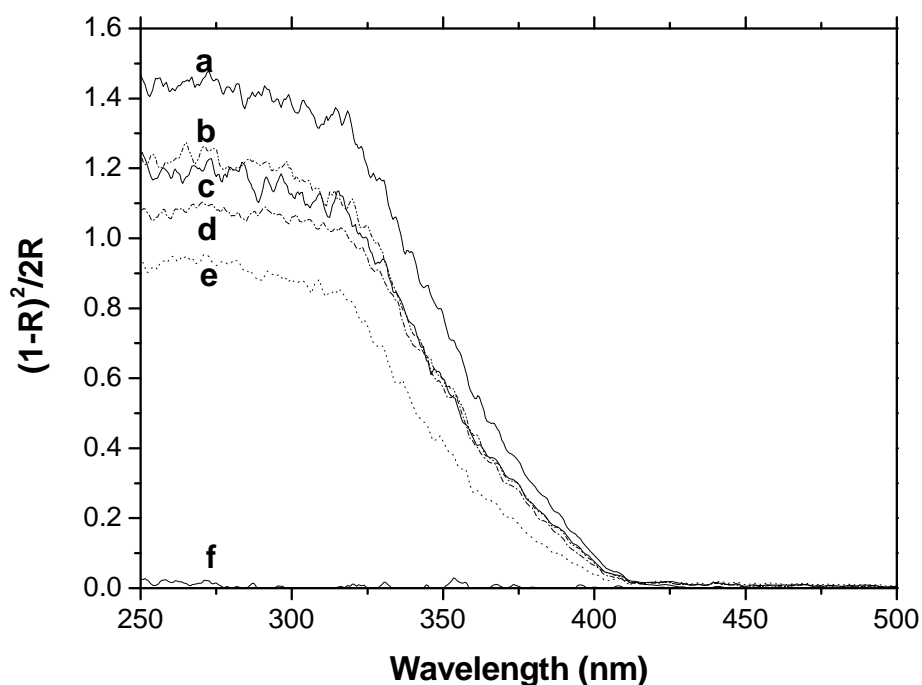


**Figure 4.5** UV-visible diffuse reflectance spectra of a)  $\text{TiO}_2$ , b) 60% $\text{TiO}_2$ /RH-MCM-41, c) 40% $\text{TiO}_2$ /RH-MCM-41, d) 20% $\text{TiO}_2$ /RH-MCM-41, e) 10% $\text{TiO}_2$ /RH-MCM-41, and f) RH-MCM-41.

Figure 4.5 shows UV-visible diffuse reflectance spectra of bare  $\text{TiO}_2$  supported  $\text{TiO}_2$  on RH-MCM-41. The results from DR-UV did not show any change

of absorption edge in the diffuse reflectance of UV spectra of TiO<sub>2</sub>/RH-MCM-41. The absorption of all catalysts depended on the amount of TiO<sub>2</sub>. RH-MCM-41 did not absorb the irradiation or enhance the absorption of the bare TiO<sub>2</sub> indicating that band gap of bare TiO<sub>2</sub> did not change after dispersion on RH-MCM-41. When comparing the absorption of 40%RH-MCM-41 and 60%RH-MCM-41, the intensities were almost the same implying that the 60 wt% loading was too much to provide a good dispersion on RH-MCM-41. The particle at this loading agglomerated and active surface decreased. Thus, the TiO<sub>2</sub> loadings of 40 wt% or less were suitable to produce good dispersions on RH-MCM-41 and the photodegradation of alachlor was expected to be improved from that on the bare TiO<sub>2</sub>.

#### 4.4.5 Characterization by zeta potential analysis

The zeta potential of RH-MCM-41, 10%TiO<sub>2</sub>/RH-MCM-41, 40%TiO<sub>2</sub>/RH-MCM-41, 60%TiO<sub>2</sub>/RH-MCM-41 and bare TiO<sub>2</sub> at 2.00, 2.90, 3.23, 4.10 and 6.08 mV, respectively, are shown in Figure 4.6. This indicated that positively charged surface increased in order of bare TiO<sub>2</sub> > TiO<sub>2</sub>/RH-MCM-41 > RH-MCM-41. From the result, TiO<sub>2</sub> was expected to dominate in charge interaction to positive ion because the increase of TiO<sub>2</sub> loading also increased pHPZC of TiO<sub>2</sub>/RH-MCM-41 and induced greater negative charge on surface of TiO<sub>2</sub>/RH-MCM-41. From these results, it could be concluded that the surfaces of 10%TiO<sub>2</sub>/RH-MCM-41s were more negatively charged and preferable to adsorb positive ion than the bare TiO<sub>2</sub> at pH greater than 3. On the other hand, adsorption of negative ion should be preferable in the pH less than 3. In case of alachlor, adsorption on solid catalysts is more preferable when solution pH approach pHPZC because it is neutral molecule.

Consequently, degradation should be preferred at pH in the range of 3-4 for 10%TiO<sub>2</sub>/RH-MCM-41.

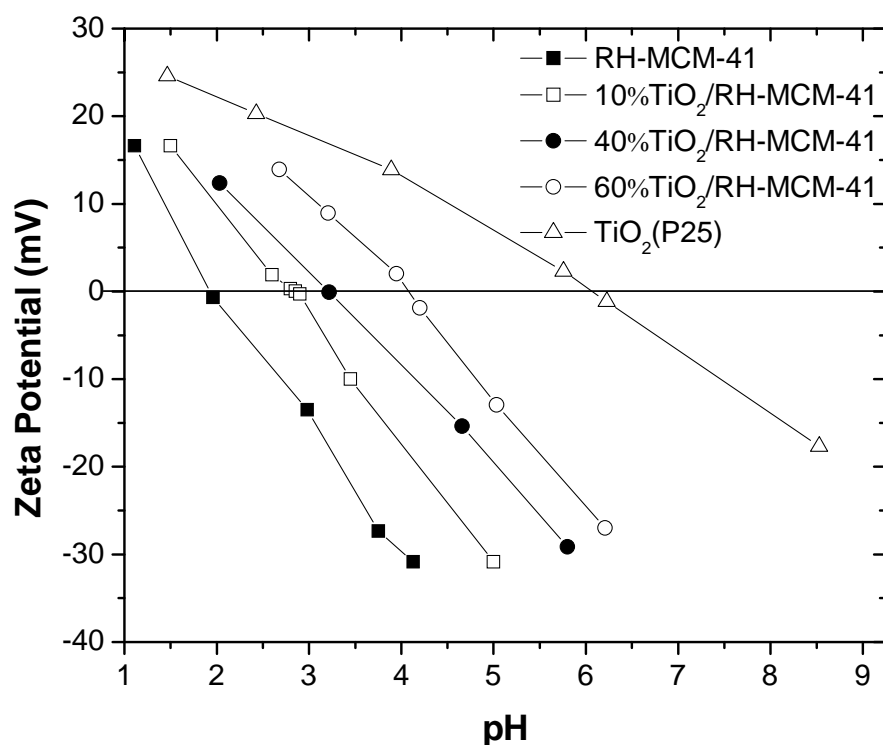


**Figure 4.6** Zeta potential of RH-MCM-41, TiO<sub>2</sub>/RH-MCM-41 and TiO<sub>2</sub> suspended in water as a function of pH.

#### 4.4.6 Photodegradation of alachlor on bare TiO<sub>2</sub> and TiO<sub>2</sub>/RH-MCM-41

##### 4.4.6.1 Effect of TiO<sub>2</sub> loading on RH-MCM-41 to photodegradation

In order to obtain the optimal amount of TiO<sub>2</sub> added on RH-MCM-41, various amounts of TiO<sub>2</sub>, 10, 20, 40 and 60 wt%, were used. Their performances for photodegradation (in Figure 4.7) showed that the degradation rate was not different significantly with different TiO<sub>2</sub> loading. All catalysts showed 100% conversion of alachlor around 15-20 min. when compared the ratio of conversion to

amount of  $\text{TiO}_2$  loading, 10 wt% was worth to use. Thus, results suggested an optimal 10% $\text{TiO}_2$ /RH-MCM-41 to achieve most effective degradation of alachlor.

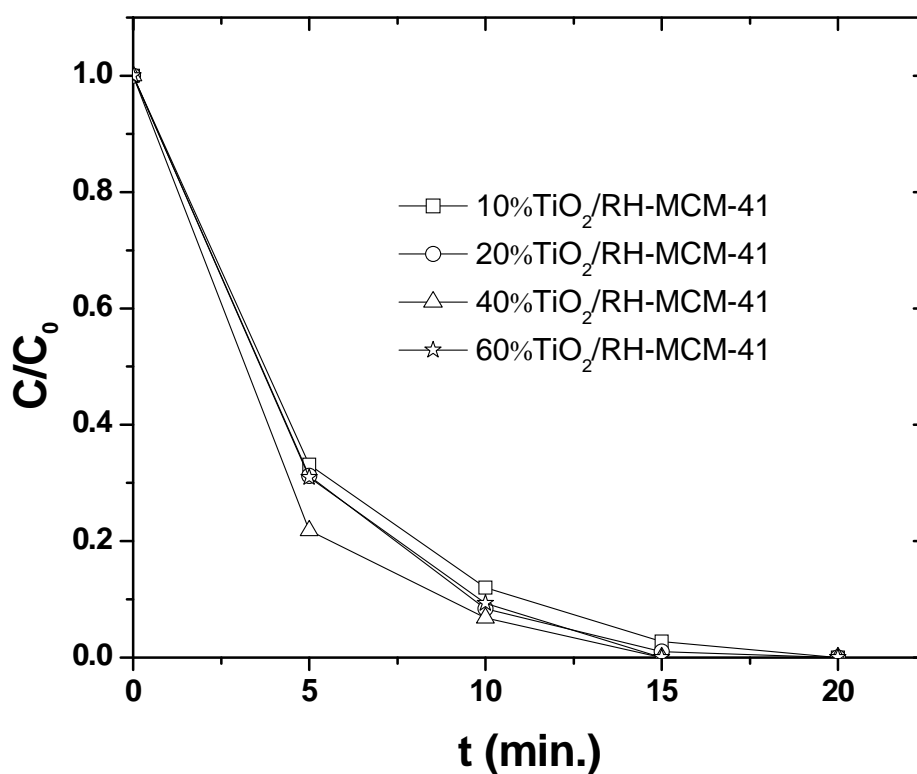


**Figure 4.7** Photocatalytic degradation of alachlor on various  $\text{TiO}_2$ /RH-MCM-41s;

$[\text{TiO}_2/\text{RH-MCM-41}] = 1 \text{ g/L}$ ,  $\text{pH} = 4$ ,  $[\text{alachlor}] = 80 \text{ }\mu\text{M}$ , UV light = 300 nm.

#### 4.4.6.2 Comparison on catalytic activity of catalysts

Photoactivity of  $\text{TiO}_2$  and  $\text{TiO}_2$ /RH-MCM-41 with various loadings are displayed in Figure 4.8. It was found that the irradiation of UV light to alachlor without catalyst exhibited small change of alachlor concentration. The conversion of alachlor on this condition was 12.58% after 30 min. Contrary,  $\text{TiO}_2$  and

TiO<sub>2</sub>/RH-MCM-41 prepared by sol-gel method showed moderate activity. The conversions of 53.21 and 76.26% were obtained on TiO<sub>2</sub> (sol-gel) and TiO<sub>2</sub>/RH-MCM-41 (sol-gel) after 30 min., respectively. In cases of nanoparticles TiO<sub>2</sub> (P25) and TiO<sub>2</sub>/RH-MCM-41 (Dispersion of TiO<sub>2</sub> (P25) on RH-MCM-41), greatest degradations were showed where 100% conversion of alachlor after 20 min on both catalysts. The reason to support would be mentioned that both later catalysts compost of proper ratio of anatase to rutile (80:20) and this ratio is more active than pure anatase, Ti-RH-MCM-41(sol-gel) and TiO<sub>2</sub>(sol-gel) (Bacsa and Kiwi, 1998). Consequently, TiO<sub>2</sub>(P25) and TiO<sub>2</sub>/RH-MCM-41(Dispersion) would be used and the catalyst will be named TiO<sub>2</sub>/RH-MCM-41 for the whole reaction.

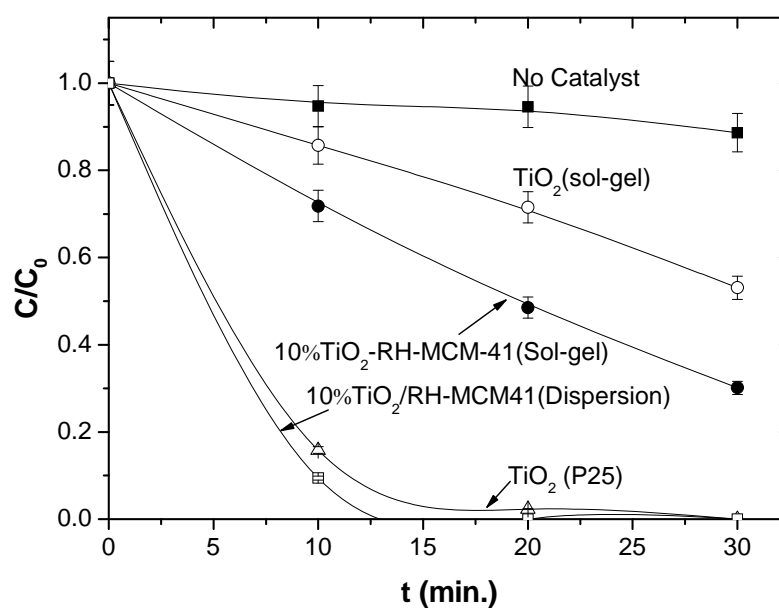


**Figure 4.8** Comparison of photocatalytic activity of various TiO<sub>2</sub>/RH-MCM-41s for photodegradation of alachlor; [modified TiO<sub>2</sub>] = 1 g/L, [TiO<sub>2</sub>] = 0.1 g/L, pH = 4, [alachlor] = 100 μM, UV light = 300 nm.

#### 4.4.6.3 Synergistic effect of support and UV light

The comparison between the photocatalytic degradation of alachlor on bare  $\text{TiO}_2$  and on  $\text{TiO}_2/\text{RH-MCM-41}$  is exhibited on Figure 4.9. In this study, the catalyst concentration and the power of UV light were fixed at 1 g/L and 300 nm because Vohra et al. (2005) had proven that the suitable amount of  $\text{TiO}_2$  for photoreaction was in the range of 0.5-1 wt. According to Figure 4.9,  $\text{TiO}_2/\text{RH-MCM-41}$  in the dark did not show any activity while the blank reaction (without catalyst) with sole UV light showed about 40% change in alachlor concentration implying that UV light is necessary for this reaction. Without UV light, there was no energy to generate  $\text{HO}^\bullet$  radical in  $\text{TiO}_2/\text{RH-MCM-41}$ . In addition, alachlor could automatically degrade but reaction time to obtain complete conversion would be too long. In the case of RH-MCM-41 with UV irradiation, the degradation rate was slightly greater than that in the blank and 50% conversion of alachlor was achieved after 30 min. This showed synergistic effect of support due to the fact that RH-MCM-41 had Brønsted acid site for adsorption and degradation of alachlor. For  $\text{TiO}_2/\text{RH-MCM-41}$  and bare  $\text{TiO}_2$ , 100% conversion of alachlor was achieved on 20 and 30 minutes for  $\text{TiO}_2/\text{RH-MCM-41}$  and bare  $\text{TiO}_2$ , respectively. This indicated the enhancement of photocatalytic degradation of alachlor by dispersing of  $\text{TiO}_2$  on RH-MCM-41 support because RH-MCM-41 provided higher OH density on the surface (Vohra et al., 2005). There are two reasons to support this hypothesis. First, the surface hydroxyl group play important role in direct participation in the reaction mechanism by trapping photo-generated holes that reach catalyst surface producing reactive surface  $\text{HO}^\bullet$  radical (Hoffmann et al., 1995). Second, surface hydroxyl group can change the adsorption of reactant molecule by both serving as active site for pollutant adsorption



and covering the site on  $\text{TiO}_2$  where electrons are trapped (Maira et al., 2000).

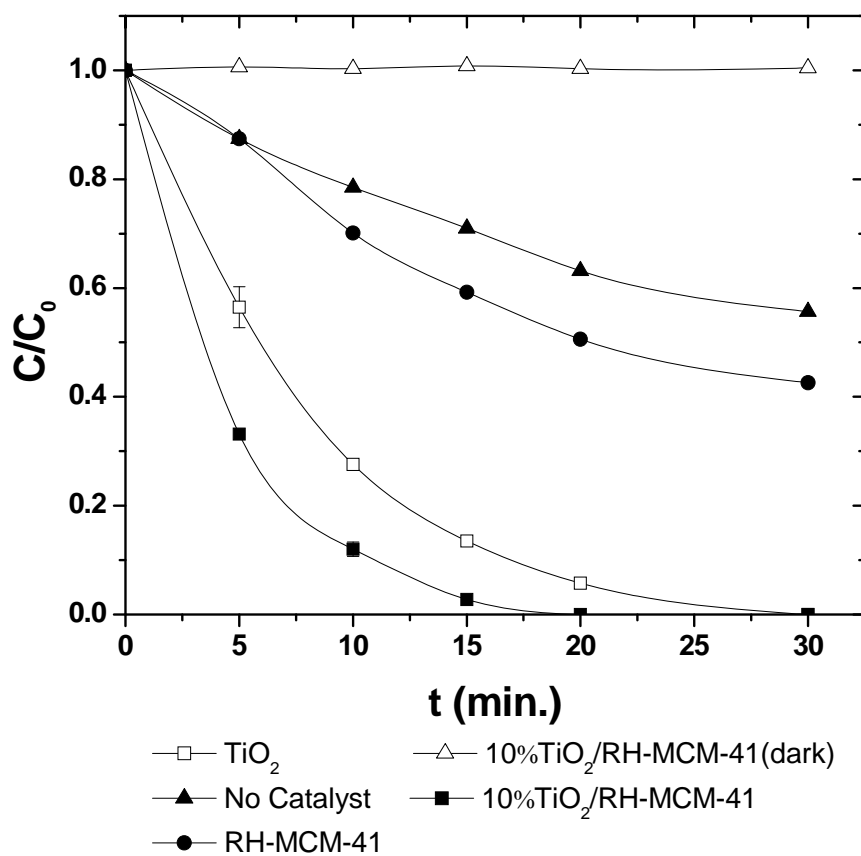


**Figure 4.9** Photocatalytic degradation of alachlor on bare  $\text{TiO}_2$ ,  $\text{TiO}_2$ /RH-MCM-41, dark control  $\text{TiO}_2$ /RH-MCM-41 and RH-MCM-41; [ $\text{TiO}_2$ /RH-MCM-41] = 1 g/L, pH = 4, [alachlor] = 80  $\mu\text{M}$ , UV light = 300 nm.

#### 4.4.6.4 Effect of alachlor concentration

Figure 4.10 shows the effect of alachlor concentration. The alachlor concentration of 80  $\mu\text{M}$  possessed the highest degradation rate. For the concentration higher than 80  $\mu\text{M}$ , the certain loading of  $\text{TiO}_2$ /RH-MCM-41 produced

a certain amount of hydroxyl radical which may not be sufficient for all alachlor molecules. For the lower concentration, alachlor molecules may adsorb more strongly on the surface and had lower degradation rate (Wang et al., 2008).

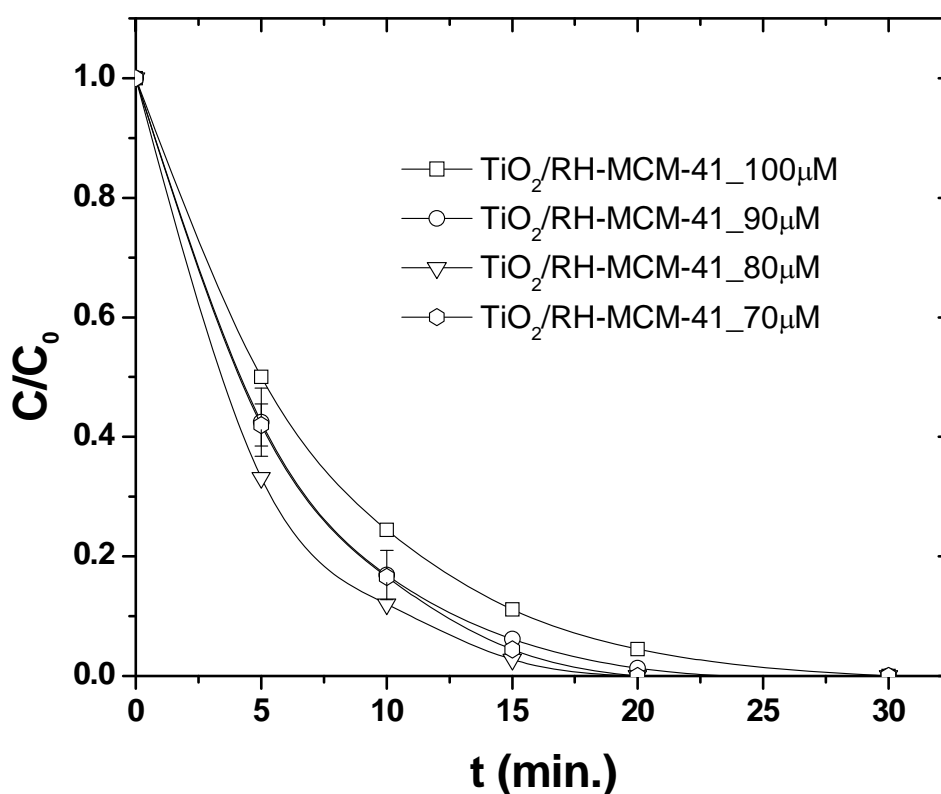


**Figure 4.10** Effect of concentration influencing photocatalytic degradation of alachlor; [TiO<sub>2</sub>/RH-MCM-41] = 1 g/L, pH = 4, UV light = 300 nm.

Further information, the initial rate of reaction was exhibited in Figure 4.11. The degradation rate agreed with the results in Figure 4.10 that the reaction proceeded rapidly when the alachlor concentration was 80 μM.

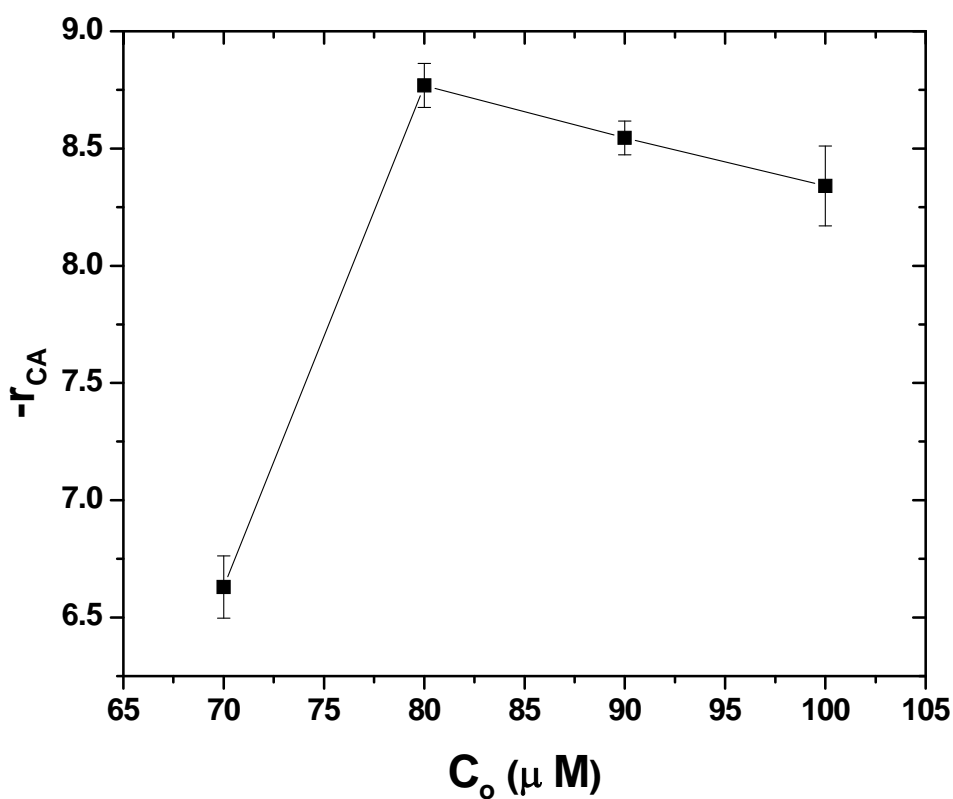


**Figure 4.11** Initial degradation rate ofalachlor by differential method; [TiO<sub>2</sub>/RH-MCM-41] = 1 g/L, pH = 4, UV light = 300 nm.

#### 4.4.6.5 Kinetics of reaction

The kinetics ofalachlor degradation was investigated to determine the reaction order. In Figure 4.12, the plot between  $\ln C_A$  versus time gave a straight line with slope and  $R^2$  of 0.23 and 0.9926, respectively corresponding to the mathematic formula below:

$$\ln(C_A) = -kt + \ln C_{A0} \quad \dots(3)$$

From the equation, rate constant ( $k$ ) of alachlor degradation was  $0.23 \text{ min}^{-1}$ . This result implied that photocatalytic degradation alachlor obeyed the pseudo-first order model as express by equation (3).

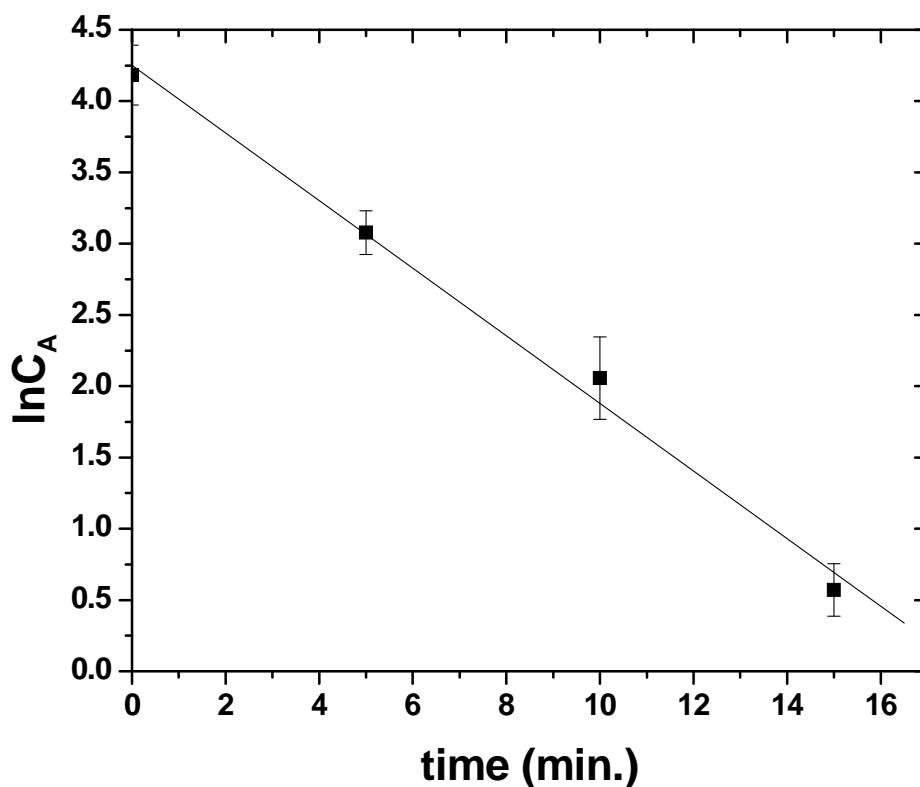


**Figure 4.12** Pseudo-first order plot from photocatalytic degradation of alachlor;  $[\text{TiO}_2/\text{RH-MCM-41}] = 1 \text{ g/L}$ ,  $\text{pH} = 4$ ,  $[\text{alachlor}] = 80 \mu\text{M}$ , UV light = 300 nm.

#### 4.4.6.6 Effect of pH to photodegradation of alachlor

Figure 4.13 exhibits the effect of pH to photocatalytic degradation of alachlor. Eventhough, pH change did not affect the charge of alachlor

molecule, surface charge was really sensitive to the pH change. In order to understand a role of pH, we already reported surface properties of TiO<sub>2</sub>/RH-MCM-41 and bare TiO<sub>2</sub> by studying zeta potential. Corresponding to the previous result, photocatalytic degradation of alachlor reached the highest efficiency at pH 4 because the surface charge of catalyst at this pH was nearly zero. The adsorption between neutral alachlor and surface functional group should be compromised in this condition.

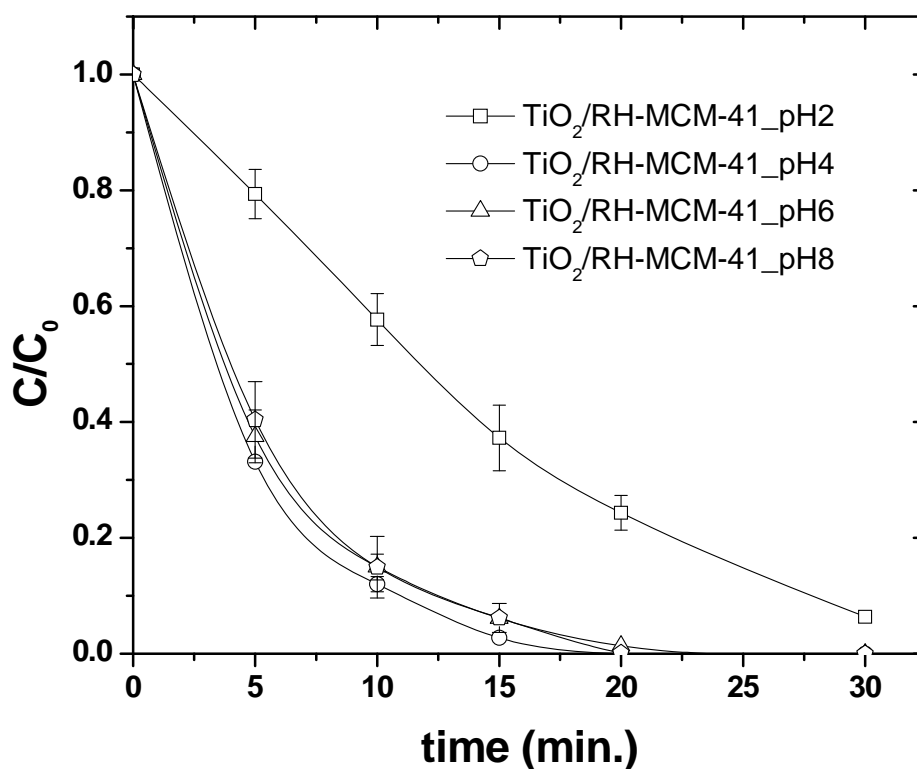


**Figure 4.13** Effect of pH influencing photocatalytic degradation of alachlor; [TiO<sub>2</sub>/RH-MCM-41] = 1 g/L, [alachlor] = 80  $\mu$ M, UV light = 300 nm.

Figure 4.14 also confirmed that degradation rate had the highest rate when the solution pH was 4. At lower pH, the surface charge was positive and the interaction between alachlor and catalyst surface was unfavorable resulting in lower degradation. At the pH higher than 4, the degradation rate decreased gradually even though the surface had negative charge. In this case, the reaction did not only occur on active site of the catalyst but also on the bulk solution. This can refer to Kim and Choi's study (Kim and Choi, 2002) which reported that the hydroxyl radical could be produced on both catalyst surface and bulk solution.

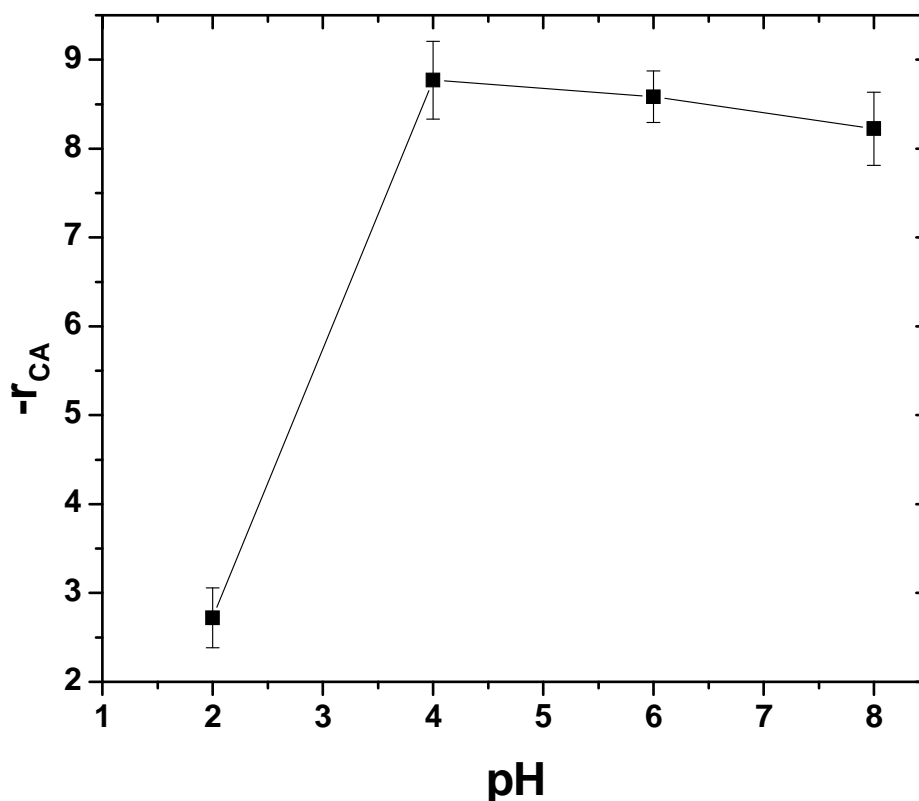


**Figure 4.14** Initial degradation rate of alachlor influencing by pH solution;  $[\text{TiO}_2/\text{RH-MCM-41}] = 1 \text{ g/L}$ ,  $[\text{alachlor}] = 80 \text{ }\mu\text{M}$ , UV light = 300 nm.

#### 4.4.7 Adsorption isotherm of alachlor

The adsorption of alachlor on 10%TiO<sub>2</sub>/RH-MCM-41 was studied in the dark condition by stirring the mixture of alachlor and catalyst and sampled after 0.5 h. There were two possible models that could explain the adsorption of alachlor: Langmuir or Freundlich isotherm. These two models were essential to be able to accurately represent the adsorption of substances on solid catalysts in the aqueous solution. The hypotheses of them are very different adsorption behavior over the range of possible adsorbate concentration. Langmuir model incorporates assumptions that adsorption occurs at a fixed number of distinct sites, all sites are energetically equivalent and each site can accommodate one sorbate molecule and no interaction between sorbate molecules on the adjacent site (Kamarudin et al., 2004). In case of Freundlich model, adsorption occurs on a flat surface, the sorbate is either chemisorbed on a distinct sites or physisorbed until only a relatively low coverage degree is reached, all sites are also energetically equivalent and the physisorption has no limit of capacity making amount of sorbates go to infinity when concentration increases (Sotelo et al., 2002; Kamarudin et al., 2004). Previously, adsorption and desorption of alachlor, metolachlor and linuron on kaolinite and montmorillonite was investigated by Torrents and Jayasundera (1997). The results showed that adsorption isotherm confirmed the Freundlich isotherm with  $K_{f(ad)}$  in the range of  $1.63 \times 10^{-3}$  to  $2.84 \times 10^{-2}$  and n values ranged from 0.78 to 1.92. However, adsorption of propachlor which is one of variety of herbicides on TiO<sub>2</sub> had a different model. Konstantinou et al. (2002) studied adsorption and photodegradation of propachlor in aqueous TiO<sub>2</sub> suspensions. The results were found that the adsorption of propachlor on TiO<sub>2</sub> fit well with Langmuir model. These indicated that the adsorption model of alachlor has been

varied by surface properties of catalyst. Consequently, the adsorption model of alachlor on TiO<sub>2</sub> dispersed mesoporous MCM-41 should be concerned carefully in this experiment. This point of view, both Langmuir and Freundlich model were examined and explained by in equation (1) and (2), respectively.

$$\frac{C_e}{q_e} = \frac{C_e}{q_{\max}} + \frac{1}{K_{ad} \times q_{\max}} \quad \dots(1)$$

$$\log(q_e) = \log(K) + \frac{1}{n} \log(C_e) \quad \dots(2)$$

Where

$C_e$  = equilibrium concentration of alachlor in solution (mg/L)

$q_e$  = amount of adsorbed alachlor on the catalyst at the equilibrium concentration (mg/g)

$q_{\max}$  = maximum adsorption amount of alachlor (mg/g)

$K_{ad}$  = apparent adsorption equilibrium concentration (mg/L)<sup>-1</sup>

$K$  = adsorption capacity constant (mg/L)<sup>-1</sup>

$n$  = adsorption layer of alachlor

The relationship between  $C_e/q_e$  and  $C_e$  was a linear like  $Y = mX + C$  which explain Langmuir model and liner relationship between  $\log(q_e)$  and  $\log(C_e)$  is able to explain Freundlich model. Whether relationship shows straight line, one will own the adsorption model of alachlor on TiO<sub>2</sub>/RH-MCM-41. The results from this research showed that the relationship between  $C_e/q_e$  and  $C_e$  did not obey Langmuir model because a linear relationship was not obtained (see Figure 4.15A). This indicated that surface-charge interaction between alachlor and TiO<sub>2</sub>/RH-MCM-41 was not only chemisorption but also physisorption. Thus, Freundlich model was studied and the results are shown in Figure 4.15B.



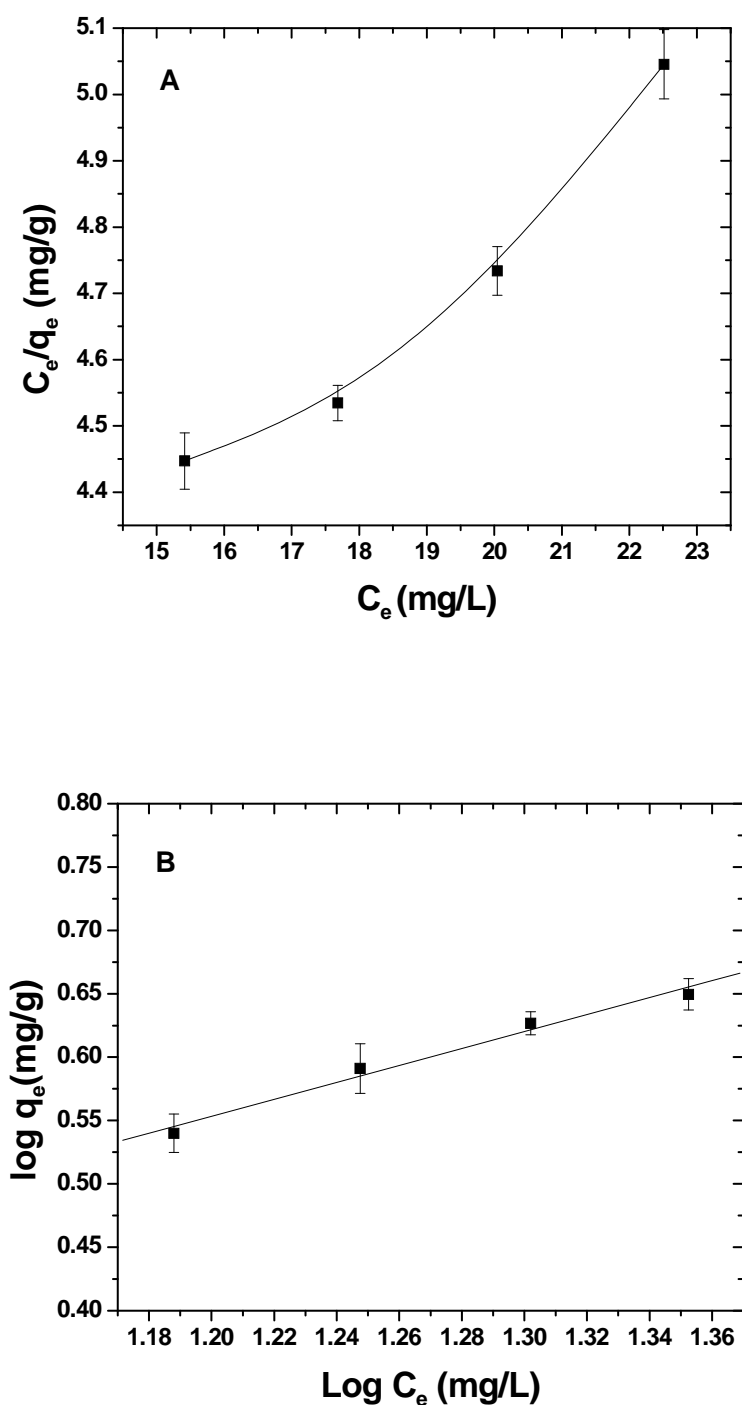


**Figure 4.15** Adsorption of alachlor on TiO<sub>2</sub>/RH-MCM-41; **A)** Langmuir isotherm **B)**

Freundlich isotherm; [TiO<sub>2</sub>/RH-MCM-41] = 1 g/L, pH = 4, [alachlor] =

80  $\mu$ M, UV light = 300 nm.

From equation (2), a straight line with the slope and  $R^2$  of 0.67 and 0.98, respectively, was obtained. A number of adsorption layers ( $n$ ) from the relationship between  $n$  and slope were 1.50 confirming the previous reasons that adsorption between organic or inorganic compounds on adsorbent should be multi-layers.

## 4.5 Conclusions

The photocatalytic performance of  $\text{TiO}_2$  could be enhanced by dispersing on mesoporous materials, RH-MCM-41, preparing for rice silica. The morphology and crystallinity of  $\text{TiO}_2$  did not change after modification. The reaction was strongly dependent on pH solution because surface functional group of solid catalysts was sensitive to pH change. The neutral surface dominated reaction by playing an important role for adsorption of a neutral alachlor molecule.  $\text{TiO}_2/\text{RH-MCM-41}$  was more preferable for photocatalytic degradation than the bare  $\text{TiO}_2$  since it possessed higher OH groups on its own surface which play an important role in catalytic acceleration.

## 3.6 References

- Bacsa, R. R., Kiwi, J. (1998). Effect of rutile phase on the photocatalytic properties of nanocrystalline titania during the degradation of *p*-coumaric acid. **Applied Catalysis B: Environmental**. 16(1): 19-29.
- Bhattacharyya, A., Kawi, S., Ray, M.B. (2004). Photocatalytic degradation of orange II by  $\text{TiO}_2$  catalysts supported on adsorbents. **Catalysis Today**. 98(3): 431–439.
- Brunauer, S., Emmett, P.H., Teller, E. (1938). Adsorption of gases in multimolecular

- layers. **Journal of the American Chemical Society**. 60(2): 309-319.
- Burrows, H. D., Canle, L. M., Santaballa, J. A., Steenken, S. (2002). Reaction pathways and mechanisms of photodegradation of pesticides. **Journal of Photochemistry and Photobiology B: Biology**. 67(2): 71-108.
- Carp, O., Huisman, C. L., Reller, A. (2004). Photoinduced reactivity of titanium dioxide. **Progress in Solid State Chemistry**. 32(1): 33-177.
- Hoffmann, M. R., Martin, S. T., Choi, W., Bahnemann, D. W. (1995). Environmental applications of semiconductor photocatalysis. **Chemical Reviews**. 95(1): 69-96.
- Kamarudin, K. S. N., Hamdan, H., Mat, H. (2004). Equilibrium model of gas adsorption on zeolite. **In: Proceeding of annual fundamental science seminar 2004 (pp. 1-5)**. Pn Norazana Ibrahim, Universiti Teknologi Malaysia Institutional Repository.
- Kim, S., Choi, W. (2002). Kinetics and mechanisms of photocatalytic degradation of  $(\text{CH}_3)_n\text{NH}_{4-n}^+$  ( $0 \leq n \leq 4$ ) in  $\text{TiO}_2$  suspension: The role of OH radicals. **Environmental Science and Technology**. 36(9): 2019-2025.
- Konstantinou, I. K., Albanis, T. A. (2004).  $\text{TiO}_2$ -assisted photocatalytic degradation of azo dyes in aqueous solution: kinetic and mechanistic investigations: A review. **Applied Catalysis B: Environmental**. 49(1): 1-14.
- Li, G., Zhao, X. S., Ray, M. B. (2007). Advanced oxidation of orange II using  $\text{TiO}_2$  supported on porous adsorbents: The role of pH,  $\text{H}_2\text{O}_2$  and  $\text{O}_3$ . **Separation and Purification Technology**. 55(1): 91-97.
- Maira, A., Yeung, K. L., Yan, C. Y., Yue, P. L., Chan, C. K. (2000). Size effects in gas-phase photo-oxidation of trichloroethylene using nanometer-sized  $\text{TiO}_2$  catalysts. **Journal of Catalysis**. 192(1): 185-196.

- Narkhede, V. S., De Toni, A., Narkhede, V. V., Guraya M., (Hans) Niemantsverdriet, J.W., van den Berg, M. W. E., et al., (2008). Au/TiO<sub>2</sub> catalysts encapsulated in the mesopores of siliceous MCM-48-Reproducible synthesis, structural characterization and activity for CO oxidation. **Microporous Mesoporous Materials**. in press.
- Sanchez-Martin, M. J., Rodriguez-Cruz M. S., Andrades, M. S., Sanchez-Camazano, M. (2006). Efficiency of different clay minerals modified with a cationic surfactant in the adsorption of pesticides: Influence of clay type and pesticide hydrophobicity. **Applied Clay Science**. 31(3): 216–228.
- Schacht, P., Noren-Franco, L., Ancheyta, J., Ramirez, S., Hernandez-Perez, I., Garcia, L. A. (2004). Characterization of hydrothermally treated MCM-41 and Ti-MCM-41 molecular sieves. **Catalysis Today**. 98 (1): 115–121.
- Sotelo, J. L., Ovejero, G., Delgado, J. A., Martínez, I. (2002). Comparison of adsorption equilibrium and kinetics of four chlorinated organics from water onto GAC. **Water Research**. 36(3): 599-608.
- Sun, B., Reddy, E. P., Smirniotis, P. G. (2005). Effect of the Cr<sup>6+</sup> concentration in Cr-incorporated TiO<sub>2</sub>-loaded MCM-41 catalysts for visible light photocatalysis. **Applied Catalysis B: Environmental**. 57(2): 139-149.
- Torrents, A., Jayasundera, S. (1997). The sorption of nonionic pesticides onto clays and the influence of natural organic carbon. **Chemosphere**. 35(7): 1549-1565.
- Vohra, M. S., Lee, J., Choi, W. (2005). Enhanced photocatalytic degradation of tetramethylammonium on silica-loaded titania. **Journal of Applied Electrochemistry**. 35(7): 757–763.
- Wang, H., Nui, J., Long, X., He, Y. (2008). Sonophotocatalytic degradation of methyl

orange by nano-sized Ag/TiO<sub>2</sub> particles in aqueous solutions. **Ultrasonics Sonochemistry**. 15(4): 386-392.

Wittayakun, J., Khemthong, P., Prayoonpokarach, S. (2008). Synthesis and characterization of zeolite NaY from rice husk silica. **Korean Journal of Chemical Engineering**. 25(4): 861-864.

Wong, C. C., Chu, W. (2003). The hydrogen peroxide-assisted photocatalytic degradation of alachlor in TiO<sub>2</sub> suspensions. **Environmental Science and Technology**. 37(10): 2310-2316.

**CHAPTER V**

**PHOTOCATALYTIC DEGRADATION OF**

**TETRAMETHYLAMMONIUM CHLORIDE ON**

**TiO<sub>2</sub>/RH-MCM-41**

**5.1 Abstract**

Photocatalytic degradation of tetramethylammonium (TMA) chloride in water on bare TiO<sub>2</sub> was compared to that on TiO<sub>2</sub> dispersed on RH-MCM-41 which was a mesoporous material synthesized with rice husk silica. The reaction equilibrium was established in 30 min. in deionized water without adjusting the solution pH. The TiO<sub>2</sub>/RH-MCM-41 had higher TMA adsorption than that of the bare TiO<sub>2</sub> and the photocatalytic degradation activity on all TiO<sub>2</sub>/RH-MCM-41s were higher than that on the bare TiO<sub>2</sub>. The highest TMA conversion of 100% was obtained from 10%TiO<sub>2</sub>/RH-MCM-41 after 90 minute while only 20% conversion was obtained from the bare TiO<sub>2</sub> with the same TiO<sub>2</sub> loading. The intermediates detected were tri-, di- and mono-methylammonium ions which were consecutively mineralized to ammonium ions. The 10%TiO<sub>2</sub>/RH-MCM-41 produced the largest amount of ammonium ion (8%) at a reaction time of 90 min.

## 5.2 Introduction

Nitrogenous organic pollutants are chemical contaminants in environment that can affect human health. An example is tetramethylammonium hydroxide  $[(\text{CH}_3)_4\text{NOH}]$ , TMAH] which is used in semiconductor industrial as a silicon etchant (Kim and Choi, 2002). The TMAH is toxic because it can irritate skin, eyes and respiratory tracts. Thus, it should be removed to prevent contamination to environment. Because TMAH is stable in water and its degradation by conventional, biological and physical methods was not effective (Bhattacharyya., et al., 2004; Li et al., 2007). Consequently, advanced oxidation processes (AOPs) have been investigated to serve this purpose. The processes involve the generation of very reactive species such as hydroxyl radical ( $\text{HO}^\bullet$ ) (Konstantinou, et al., 2004). Bare  $\text{TiO}_2$  is usually used in the presence of UV to generate hole-electron pair and transfer to degrade pollutant molecules. Photodegradation of tetramethylammonium hydroxide derivatives, tetramethylammonium chloride (TMA), was studied on bare  $\text{TiO}_2$  at various pH solutions by Kim and Choi (2002). The catalyst was effective in both acid and alkaline solution. The reasons to explain as followed. First, surface charge interaction between TMA and solid catalyst influenced degradation rate of the reaction at alkaline solution. Secondly, charge repulsion between TMA and solid catalyst was weak and hydroxyl radicals could be produced on both the functionalized-hydroxyl surface and in bulk solution. Consequently, the reaction could proceed in acidic solution. However, when the pH equaled to pH point of zero charge ( $\text{pH}_{\text{PZC}}$ ) of bare  $\text{TiO}_2$  which was 6.7, the bare  $\text{TiO}_2$  gave low activity of TMA photocatalytic degradation because tiny  $\text{TiO}_2$  particles aggregated and the number of active sites decreased. Furthermore, electron/hole recombination can happen on the surface of bare

TiO<sub>2</sub> (Zhang and Wang, 1998). When the size of TiO<sub>2</sub> particles decreased, the surface area increased and generated electron and hole can recombine on the surface of TiO<sub>2</sub>. On the other hand, when the size of TiO<sub>2</sub> is increased, the path length to transfer electron from conduction band to surface increased and the possibility of electron/hole recombination increased. In another experiment, Vohra et al. (2005) improved photocatalytic activity of TMA degradation on bare TiO<sub>2</sub> by adding Si to produce Si-TiO<sub>2</sub>. The activity at pH 5 was improved from 32% on bare TiO<sub>2</sub> to 100% on Si-TiO<sub>2</sub>. The electron/hole recombination was suppressed by surface hydroxyl groups of SiO<sub>2</sub>. However, the adsorption of TMA on TiO<sub>2</sub> was negligible and the reaction was slow (2 h) because SiO<sub>2</sub> possessed low surface area (245 g/cm<sup>3</sup>) and had non-uniformed pores. In this work, TiO<sub>2</sub> particles were dispersed on RH-MCM-41, a mesoporous material synthesized with rice husk silica which possessed a high specific surface area (1231 cm<sup>3</sup>) and uniform pore size (Artkla et al., 2008). This RH-MCM-41 was further dispersed by TiO<sub>2</sub> and used as a catalyst to test photoactivity for TMA degradation. The dispersion of TiO<sub>2</sub> could prevent agglomeration and maintain catalytic activity. Moreover, the reaction was pH dependent and it would be more practical if the reaction could be carried out at pH 7. High specific surface area of RH-MCM-41 composed of -OH surface functionalized was expected to enhance the catalytic activity. Hole-electron recombination at pH 7 would be suppressed and active species would be easily transferred to degrade pollutants. The parameters that influence photodegradation of TMA including TMA concentration, catalyst concentration, TiO<sub>2</sub> loadings and solution pH were investigated. The TMA adsorption model and degradation kinetics were also investigated in this study.



## 5.3 Experimental

### 5.3.1 Chemicals and Materials

Chemicals for photodegradation of TMA on TiO<sub>2</sub>/RH-MCM-41 were: RH-MCM-41, TiO<sub>2</sub>/RH-MCM-41, TiO<sub>2</sub> Degussa P25 (Aldrich), (CH<sub>3</sub>)<sub>4</sub>NCl (ACROS Organics), (CH<sub>3</sub>)<sub>3</sub>NHCl (Aldrich), (CH<sub>3</sub>)<sub>2</sub>NH<sub>2</sub>Cl (Sigma), CH<sub>3</sub>NH<sub>3</sub>Cl (Sigma), NH<sub>4</sub>Cl (Aldrich), (C<sub>2</sub>H<sub>5</sub>)<sub>4</sub>NCl (Sigma), CH<sub>3</sub>SO<sub>2</sub>(OH) (Aldrich), Na<sub>2</sub>CO<sub>3</sub> (S.P.C. GR Reagent, Japan), NaHCO<sub>3</sub> (Kanto, Japan), CH<sub>3</sub>CN (Aldrich), HCl (S.P.C. GR Reagent, Japan), and LiOH (S.P.C. GR Reagent, Japan). A Barnstead water purification setup was employed to obtain the deionized water (18 MΩ cm).

### 5.3.2 Apparatus and equipments

The apparatus and equipments for photodegradation of TMA on TiO<sub>2</sub>/RH-MCM-41 included glass wares, magnetic stirrer, balance, sonicator, pyrex reactor, pH meter, Xe-arc lamp (300 W, Oriel), timer, micropipette PTFE filters (Millipore), syringe and ion chromatograph (IC, Dionex-120).

The synthesis of RH-MCM-41 and the preparation of TiO<sub>2</sub>/RH-MCM-41 were similar to the procedure described in chapter IV.

### 5.3.3 Photocatalytic degradation of TMA

All experiments were carried out in a pyrex reactor (33 mL) with a quartz window. A Xe-arc lamp (300 W, Oriel) was used as the illumination. All bare TiO<sub>2</sub> and TiO<sub>2</sub>/RH-MCM-41 suspensions were prepared at a concentration of 0.25-2.0 g/L and were dispersed by simultaneous sonication and shaking for 30 s. An aliquot of the substrate stock solution (1 mM) was subsequently added to the suspension to

give a desired concentration. The initial pH ( $\text{pH}_i$ ) of the suspension was adjusted with HCl or LiOH standard solutions. The mixture was irradiated by UV light and sample aliquots of 1 mL were collected at appropriate time intervals and filtered through 0.45- $\mu\text{m}$  PTFE filters. The concentration of TMA and its mineralized products were analyzed by a Dionex ion chromatograph equipped with a conductivity detector.

Effect of  $\text{TiO}_2$  loading on RH-MCM-41 was studied by varying the amount of  $\text{TiO}_2$  from 10 to 60 wt. %. The catalyst concentration was also varied from 0.25 to 2.0 g/L to optimize the condition for reaction. The reaction was also compared activity of with the same amount of  $\text{TiO}_2$  between bare  $\text{TiO}_2$  and  $\text{TiO}_2/\text{RH-MCM-41}$ . The effect of pH was studied in the range of 3 to 11. Furthermore, the catalytic activity of controlled reactions in the dark and under UV irradiation was compared. Total Organic Carbon (TOC) of all samples was analyzed with a total organic carbon analyzer (TOC, Shimadzu TOCVCSH) which detected  $\text{CO}_2$  evolution. All data were used for the determination of the reaction order and kinetics.

#### **5.3.4 Adsorption isotherm determination on catalysts**

Adsorption of TMA was investigated by mixing catalyst powder at 1 g/L in 30 mL TMA (80-120  $\mu\text{M}$ ). The solution pH was adjusted by  $\text{HNO}_3$  and LiOH standard solutions. The mixture was sonicated for 30 s to suspend finely catalyst powder in solution and stirred in the dark for 30 min. After 30 s, sample aliquots of 1 mL were collected at appropriate time intervals, filtered through 0.45- $\mu\text{m}$  PTFE filters and analyzed by a Dionex ion chromatograph. The eluent for TMA analysis, was 10 mM methanesulfonic acid. The changes in concentration of TMA were determined from calibration method.

## 5.4 Results and Discussion

### 5.4.1 Photodegradation of TMA on bare TiO<sub>2</sub> and TiO<sub>2</sub>/RH-MCM-41

#### 5.4.1.1 Effect of TiO<sub>2</sub> content on RH-MCM-41 to photodegradation

In order to obtain the optimal loading of TiO<sub>2</sub> on RH-MCM-41, various loadings 10, 20, 40 and 60 wt. %, were loaded. The catalytic activities were compared in Figure 5.1. The initial TMA concentration on each catalyst was not the same due to the difference in adsorption. The conversions of TMA with various TiO<sub>2</sub> loadings were similar and all catalysts gave a nearly complete TMA conversion after 90 min. Thus, only 10% TiO<sub>2</sub> loading was adequate for this reaction.

#### 5.4.1.2 Effect of catalyst concentration

The ratio between catalyst amount and TMA volume was optimized in order to obtain the best condition for this reaction. Results in Figure 5.2 showed that the TMA degradation increased with the catalyst amount. The initial TMA concentration was different on each catalyst because the adsorption increased with the amount of catalyst. Both catalysts with 1.0 g/L and 2.0 g/L ratio gave a complete conversion after 90 min. but the initial TMA concentration for the 1.0 g/L was higher. Thus, the catalyst with 1.0 g/L was considered to be the optimum ratio and used in the further study.

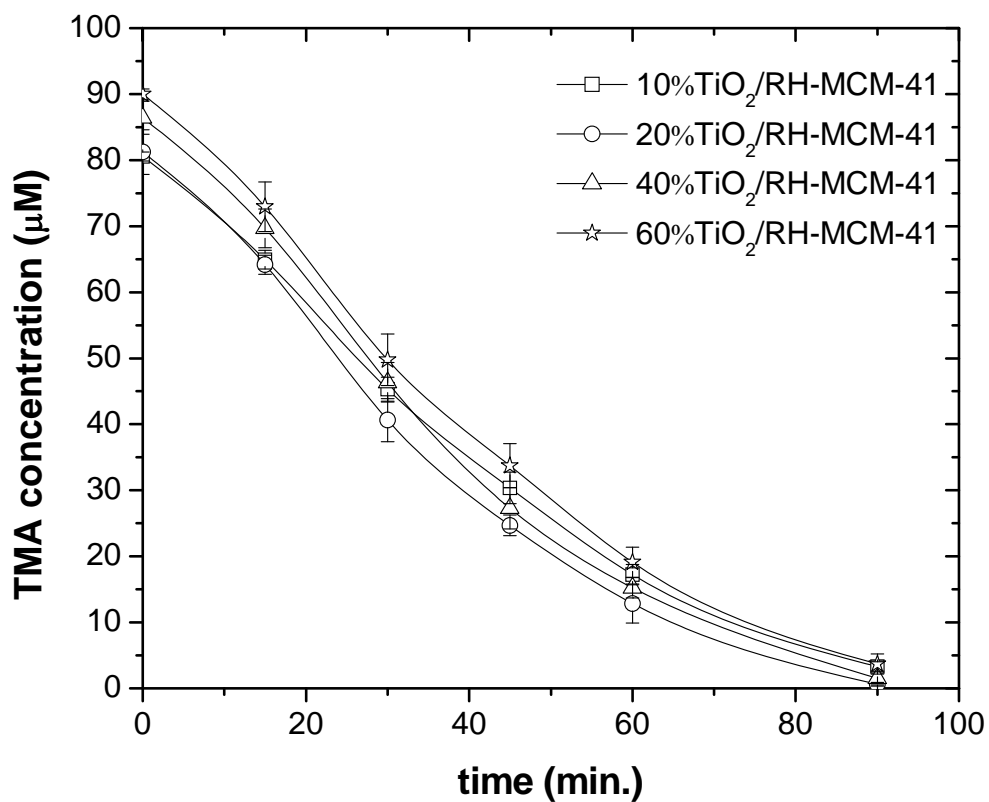


**Figure 5.1** Effect of  $\text{TiO}_2$  loadings in  $\text{TiO}_2/\text{RH-MCM-41}$  on photocatalytic degradation rate of TMA;  $[\text{TMA}] = 100 \mu\text{M}$ ,  $\text{pH} = 7$ .

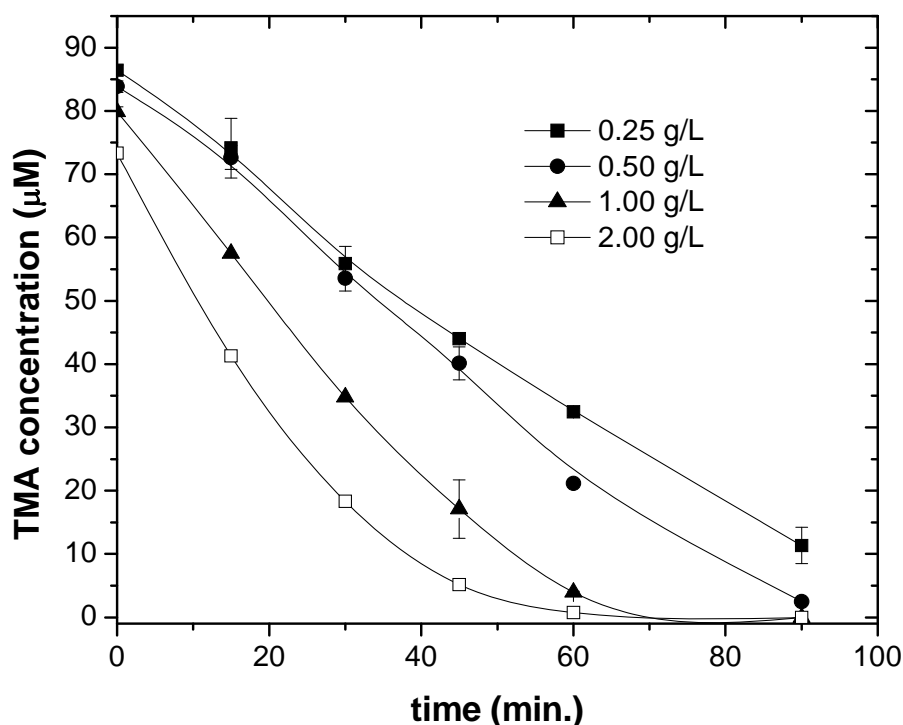


**Figure 5.2** Effect of catalyst concentration on photocatalytic degradation of TMA; [TMA] = 100  $\mu\text{M}$ , pH = 7.

#### 5.4.1.3 Effect of pH to photodegradation of TMA on $\text{TiO}_2/\text{MCM-41}$

Figure 5.3 exhibited the effect of pH to photocatalytic degradation of TMA. Even though, pH change did not affect the charge of TMA molecule, surface charge was sensitive to pH change. The surface properties of  $\text{TiO}_2/\text{RH-MCM-41}$  and bare  $\text{TiO}_2$  were different as confirmed by studying zeta potential. As a result, photocatalytic degradation of TMA reached the highest efficiency at pH 7 because the surface charge of catalyst at this pH was negative. The adsorption between TMA and surface functional group should be compromised at this condition.

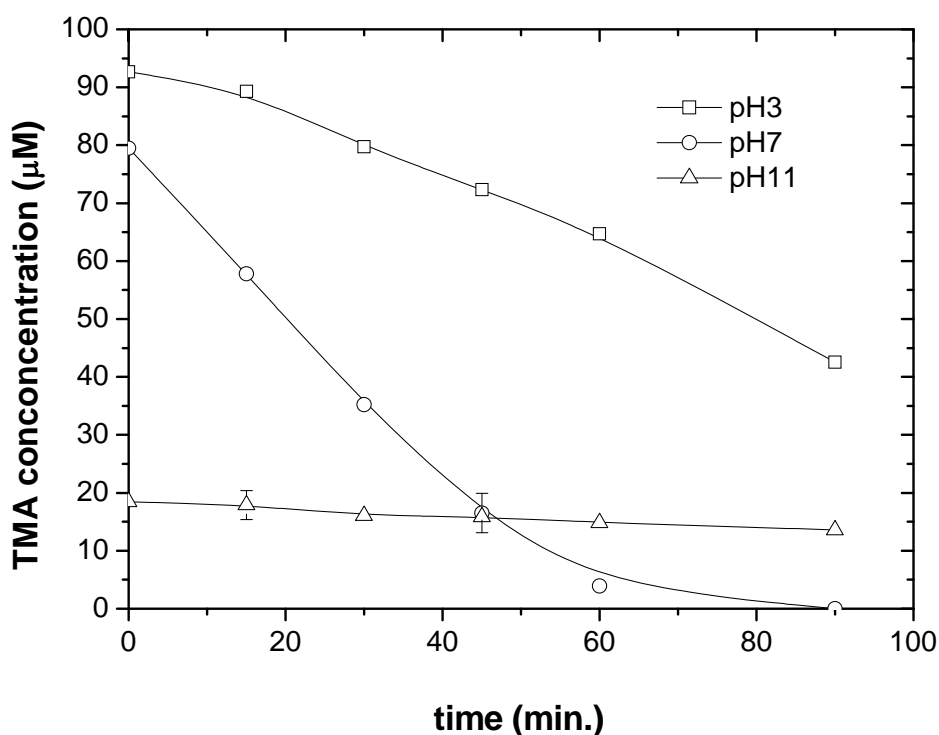


**Figure 5.3** Effect of pH solution on photocatalytic degradation of TMA; [TMA] = 100  $\mu\text{M}$ , [10%TiO<sub>2</sub>/RH-MCM-41] = 1 g/L.

At the pH 3, photocatalytic degradation proceeded although there was repulsion between ammonium ions and the surface of the catalyst. In this case, the reaction did not only occur on active site of the catalyst but also in the bulk solution. This could be explained as in the previous study that the hydroxyl radical could be produced on both catalyst surface and in bulk solution (Kim and Choi, 2002). Taking into account of the reaction at alkali solution (pH > 7), the degradation rate was dramatically dropped when solution pH was further increased. The reasons to support were as followed. Firstly, RH-MCM-41 structure could not withstand alkaline condition for a long time. It was reported that RH-MCM-41 structure was completely

ruined after soaking at pH 11 for 48 h (Pérez et al., 2000). Secondly, when considered the result from Figure 5.3, the conversion was nil at this and the adsorption in the dark after 30 min was large. It was likely that TMA adsorbed strongly on negatively charged surface. In addition, the degradation efficiency with pH could be seen from Figure 5.4 where the initial degradation rate increased with pH until 7. Further increasing of solution pH no longer enhanced photocatalytic activity because of stability of the TiO<sub>2</sub>/RH-MCM-41 structure as mentioned previously. Similar to TiO<sub>2</sub>/RH-MCM-41, degradation rate of TMA on bare TiO<sub>2</sub> increased with pH solution excepting at pH 7. The initial degradation rate was dramatically decreased because of stability of bare TiO<sub>2</sub> which will be explained in the next section.

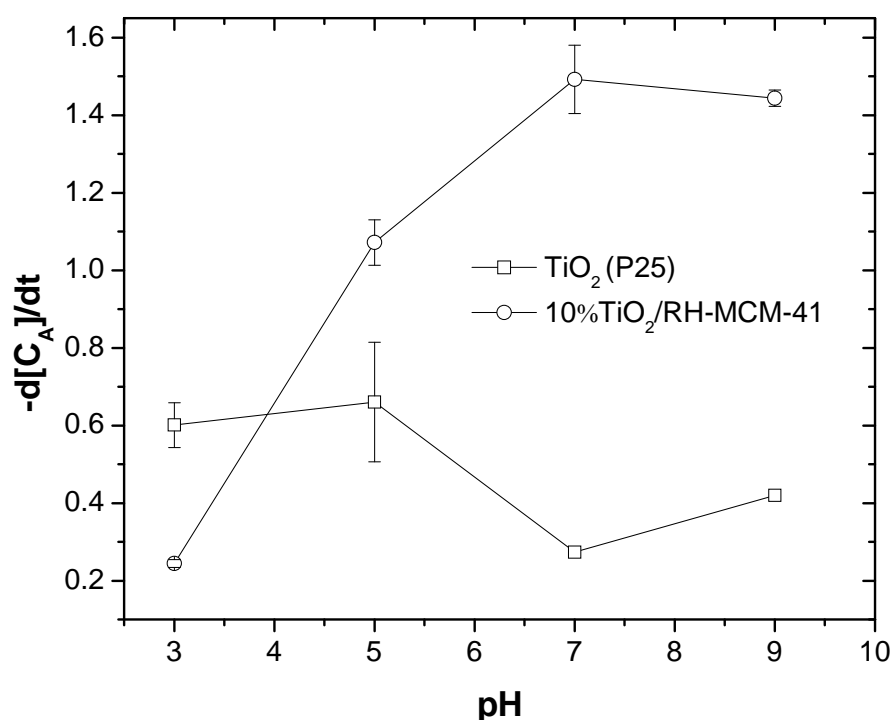


**Figure 5.4** Effect of solution pH on degradation rate of TMA; [TMA] = 100  $\mu$ M, [TiO<sub>2</sub>/RH-MCM-41] = 1 g/L, [TiO<sub>2</sub>] = 0.1 g/L.

#### 5.4.1.4 Synergic effect of support and UV light

Comparison of photodegradation of TMA on bare  $\text{TiO}_2$ , RH-MCM-41 and 10%  $\text{TiO}_2/\text{RH-MCM-41}$  is shown in Figure 5.5. At the initial stage, TMA adsorbed on all samples in the order  $\text{TiO}_2/\text{RH-MCM-41} > \text{RH-MCM-41} > \text{bare TiO}_2$ . The concentration of TMA in the presence of only RH-MCM-41 and without irradiation was constant throughout the 90 min testing period. While the mixture between TMA and RH-MCM-41 under UV-irradiation gave about 5% TMA conversion. This conversion could be from functionalized-hydroxyl surface of RH-MCM-41 (Maira et al., 2000). The TMA conversion on the bare  $\text{TiO}_2$  was about 25% while a complete conversion was obtained on  $\text{TiO}_2/\text{RH-MCM-41}$  with the similar  $\text{TiO}_2$  weight. This evidence confirmed that the photodegradation of TMA could be enhanced when the  $\text{TiO}_2$  was dispersed on RH-MCM-41.

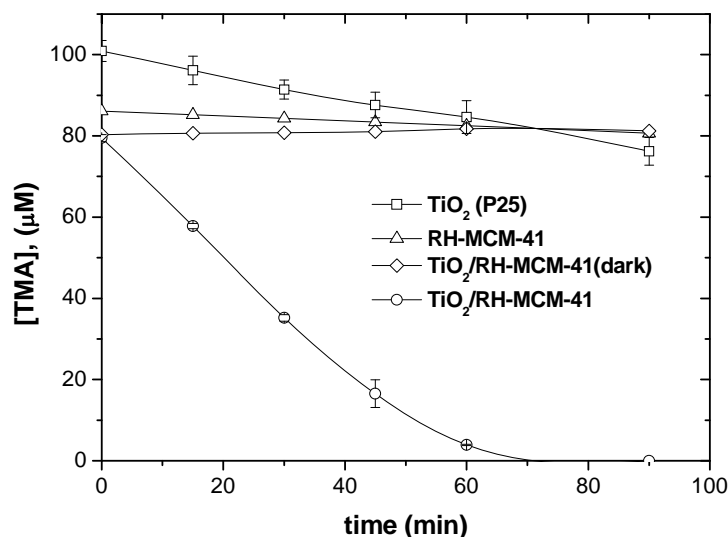


**Figure 5.5** Photocatalytic degradation of TMA on  $\text{TiO}_2$ , RH-MCM-41 and  $\text{TiO}_2/\text{RH-MCM-41}$ ;  $[\text{RH-MCM-41}] = 1 \text{ g/L}$ ,  $[\text{TiO}_2/\text{RH-MCM-41}] = 1 \text{ g/L}$ ,  $[\text{TiO}_2] = 0.1 \text{ g/L}$ ,  $\text{pH} = 7$ .



In conclusion, the corporation between  $\text{TiO}_2$  and RH-MCM-41 resulted in photogeneration of hydroxyl radical, stabilization of catalyst structure and removal of electron-hole recombination. There were three reasons to confirm that RH-MCM-41 assisted the reaction. First, RH-MCM-41 provided higher OH density on the surface (Vohra et al., 2005). Second, The surface hydroxyl groups play an important role in direct participation in the reaction mechanism by trapping photogenerated holes that reach catalyst surface producing reactive surface  $\text{HO}^\bullet$  radical (Maira et al., 2000). Third, surface hydroxyl group can change the adsorption of reactant molecule by serving as active site for pollutant adsorption and covering the site on bare  $\text{TiO}_2$  where electron could be trapped (Hoffmann et al., 1995). This method is much more important in producing oxygen as well as hindering electron-hole recombination (Carp, et al., 2004) indicating the enhancement of photocatalytic degradation of TMA by dispersing of  $\text{TiO}_2$  on RH-MCM-41.

The product distributions detected during the degradation of TMA on  $\text{TiO}_2/\text{RH-MCM-41}$  are shown in Figure 5.6. Products from photodegradation of TMA are mainly tri-, di- and monomethylammonium with trace amount of ammonium and nitrate ions. When the bare  $\text{TiO}_2$  catalyst was employed (Figure 5.6A), the only detected products were tri- and dimethylamine which increased slightly with time. When the 10% $\text{TiO}_2/\text{RH-MCM-41}$  was used (Figure 5.6B), the degradation products after 20 min were tri- and dimethylammonium. The amount of both ions increased with time until 45 and 60 min, respectively and then started to decreased.

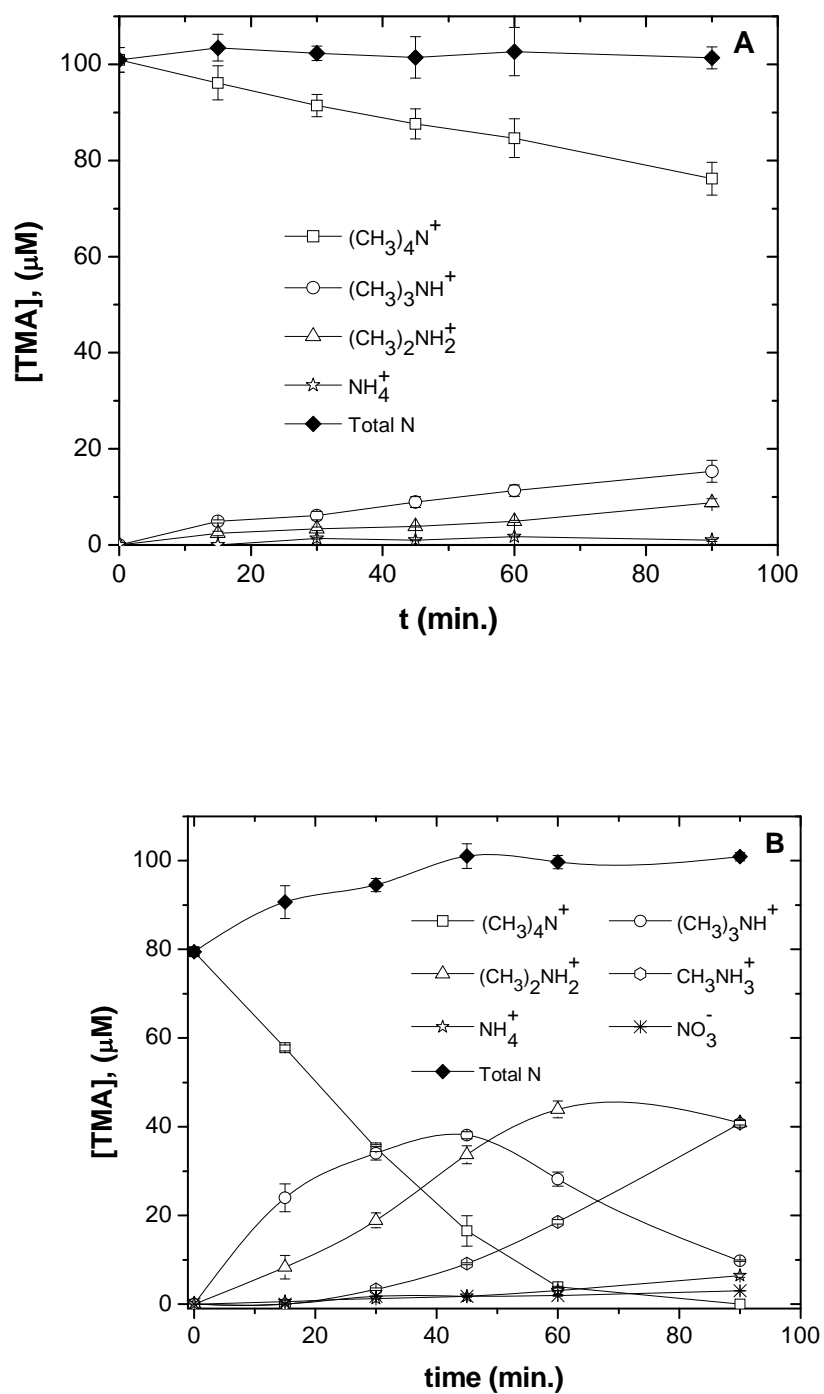


**Figure 5.6** Product distribution from photodegradation of TMA: A) bare TiO<sub>2</sub> and B)

TiO<sub>2</sub>/RH-MCM-41; [TMA] = 100 μM, [TiO<sub>2</sub>/RH-MCM-41] = 1 g/L,

[TiO<sub>2</sub>] = 0.1 g/L, pH7, UV light = 300 nm.

The monomethylammonium ions was detected after 20 min as a minor product and increased with time to become a major product after 90 min. At this period, only small amount of mineralized products, ammonium and nitrate, were detected. In addition, the evolution of CO<sub>2</sub> was investigated by measuring the decrease of total organic carbon (TOC) which showed in Figure 5.7. Usually, CO<sub>2</sub> evolution can be estimated from the ratio of TOC<sub>i</sub>/TOC<sub>f</sub>, where TOC<sub>i</sub> and TOC<sub>f</sub> were initial and final TOC, respectively. The CO<sub>2</sub> evolution increased with pH solution but only 25% of CO<sub>2</sub> was generated at pH about 3 from photodegradation on both catalysts.

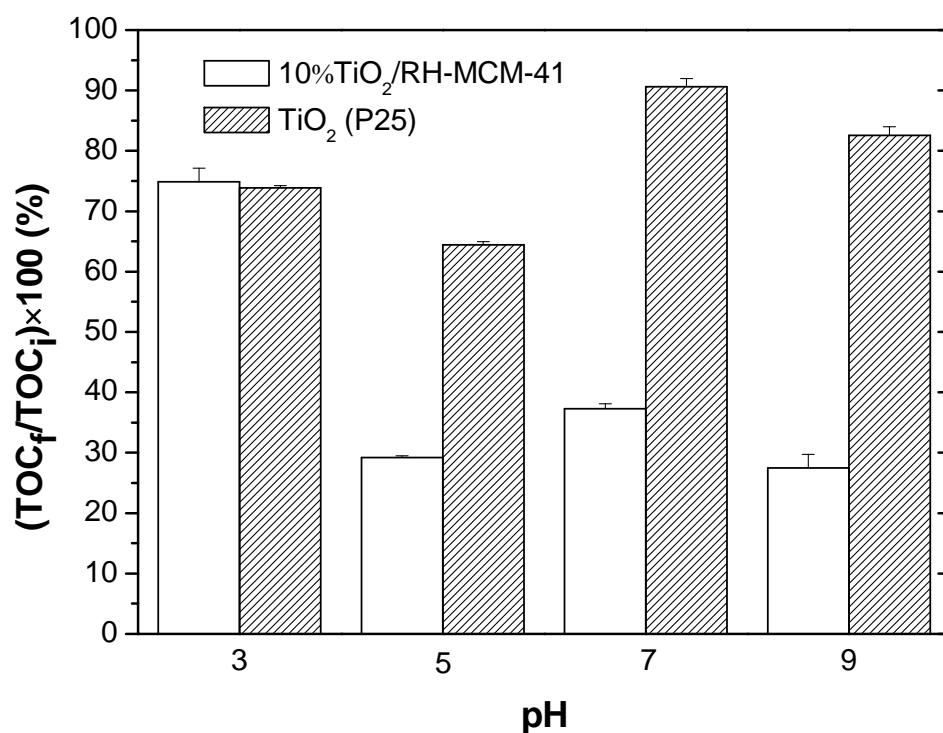


**Figure 5.7** TOC removal from photodegradation of TMA; [TMA] = 100 μM, pH =7,

[TiO<sub>2</sub>/RH-MCM-41] = 1 g/L, [TiO<sub>2</sub>] = 0.1 g/L, UV light = 300 nm.

Like the results from nitrogenous compounds, poorly photocatalytic activity caused by charge repulsion between TMA and surface functional group of solid catalysts. The degradation of TMA on TiO<sub>2</sub>/RH-MCM-41 gave greater CO<sub>2</sub> than that on bare TiO<sub>2</sub> in the pH range of 5 to 9. 70% and 35% of CO<sub>2</sub> was generated on photocatalytic degradation of TMA on TiO<sub>2</sub>/RH-MCM-41 and bare TiO<sub>2</sub> at pH 5, respectively. This clue also told firmly that photocatalytic activity of TiO<sub>2</sub>/RH-MCM-41 was greater than that of bare TiO<sub>2</sub>.

#### 5.4.1.5 Kinetics of reaction

The kinetics of TMA degradation was investigated as the reaction order (see Figure 5.8). The plot between  $\ln C_A$  versus time was straight line with slope and R<sup>2</sup> of 0.029 and 0.9815, respectively following equation:

$$\ln(C_A) = -kt + \ln C_{A_0} \quad \dots(1)$$

From the equation, rate constant (k) of TMA degradation was 0.029 min<sup>-1</sup>. This result implied that photocatalytic degradation of alachlor obeyed the pseudo-first order model as expressed by equation (1).

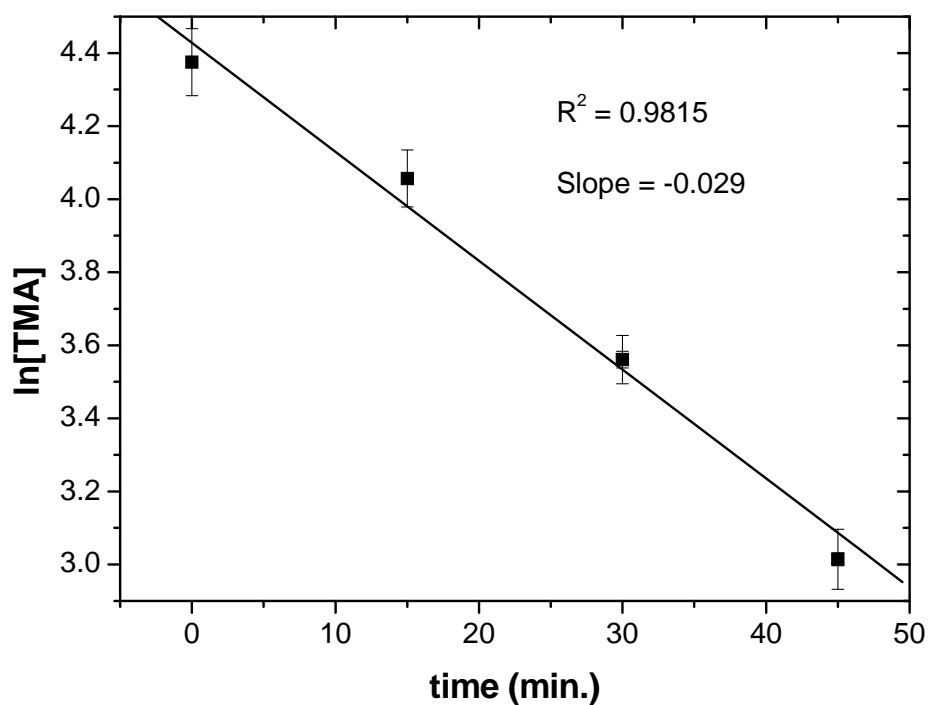


**Figure 5.8** Reaction order of TMA photodegradation on  $\text{TiO}_2/\text{RH-MCM-41}$ ;  $[\text{TMA}] = 100 \mu\text{M}$ ,  $[\text{TiO}_2/\text{RH-MCM-41}] = 1 \text{ g/L}$ ,  $\text{pH} = 7$ , UV light = 300 nm.

#### 5.4.2 Adsorption of TMA on bare $\text{TiO}_2$ and $\text{TiO}_2/\text{RH-MCM-41}$

Adsorption of TMA was investigated after mixing the solution with solid catalysts and stirring in the dark for 30 min. Results are shown in 5.9. After an adsorption equilibrium was established.  $\text{TiO}_2/\text{RH-MCM-41}$  had a higher amount of adsorbed TMA the bare  $\text{TiO}_2$ .

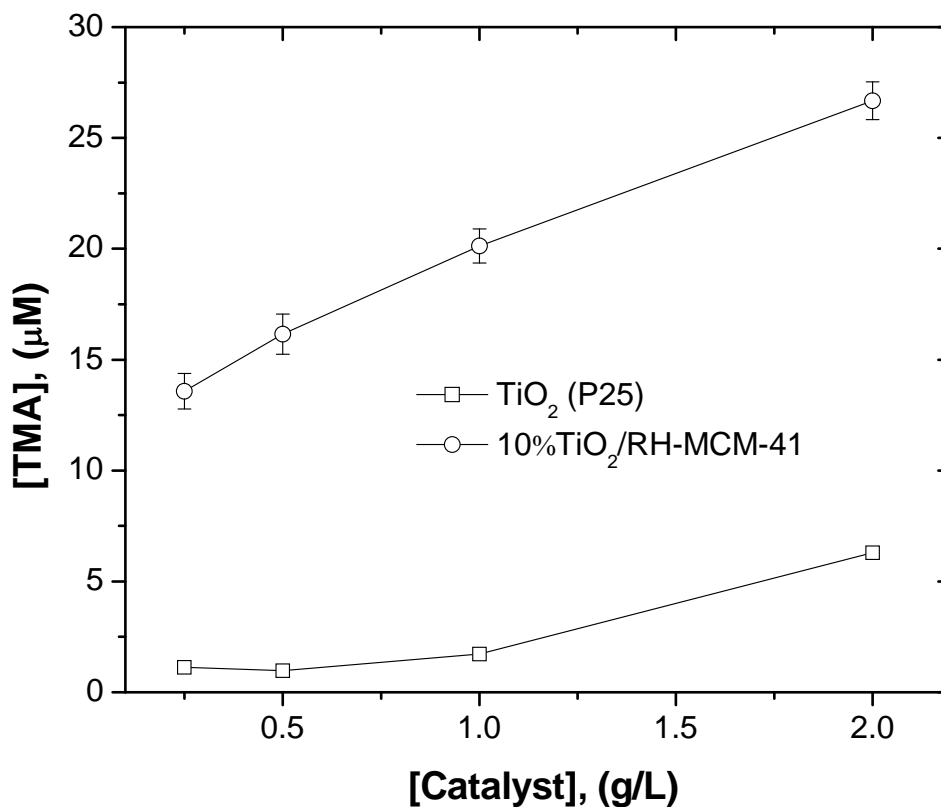


**Figure 5.9** Adsorption of TMA on TiO<sub>2</sub> and TiO<sub>2</sub>/RH-MCM-41; [TiO<sub>2</sub>/RH-MCM-41] = 1 g/L, [TiO<sub>2</sub>] = 0.1 g/L, pH = 7.

The amount adsorbed on TiO<sub>2</sub>/RH-MCM-41 was increased linearly with catalyst concentration. On the other hand, the bare TiO<sub>2</sub> showed a small change in TMA adsorption. This result agreed with the work done by Vohra et al. (2005) in which the adsorption of TMA on bare TiO<sub>2</sub> was nearly zero due to surface properties of bare TiO<sub>2</sub>. Because pH solution in this part of experiment was 7 which closed to p*H*<sub>PZC</sub> of bare TiO<sub>2</sub>, its surface charge was also neutral. Consequently, adsorption of ammonium ions was not preferable at this condition.

Adsorption model of TiO<sub>2</sub>/RH-MCM-41 was investigated in various TMA concentrations. Several adsorptive parameters were concerned including the equilibrium concentration of TMA in solution, the amount of adsorbed TMA on the catalyst at the equilibrium concentration, the maximum adsorption amount and the apparent adsorption equilibrium concentration. The data were plotted in Figure 5.10 according to Langmuir equation (2).

$$\frac{C_e}{q_e} = \frac{C_e}{q_{max}} + \frac{1}{K_{ad} \times q_{max}} \quad \dots(2)$$

Where

$C_e$  = equilibrium concentration of TMA in solution (mg/L)

$q_e$  = amount of adsorbed TMA on the catalyst at the equilibrium concentration  
(mg/g)

$q_{max}$  = maximum adsorption amount of TMA (mg/g)

$K_{ad}$  = apparent adsorption equilibrium constant (mg/L)<sup>-1</sup>

The relationship between  $C_e/q_e$  and  $C_e$  in Figure 5.10 gave a straight line with the slope and R<sup>2</sup> of 0.12 and 0.9999, respectively. The maximum adsorption amount of TMA on TiO<sub>2</sub>/RH-MCM-41 ( $q_{max}$ ) which calculated for reciprocal ratio of slope was 8.34 mg/g and adsorption constant ( $K_{ad}$ ) was  $2.90 \times 10^{-2}$  (mg/L)<sup>-1</sup>. Because adsorption of TMA was monolayer, the interactions between adsorbed molecules were not significant.

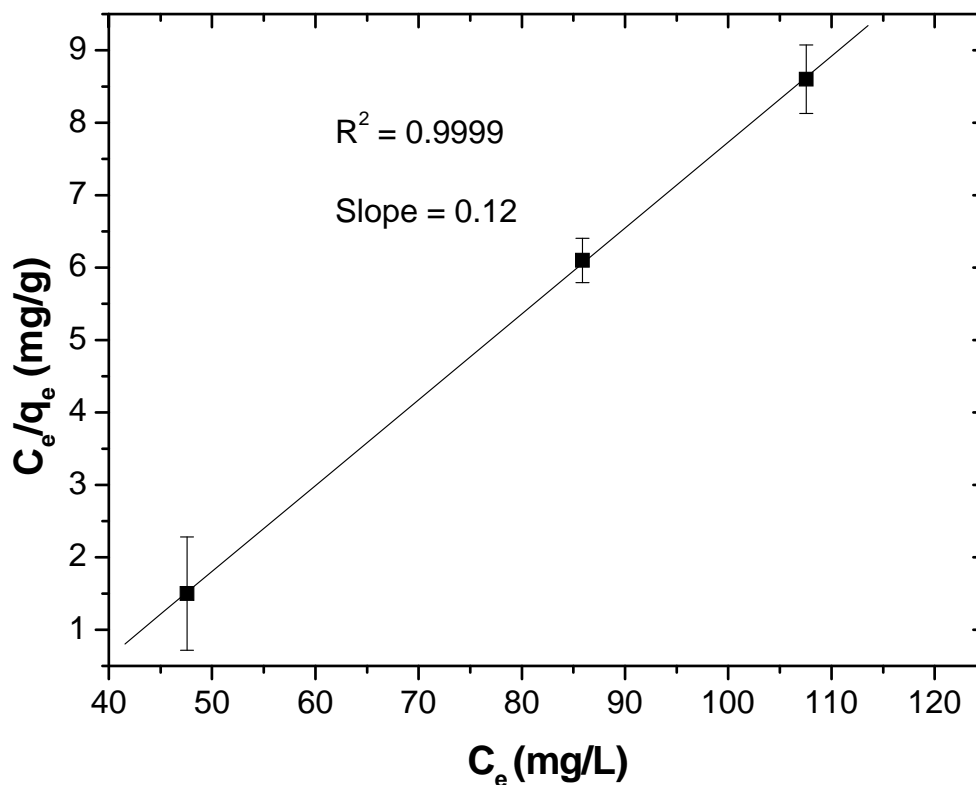


**Figure 5.10** Equilibrium adsorption isotherm of TMA adsorption on  $\text{TiO}_2/\text{RH-MCM-41}$  fitted to Langmuir model;  $[\text{TiO}_2/\text{RH-MCM-41}] = 1 \text{ g/L}$ ,  $\text{pH} = 7$ .

## 5.5 Conclusions

The photocatalytic performance of bare  $\text{TiO}_2$  particles could be enhanced by dispersing them on RH-MCM-41. The morphology and crystallinity of the bare  $\text{TiO}_2$  were not changed after modifying RH-MCM-41. Zeta potential played a key role in surface change of catalysts. Photocatalytic activity of bare  $\text{TiO}_2$  on tetramethylamine was increased by loading proper amount of  $\text{TiO}_2$  on MCM-41 (10%wt.). Adsorption



of TMA on 10%TiO<sub>2</sub>/RH-MCM-41 obeyed Langmuir model which was characteristic adsorption between charge molecule and solid catalysts. The suitable condition for this study is pH7, 10%wt. of TiO<sub>2</sub> loading and 1 g/L of catalyst concentration. The reaction was strongly dependent on pH solution and preferred neutral solution. Photocatalytic activity of TMA on TiO<sub>2</sub>/RH-MCM-41 was greater than that on bare TiO<sub>2</sub>. A complete conversion of TMA was achieved after 90 min. Tri- di- and monomethylamine were detected as the intermediates while ammonium, nitrate and CO<sub>2</sub> were detected as mineralized products. The surface functional groups changing with solution pH played an important role for photocatalytic degradation of tetramethylamine. RH-MCM-41 prevented bare TiO<sub>2</sub> from particle aggregation and electron hole recombination and enhanced photocatalytic activity of it. Order of reaction was found to be pseudo-first order.

## 5.6 References

- Artkla, S., Gridsadanuruk, N., Neramittagapong, S., Wittayakun, J. (2008). Characterization and catalytic performance on transesterification of palm olein of potassium oxide supported on RH-MCM-41 from rice husk silica. **Suranaree Journal of Science and Technology**. 15(2): 133-138.
- Bhattacharyya, A., Kawi, S., Ray, M.B. (2004). Photocatalytic degradation of orange II by TiO<sub>2</sub> catalysts supported on adsorbents. **Catalysis Today**. 98(3): 431-439.
- Carp, O., Huisman, C. L., Reller, A. (2004). Photoinduced reactivity of titanium dioxide. **Progress in Solid State Chemistry**. 32(1): 33-177.
- Hoffmann, M. R., Martin, S. T., Choi, W., Bahnemann, D. W. (1995). Environmental applications of semiconductor photocatalysis. **Chemical Reviews**. 95(1): 69-96.

- Kim, S., Choi, W. (2002). Kinetics and mechanisms of photocatalytic degradation of  $(\text{CH}_3)_n\text{NH}_{4-n}^+$  ( $0 \leq n \leq 4$ ) in  $\text{TiO}_2$  suspension: The role of OH radicals. **Environmental Science and Technology**. 36(9): 2019-2025.
- Konstantinou, I. K., Albanis, T. A. (2004).  $\text{TiO}_2$ -assisted photocatalytic degradation of azo dyes in aqueous solution: kinetic and mechanistic investigations: A review. **Applied Catalysis B: Environmental**. 49(1): 1-14.
- Li, G., Zhao, X. S., Ray, M. B. (2007). Advanced oxidation of orange II using  $\text{TiO}_2$  supported on porous adsorbents: The role of pH,  $\text{H}_2\text{O}_2$  and  $\text{O}_3$ . **Separation and Purification Technology**. 55(1): 91-97.
- Maira, A., Yeung, K. L., Yan, C. Y., Yue, P. L., Chan, C. K. (2000). Size effects in gas-phase photo-oxidation of trichloroethylene using nanometer-sized  $\text{TiO}_2$  catalysts. **Journal of Catalysis**. 192(1): 185-196.
- Pérez, C. N., Moreno, E., Henriques, C. A., Valange, S., Gabelica, Z., Monteiro, J. L. F. (2000). On the stability of MCM-41 after ion-exchange and impregnation with cesium species in basic media. **Microporous Mesoporous Materials**. 41(1): 137-148.
- Vohra, M. S., Lee, J., Choi, W. (2005). Enhanced photocatalytic degradation of tetramethylammonium on silica-loaded titania. **Journal of Applied Electrochemistry**. 35(7): 757-763.
- Zhang, Z., Wang, C-C., Zakaria, R., Ying, J. Y. (1998). Role of particle size in nanocrystalline  $\text{TiO}_2$ -based photocatalysts. **Journal of Physical Chemistry B**. 102(52): 10871-10878.

# CHAPTER VI

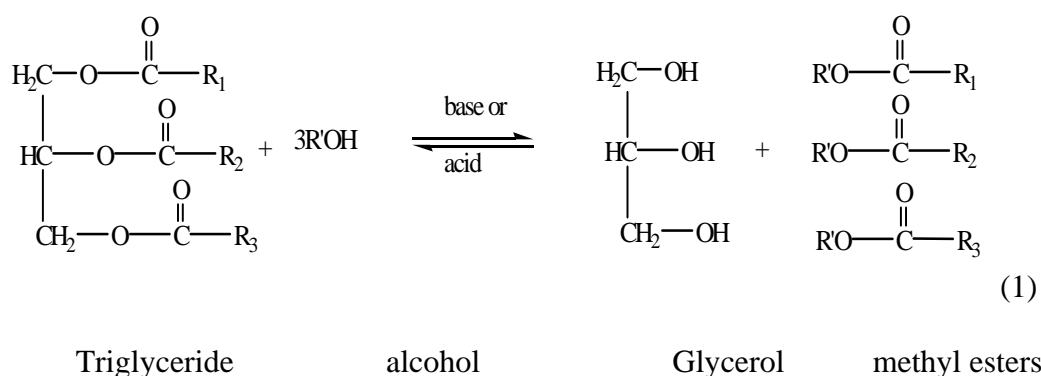
## TRANSESTERIFICATION OF PALM OLEIN OIL WITH METHANOL ON K<sub>2</sub>O/RH-MCM-41

### 6.1 Abstract

Mesoporous material, RH-MCM-41, was synthesized with rice husk silica source by hydrothermal method. The obtained material showed characteristic X-ray diffraction peaks of the (100), (110) and (200) planes at 2.3, 4.0 and 4.7 degree, respectively; and possessed high specific surface area of 1,231 m<sup>2</sup>/g and narrow pore size distribution in the range of 1.8-4.2 nm. It was used as a catalytic support for potassium oxide (K<sub>2</sub>O) from CH<sub>3</sub>COOK precursor to produce K<sub>2</sub>O/RH-MCM-41 with K<sub>2</sub>O loading of 4, 8 and 12% wt. Upon loading with K<sub>2</sub>O, RH-MCM-41 surface area decreased significantly indicating the collapse of mesoporous structure and the tendency to collapse increased with K<sub>2</sub>O loading. The catalytic activities of K<sub>2</sub>O/RH-MCM-41 catalysts were tested for biodiesel production from palm olein oil and methanol via transesterification at 50, 75 and 100 °C. The catalyst with 8% K<sub>2</sub>O loading gave the highest conversion at all tested temperature. At this loading, the activity increased with temperature and the highest conversion was 84% at 100 °C. Products from transesterification were mainly methyl palmitate (C16) and unsaturated methyl ester (oleate, linoleate and linolinate, C18).

## 6.2 Introduction

Because of the rapid growth of world population, diesel fuels are consumed in very large scale per day. Major of the world energy needs are supplied for thought petrochemical source, coal, and natural gases (Meher et al., 2006; Fukuda et al., 2001). In the near future, it will be lack of diesel fossil resources. Alternative renewable fuel sources are needed and biodiesel is among the best choices that can satisfy the desire for renewable energy sources. Biodiesel, referred to a non-petroleum-based diesel fuel consisting of short chain alkyl (methyl or ethyl) esters, can be made from renewable biological sources such as vegetable oils and animal fats via transesterification reaction to produce alkyl esters and glycerol (equation 1).



After processing, the main chemical substances compose of carbon 77%, hydrogen 12%, oxygen 11%, traces amount of nitrogen and sulfur (Encinar et al., 2005). Conventionally, the homogeneous base catalyst such as NaOH, KOH and NaOCH<sub>3</sub> are preferred because they produce high yield of the alkyl ester product, the reaction time is short (about 2 h) and the cost of raw materials is low. Unfortunately, the use of base catalysts is limited only on the well-refined vegetable oil with less than 2.0% free fatty acid (FFA) in order to avoid the formation of soap, undesired

by-product. In addition, it is difficult to separate ester products from glycerol by-products in homogeneous catalysis and the yield of methyl esters is low (Ma and Hanna, 1999). Consequently, the area of heterogeneous catalysis holds the most promise for available continuous processes. Non-solubility of heterogeneous catalysts in alcohol facilitates the separation of biodiesel and solid catalysts. Furthermore, surface functional group of them can be tailored for active site by adding metal or metal oxide. Here we reported the preparation of RH-MCM-41 and K<sub>2</sub>O/RH-MCM-41 and characterization by XRD, BET and XANES. The catalysis of K<sub>2</sub>O/RH-MCM-41 for the biodiesel production was also studied to understand the effects of reaction temperature and potassium oxide content.

## 6.3 Experimental

### 6.3.1 Chemicals and Materials

Chemicals for biodiesel production included methanol (99.8% CH<sub>3</sub>OH, Merck), Triglyceride (palm olein oil) used as a raw material for reaction consisting of 39.8% wt. palmitic acid (C16:0), 54.0% wt. unsaturated acids [oleic acid (C18:1), linoleic acid (C18:2) and linolenic acid (C18:3)] and 4.4% wt. stearic acid (C18:0) (Department of Thailand Agriculture, 2007), K<sub>2</sub>O/RH-MCM-41, hexane (85% C<sub>6</sub>H<sub>14</sub>, Ajax), and sodium sulfate anhydrous (Na<sub>2</sub>SO<sub>4</sub>, analysis grade, Carlo Erba). The standard kit of methyl ester (C6:0-C24:0, aldrich) was used for GC analysis and Methyl heptadecanoate (C17:0) was used as internal standard.

### 6.3.2 Apparatus and instruments

Apparatus and equipments for transesterification palm olein oil with methanol on  $K_2O/RH-MCM-41$  included graduated cylinder, erlenmeyer flask, magnetic stirrer, balance, reflux column, round bottom flask, micropipette, separatory funnel, refrigerator, evaporator, gas chromatograph (Shimadzu GC14-A) equipped with an FID detector.

### 6.3.3 Preparation of $K_2O/RH-MCM-41$

$RH-MCM-41$  was synthesized with a method similar to the explanation in chapter III and used without modification.  $K_2O/RH-MCM-41$  was prepared by impregnation method adapted from literature with  $K_2O$  loading of 4, 8 and 12% wt (Xie et al., 2006). The dried  $RH-MCM-41$  was mixed with  $CH_3COOK$  in methanol solution and vigorously stirred for 3 h. Finally, the mixture was washed with distilled water, calcined at  $500^\circ C$  for 5 h and characterized by XRD, Nitrogen adsorption-desorption and XANES.

### 6.3.4 Characterization of $K_2O/RH-MCM-41$

The crystalline phase of  $RH-MCM-41$  and  $K_2O/RH-MCM-41$  were analyzed using powder X-ray diffraction (XRD: Bruker axs D5005 diffractometer) with  $CuK_\alpha$  radiation. The X-ray was generated with a current of 40 mA and a potential of 40 kV. The catalyst powder (0.20 g) was pressed in a sample holder and scanned from 1.5 to 10 degrees ( $2\theta$ ) in steps of 0.05 degrees per min. The powder patterns of the samples were recorded at the same time and with the same amount of material, so that the intensity of the peak height (100) could be compared.

Nitrogen adsorption-desorption isotherms were determined at  $-196\text{ }^{\circ}\text{C}$  from a relative pressure of 0.001-0.99 on a microporemetrics analyzer (ASAP 2010 V). Before measurement, each sample was degassed at  $300\text{ }^{\circ}\text{C}$  for 12 h. The pore size and pore volumes were calculated from the desorption branches of the isotherm using Barrett-Joyner-Halenda (BJH) method.

XANES spectra of  $\text{K}_2\text{O}/\text{RH-MCM-41}$  and reference compound were measured in the energy region of the potassium K-edge in transmission mode at XAFS beamline (BL-8) of Synchrotron Light Research Institute (Public Organization) in Suranaree University of Technology. The X-ray beam 2s emitted by a storage ring running at 1.2 GeV. X-rays were monochromatized using a Si(111) two-crystal monochromator with energy resolution of  $1.0\times 10^{-4}$ - $5.0\times 10^{-4}$ . The monochromator covers the photon range 1830–8000 eV. Each sample (0.3 g) was pressed into a self-supporting wafer with an approximate thickness of 0.3 mm, placed in a holder, and mounted in a cell. The cell was evacuated and installed at the beamline.

XANES spectra of samples were scanned at K  $\text{K}_{\alpha}$  edge (3608) with integration for 0.2 at each energy step in the range from 50 eV below the absorption edge to 150 eV beyond the edge with transmission mode. The pre-edge in the XANES region were normalized with the software ATHENA. The edge shifts were corrected to standard reference compounds to figure out characteristics of the samples.

### **6.3.5 Catalytic testing for transesterification**

Palm olein oil (4.0 mL) was preheated to reaction temperature and added to a mixture between methanol (10.0 mL) and catalyst (0.3 g). The mixture was stirred for 7 h at 50, 75 or  $100\text{ }^{\circ}\text{C}$ . During the reaction, a pale yellowish liquid was formed and

the viscosity of the mixture decreased significantly. The pale yellowish solution was evaporated to remove the excess methanol and the resulting liquid was separated from the catalyst by gravity under refrigeration. The obtained yellowish solution which contained fatty acid methyl ester (FAME) was analyzed by gas chromatography on a Shimadzu GC14-A.

## 6.4 Results and discussion

### 6.4.1 Characterizations of K<sub>2</sub>O/RH-MCM-41

XRD patterns of RH-MCM-41 and K<sub>2</sub>O/RH-MCM-41 with K<sub>2</sub>O loading of 4, 8, and 12% wt. are shown in Figure 6.1 Spectrum of RH-MCM-41 showed the characteristic reflections of the (100), (110) and (200) planes of hexagonal structure at 2.3, 4.0 and 4.7 degree, respectively, similar to that of MCM-41 from literature (Papp et al., 2005). When RH-MCM-41 was loaded with potassium oxide, the only peak observed was that of the (100) plane and the intensity decreased with the amount of K<sub>2</sub>O. This indicated that mesoporous structure of RH-MCM-41 collapsed upon K<sub>2</sub>O addition. The position of the (100) peak also shifted to higher value with the K<sub>2</sub>O amount indicating the decrease of d spacing. The position of the (100) peak, unit cell width ( $a^*$ ), calculated  $d_{100}$  are showed in Table 1. Thus, the K<sub>2</sub>O loading affected the RH-MCM-41 hexagonal structure and the surface area of RH-MCM-41 was expected to decrease upon K<sub>2</sub>O loading. For 12%K<sub>2</sub>O/RH-MCM-41, the (100) peak was barely observable indicating that its mesoporous structure collapsed almost completely. Although it was still unclear about structure of the collapsed RH-MCM-41, the catalysis of 12%K<sub>2</sub>O/RH-MCM-41 was investigated and compared with that of 12%K<sub>2</sub>O/RH-SiO<sub>2</sub> which was less porous to observe the influence of support.



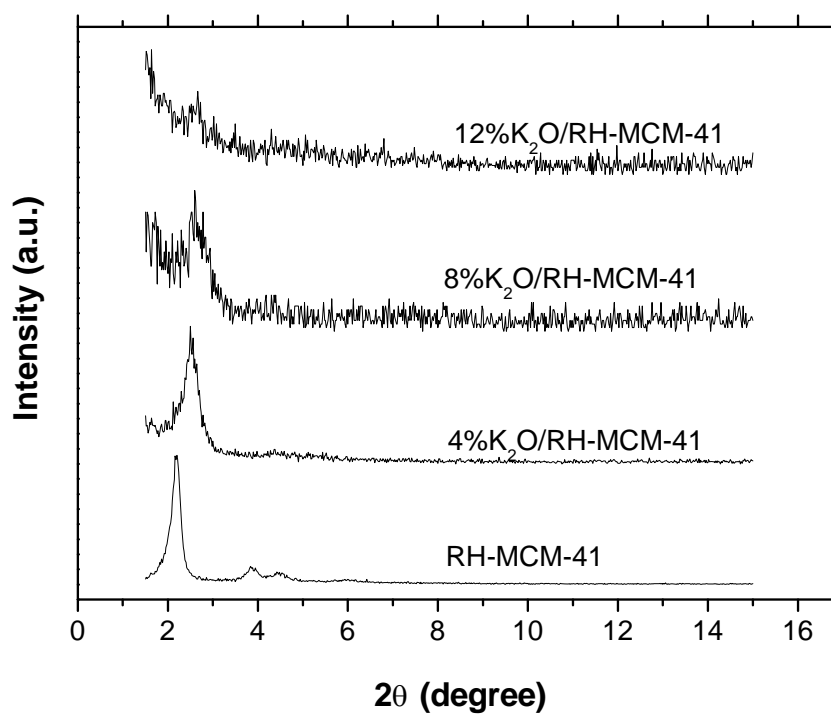


**Figure 6.1** XRD patterns of (a) RH-MCM-41, (b) 4%K<sub>2</sub>O/RH-MCM-41, (c) 8%K<sub>2</sub>O/RH-MCM-41 and (d) 12%K<sub>2</sub>O/RH-MCM-41.

**Table 6.1** Structure properties data of RH-MCM-41 and K<sub>2</sub>O/RH-MCM-41.

Materials	2 $\theta$	a* (Å)	d <sub>100</sub> (Å)
RH-MCM-41	2.3	43.6	37.8
4%K <sub>2</sub> O/RH-MCM-41	2.5	39.4	34.1
8%K <sub>2</sub> O/RH-MCM-41	2.6	38.6	33.4
12%K <sub>2</sub> O/RH-MCM-41	2.7	37.5	32.5

\* Unit cell parameter of RH-MCM-41 and K<sub>2</sub>O/RH-MCM-41 of the 100 plan,

calculated form  $a_{100} = \frac{2}{\sqrt{3}} d_{100}$

The nitrogen adsorption-desorption isotherms of RH-MCM-41 and K<sub>2</sub>O/RH-MCM-41 are displayed in Figure 6.2. RH-MCM-41, Figure 6.2a, and 4%K<sub>2</sub>O/RH-MCM-41, Figure 6.2b, gave Type-IV isotherm with three well-defined stages. In the first step, the adsorption at relative pressure around 0.0-0.2, concaved to the P/P<sub>0</sub> axis due to monolayer adsorption in external surface which were large pores. The lower adsorption volume on 4%K<sub>2</sub>O/RH-MCM-41 indicated lower surface area. The adsorption at relative pressure of 0.2-0.4 for RH-MCM-41 and 0.4-0.8 for K<sub>2</sub>O/RH-MCM-41 were an adsorption in mesopores.

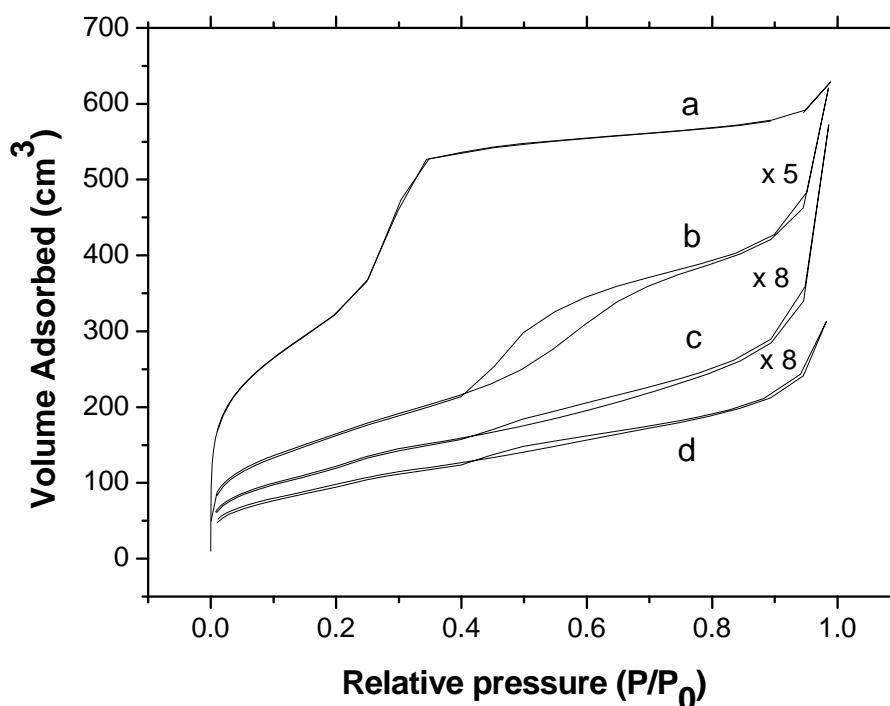


**Figure 6.2**  $N_2$  adsorption-desorption isotherm of RH-MCM-41 and  $K_2O/RH-MCM-41$ ; (a) RH-MCM-41, (b) 4% $K_2O/RH-MCM-41$ , (c) 8% $K_2O/RH-MCM-41$  and (d) 12% $K_2O/RH-MCM-41$ .

The mesopores of 4% $K_2O/RH-MCM-41$  were smaller than those in RH-MCM-41 and thus, required higher pressure. The last step was a plateau until the relative pressure approached one and the adsorption volume increased again to form condensation on the surface. The isotherms of 8% $K_2O/RH-MCM-41$ , Figure 6.2c, and 12% $K_2O/RH-MCM-41$ , Figure 6.2d, were different from that of 4% $K_2O/RH-MCM-41$  in which the adsorption in mesopores at relative pressure 0.4-0.8 disappeared indicating more collapse of the MCM-41 mesoporous structure. In addition, the adsorption amount at low relative pressure on 8% $K_2O/RH-MCM-41$  and

12%K<sub>2</sub>O/RH-MCM-41 compared to that on 4%K<sub>2</sub>O/RH-MCM-41 indicating lower surface area. These results confirmed the XRD results that the increase of K<sub>2</sub>O content on RH-MCM-41 ruined mesoporous structure.

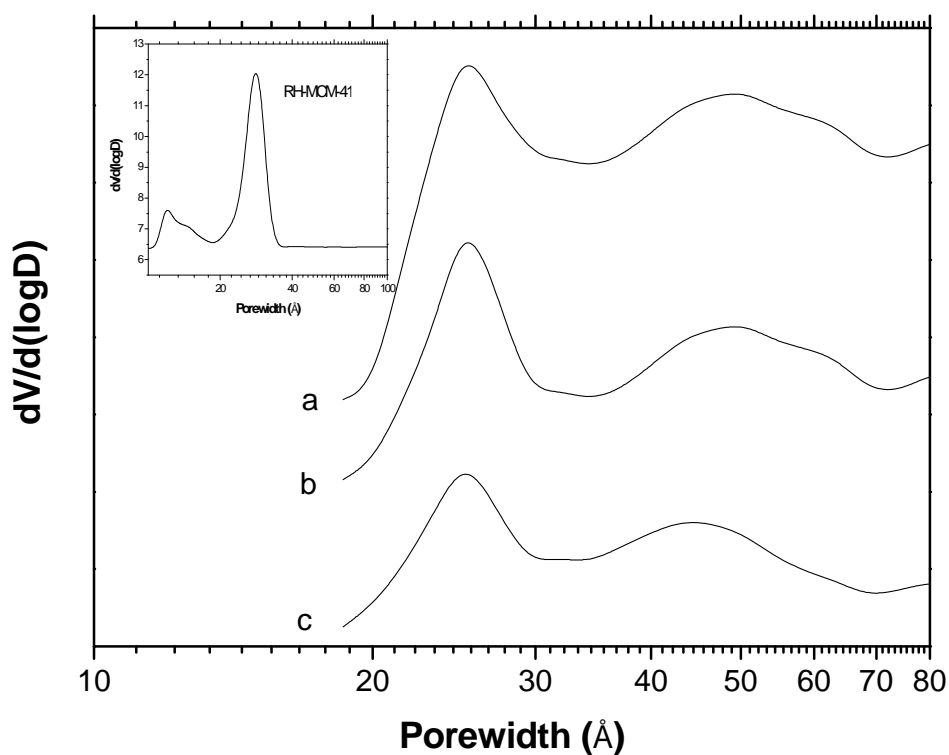


**Figure 6.3** Pore size distribution of RH-MCM-41 and K<sub>2</sub>O/RH-MCM-41; (a) 4%K<sub>2</sub>O/RH-MCM-41, (b) 8%K<sub>2</sub>O/RH-MCM-41 and (c) 12%K<sub>2</sub>O/RH-MCM-41.

The pore size distribution of mesopore in RH-MCM-41 and K<sub>2</sub>O/RH-MCM-41 are presented in Figure 6.3. The pore diameter of RH-MCM-41 was centered at 28.04 Å while the pore size distribution of all K<sub>2</sub>O/RH-MCM-41 still was slightly decreased into 25.37 Å.

The total pore volume and specific surface area of RH-MCM-41 and K<sub>2</sub>O/RH-MCM-41 are presented in Table 6.2. There was a dramatic decrease of surface area and pore size with the addition of K<sub>2</sub>O on RH-MCM-41. In K<sub>2</sub>O/RH-MCM-41 samples, the pore size and surface area decreased with K<sub>2</sub>O content. The table also concluded the BET results of RH-SiO<sub>2</sub> and 8% K<sub>2</sub>O/RH-SiO<sub>2</sub>. These data were used for comparison in the section below.

**Table 6.2** Pore volume and surface area of RH-SiO<sub>2</sub>, RH-MCM-41, K<sub>2</sub>O/RH-SiO<sub>2</sub> and K<sub>2</sub>O/RH-MCM-41.

Materials	V <sub>p</sub> (cm <sup>3</sup> /g)*	S <sub>BET</sub> (m <sup>2</sup> /g)
RH-SiO <sub>2</sub>	0.110	234.2
RH-MCM-41	0.970	1231.4
4% K <sub>2</sub> O/RH-MCM-41	0.190	118.5
8% K <sub>2</sub> O/RH-MCM-41	0.110	55.8
8% K <sub>2</sub> O/RH-SiO <sub>2</sub>	0.003	6.1
12% K <sub>2</sub> O/RH-MCM-41	0.060	44.7

\* Total pore volumes, calculated from N<sub>2</sub> desorption by BJH method.

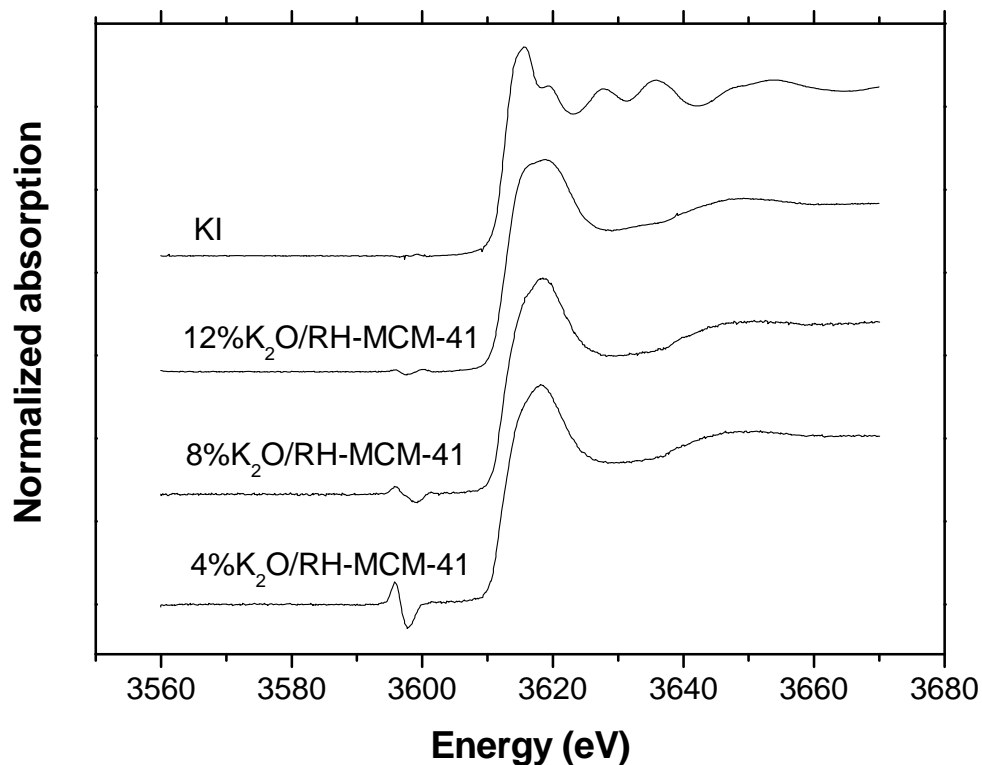


**Figure 6.4** K K-edge XANES spectra of K<sub>2</sub>O/RH-MCM-41 and KI reference.

Normalized K K-edge spectra of K<sub>2</sub>O/RH-MCM-41 and reference sample of KCl are plotted in Figure 6.4 using ATHENA software. In this study, the spectra of all samples were similar, showing features in the energy range 3605–3635 eV. The particular binding energy of K on RH-MCM-41 samples was 3609.04 eV corresponding to KI reference. It implied that oxidation state of K was +1 and located in oxide form. The remark features of these structures were determined by the structural arrangements of the atoms surrounding the K absorber and electronic contributions to the K<sup>+</sup> cation depending on interactions with its direct surrounding (Marcelli et al., 2006).

#### 6.4.2 Catalytic Activity of $K_2O/RH-MCM-41$ and $K_2O/RH-SiO_2$

The conversions of fatty acids were displayed in Figure 6.5-7 in which the formation of methyl palmitate (C16:0), unsaturated methyl esters, including methyl oleate (C18:1), methyl linoleate (C18:2) and methyl linolenate (C18:3), and methyl stearate (C18:0) were plotted versus catalysts with different  $K_2O$  loading, respectively. The formation of methyl esters occurred depending on the amount of fatty acids in the raw material and the most active catalyst for transesterification was 8%  $K_2O/RH-MCM-41$ . In addition, the conversion 8%  $K_2O/RH-MCM-41$  also depended on temperature. However, the conversion at 100 °C was not significantly higher than that at 75 °C (namely, 84% VS. 82%). As a result, the temperature at 75 °C was considered to be the more suitable condition with regards to energy saving.

To compare catalysts on different supports, the catalytic activity of 8%  $K_2O/RH-MCM-41$  and that of 8%  $K_2O/RH-SiO_2$  were determined at 100 °C and the results are compared in Figure 6.8. The 8%  $K_2O/RH-MCM-41$  gave higher conversion of both C-16 and C-18 than 8%  $K_2O/RH-SiO_2$ . This might be contributed to the difference in the surface area because the first one had higher surface area (56 VS 6  $m^2/g$ ).

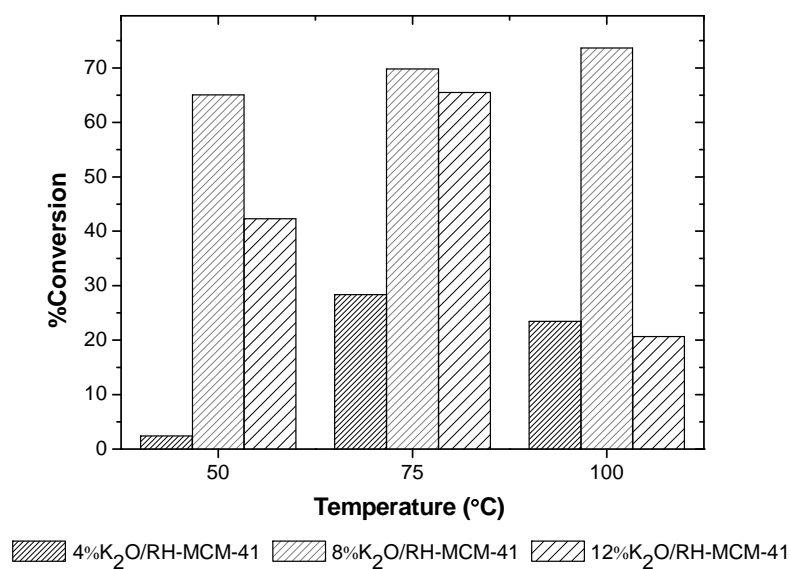


**Figure 6.5** Formation of methyl palmitate on K<sub>2</sub>O/RH-MCM-41 at various temperatures.

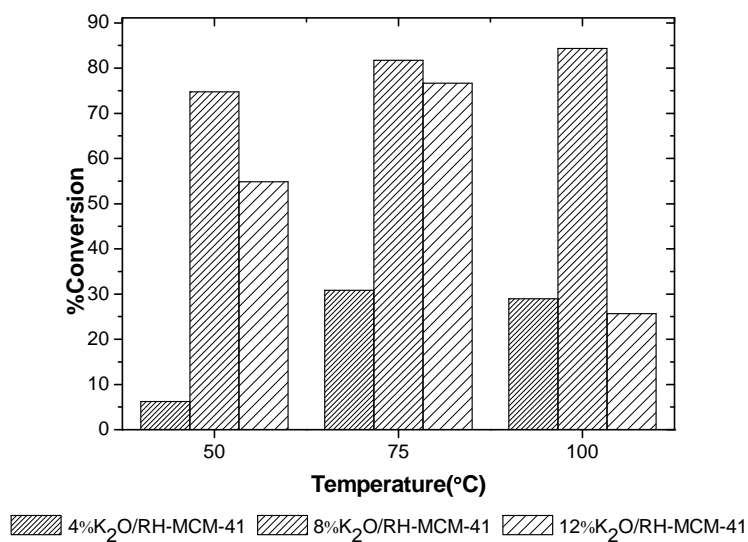


**Figure 6.6** Formation of unsaturated methyl esters (methyl oleate, C<sub>18</sub>:1; methyl linoleate, C<sub>18</sub>:2 and methyl linolenate, C<sub>18</sub>:3) on K<sub>2</sub>O/RH-MCM-41 at various temperatures.



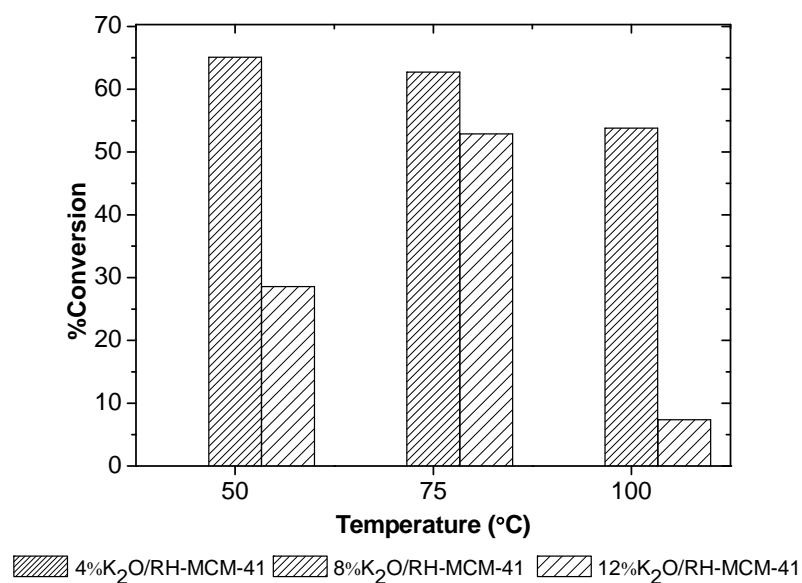


**Figure 6.7** Formation of methyl stearate (C18:0) on K<sub>2</sub>O/RH-MCM-41 at various temperatures.

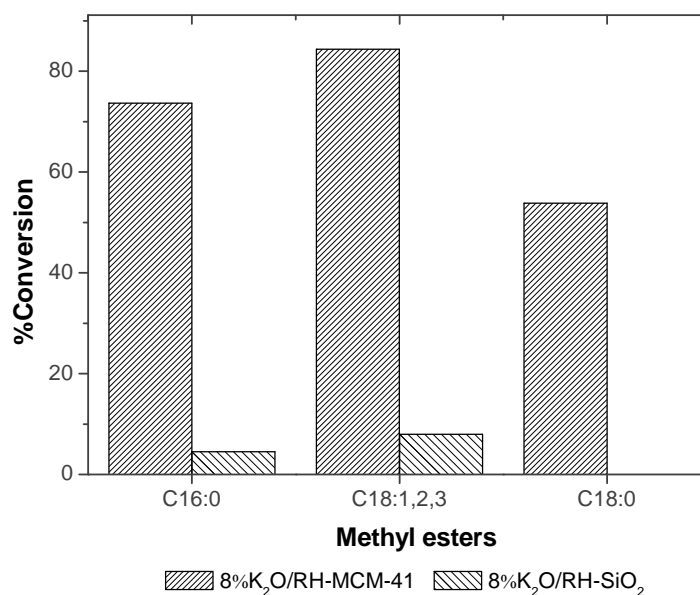


**Figure 6.8** Catalytic activity of 8% K<sub>2</sub>O supported on RH-MCM-41 and RH-SiO<sub>2</sub> at 100 °C.

## 6.5 Conclusions

The K<sub>2</sub>O/RH-MCM-41 was active for the transesterification of palm olein oil with methanol. The performance depended with the K<sub>2</sub>O loading and temperature. The highest conversion was observed on 8%K<sub>2</sub>O/RH-MCM-41 at 100 °C. Both saturated methyl ester (C16:0) and unsaturated methyl esters (C18:1, C18:2 and C18:3) were obtained with approximately 70-80% yield.

## 6.6 References

- Department of Thailand Agriculture. (2007). **Oil palm research center** [On-line], Available from: <http://www.doa.go.th/palm/linkTechnical/process-Oilpalm.html>. Accessed Dec 11, 2007.
- Encinar, J.M., Gonzalez, J.F., and Rodriguez-Renares, A. (2005). Biodiesel from used frying oil: variables affecting the yields and characteristics of the biodiesel. **Industrial and Engineering Chemistry Research**. 44(15): 5491-5499.
- Fukuda, H., Kondo, A., Noda, H. (2001). Biodiesel fuel production by transesterification of oils. **Journal of Bioscience and Bioengineering**. 92(5): 405-416.
- Ma, F., Hanna, M.A. (1999). Biodiesel production: a review. **Bioresource Technology**. 70(1): 1-15.
- Meher, L.C., Vidya Sagar, D., Naik, S.N. (2006). Technical aspects of biodiesel production by transesterification–A review. **Renewable & Sustainable Energy Rev**. 10(3): 248-268.
- Marcelli, A., Cibin, G., Cinque, G., Mottana, A., Brigatti M. F. (2006). Polarized

XANES spectroscopy: The K edge of layered K-rich silicates. **Radiation Physics and Chemistry**. 75(11): 1596-1607.

Papp, A., Molnár, Á., Mastalir, Á. (2005). Catalytic investigation of Pd particles supported on MCM-41 for the selective hydrogenations of terminal and internal alkynes. **Applied Catalysis A: General**. 289(2): 256-266.

Xie, W., Huang, X. and Li, H. (2006). Soybean oil methyl ester preparation using NaX zeolite loaded with KOH as a heterogeneous catalyst. **Bioresource Technology**. 98(4): 936-939.

## CHAPTER VII

### CONCLUSIONS

This work used rice husk which is an agricultural solid waste as a raw material for silica production through acid leaching method. The purity of the obtained silica was 98% and it was used as silica source for syntheses of mesoporous materials referred to as RH-MCM-41 via hydrothermal method. The gel molar ratio in the RH-MCM-41 synthesis was  $1.0\text{SiO}_2 : 0.25\text{CTAB} : 180\text{H}_2\text{O}$  and the gel pH was adjusted to 11.5 before crystallization for 1-3 days and calcination at 500 °C. The product from a longer crystallization time had a higher crystallinity and thicker hexagonal pore walls. All RH-MCM-41s possess high specific surface area ( $> 1000 \text{ m}^2/\text{g}$ ) and narrow pore size distribution (20-35 Å). The RH-MCM-41 was used as a support material for  $\text{TiO}_2$  and  $\text{K}_2\text{O}$ .

The 10wt% Ti-RH-MCM-41 was synthesized with rice husk silica by adding TBOT into the synthetic gel of RH-MCM-41 with the gel molar ratio of  $1.0\text{SiO}_2 : 0.05\text{TBOT} : 3.0\text{NaOH} : 0.25\text{CTAB} : 180\text{H}_2\text{O}$ . In addition,  $\text{TiO}_2/\text{RH-MCM-41}$  with similar Ti content (10 wt%) was prepared by grafting a gel of  $\text{TiO}_2$  onto the preformed RH-MCM-41. Both Ti-RH-MCM-41 and  $\text{TiO}_2/\text{RH-MCM-41}$  were characterized by various techniques. The Ti-MCM-41 had mesoporous structure and surface area of  $1006 \text{ m}^2/\text{g}$  which ensured good Ti dispersion. The Ti oxidation state was IV and it was tetrahedrally coordinated to oxygen atoms. The  $\text{TiO}_2/\text{RH-MCM-41}$  also had hexagonal structure of RH-MCM-41 and the form of  $\text{TiO}_2$  was anatase. Both catalysts were tested for photodegradation of methyl orange. The  $\text{TiO}_2/\text{RH-MCM-41}$

was more active than Ti-RH-MCM-41 because it possessed anatase TiO<sub>2</sub> phase which is active sites for photodegradation. The optimum weight to volume ratio of TiO<sub>2</sub>/RH-MCM-41 to methyl orange solution was 5 g/L and the optimum concentration of methyl orange was 2.0 ppm. The photocatalytic degradation of methyl orange on TiO<sub>2</sub>/RH-MCM-41 obeyed pseudo-first order.

Another TiO<sub>2</sub>/RH-MCM-41 was prepared by dispersing TiO<sub>2</sub> (Degussa P25) on RH-MCM-41 in DI water and calcined at 300 °C for 6 h. Characterization by XRD demonstrated well-define ordered hexagonal array which is characteristic of MCM-41. The crystallinity was diminished by loading of TiO<sub>2</sub> but its interplanar distance did not change. The surface areas of TiO<sub>2</sub>/RH-MCM-41 was lower than that of RH-MCM-41 and pore size of was in the range of 20-35Å. The band gap energy of TiO<sub>2</sub> did not change after dispersion on RH-MCM-41. The pH point of zero charge (pH<sub>pzc</sub>) of TiO<sub>2</sub>/RH-MCM-41 increased with loadings of TiO<sub>2</sub> (P25) from 2.0 (RH-MCM-41) to 6.8 (bareTiO<sub>2</sub>) indicating that proper adsorption which enhance photodegradation was tunable by varying pH solution. This pH<sub>pzc</sub> also controlled zeta potential which played a key role in surface change of catalysts. Photodegradation of alachlor on TiO<sub>2</sub>/RH-MCM-41 prepared from grafting, TiO<sub>2</sub>/RH-MCM-41 prepared by dispersing Degussa P-25 and bare TiO<sub>2</sub> were compared. The photoactivity of the dispersing TiO<sub>2</sub>/RH-MCM-41 was greater than that of grafting TiO<sub>2</sub>/RH-MCM-41 and bare TiO<sub>2</sub>. The reaction was preferable at a natural pH (pH = 3-4) because surface functional groups of solid catalysts were sensitive to pH change. The neutral surface dominated reaction by playing an important role for adsorption of a neutral alachlor molecule. The effect of TiO<sub>2</sub> loading from 10 to 60wt% was almost negligible and the 10%TiO<sub>2</sub>/RH-MCM-41 was sufficient for the reaction. Concentration of alachlor strongly affected

degradation rate and the optimal concentration of 80  $\mu\text{M}$  was significant to control active site of catalyst and UV blocking. Kinetics of the reaction obeyed pseudo first order and the adsorption of alachlor on solid catalysts obeyed Freundlich isotherm for neutralized functional surface.

The photocatalytic performance of  $\text{TiO}_2$  nanoparticles (Degussa P25) on RH-MCM-41, dispersing  $\text{TiO}_2/\text{RH-MCM-41}$ , was further studied for photo-degradation tetramethylammonium (TMA) chloride. The TMA adsorption on  $\text{TiO}_2/\text{RH-MCM-41}$  was much higher than that on the bare  $\text{TiO}_2$  and was described by Langmuir model. A significant improvement in the photocatalytic activity was obtained with the hybrid catalyst and the optimal  $\text{TiO}_2$  loading was 10 wt%. The increase in the mass of the hybrid catalyst (with a fixed %  $\text{TiO}_2$  loading) caused a significant improvement in the photocatalytic activity whereas the increase in %  $\text{TiO}_2$  loading on the support (with a fixed mass of the hybrid catalyst) did not enhance the photodegradation activity. The photodegradation activity of 10%  $\text{TiO}_2/\text{RH-MCM-41}$  strongly depended on the solution pH and was maximal around the neutral pH while that of bare  $\text{TiO}_2$  photocatalyst showed the reverse dependence on pH. A complete photocatalytic conversion of TMA was achieved in 90 min irradiation. Tri- di- and monomethylamine were generated as the main intermediates along with ammonium and nitrate as minor products. Photo-degradation with  $\text{TiO}_2/\text{RH-MCM-41}$  was much faster not only for the removal of the parent substrate (TMA) but also its mineralization.

Finally,  $\text{K}_2\text{O}/\text{RH-MCM-41s}$  were prepared by impregnation of potassium acetate on  $\text{RG-MCM-41}$  and calcined at 500  $^\circ\text{C}$  for 5 h to obtain 4%, 8% and 12%  $\text{K}_2\text{O}/\text{RH-MCM-41}$ . The prepared  $\text{K}_2\text{O}/\text{RH-MCM-41}$  was characterized by XRD and

nitrogen adsorption-desorption analysis. The crystallinity of RH-MCM-41 diminished by loading of  $K_2O$  coincided to the decrease of specific surface area and volume adsorbed. The  $K_2O/RH-MCM-41$  had higher surface area and volume adsorbed than that of  $K_2O/RH-SiO_2$ . Consequently, all catalysts were further tested for the transesterification of palm olein with methanol. The results showed that there was no generation of biodiesel on both neat  $RH-SiO_2$  and  $RH-MCM-41$ . The  $K_2O$  on  $RH-MCM-41$  was active for transesterification and the reaction depended on  $K_2O$  loading and temperature. The  $K_2O/RH-MCM-41$  gained greater activity in biodiesel production than that of  $K_2O/RH-SiO_2$ . The highest conversion was found on 8%  $K_2O/RH-MCM-41$  at 100 °C. Both saturated methyl ester (C16:0) and unsaturated methyl esters (C18:1, C18:2 and C18:3) were obtained with approximately 70-80% yield. It can be rationalized that specific surface area was responsible to provide adsorptive site of reagents and reaction rate is preferable on  $K_2O/RH-MCM-41$  to  $K_2O/RH-SiO_2$ .

## **APPENDIX**



## THESIS OUTPUT

1. Artkla, S., Grisdanurak, N., Neramittagapong, S., Wittayakun, J. (2008). Characterization and catalytic performance on transesterification of palm olein of potassium oxide supported on RH-MCM-41 from rice husk silica, **Suranaree J. Sci. Technol.**, 15(2): 133-138.
2. Artkla, S., Choi, W., Wittayakun, J. (2009). Enhancement of catalytic performance of MCM-41 synthesized with rice husk silica by addition of titanium dioxide for photodegradation of alachlor, **Environment Asia**, 2(1): 41-48.
3. Artkla, S., Grisdanurak, N., Wantala, K., Srinameb, B., Wittayakun, J. Characteristics and photocatalytic degradation of methyl orange on Ti-RH-MCM-41 and TiO<sub>2</sub>/RH-MCM-41, Korean Journal of Chemical and Engineering, **Accepted.**
4. Artkla, S., Kim, W., Choi, W., Wittayakun, J. Highly enhanced photocatalytic degradation of tetramethylammonium on the hybrid catalyst of titania and MCM-41 obtained from rice husk silica, Applied Catalysis B: Environmental, **Accepted.**

## CURRICULUM VITAE

Surachai Artkla was born on March 13, 1981 in Yasothon, Thailand. He received a B. Sc. with honors in chemistry from Ubon Ratchathani University, Ubon Ratchathani in 2004; a Grad. Dip. in science teaching profession from Silpakorn University, Nakhonpatom in 2005 and a Ph. D. in chemistry from Suranaree University of Technology, Nakhon Ratchasima, Thailand in 2009. He will start working at Roi-Et Rajabhat University in 2009.

### Publications

1. Artkla, S., Grisdanurak, N., Neramittagapong, S., Wittayakun, J. (2008). Characterization and catalytic performance on transesterification of palm olein of potassium oxide supported on RH-MCM-41 from rice husk silica, **Suranaree J. Sci. Technol.** 15(2): 133-138.
2. Artkla, S., Choi, W., Wittayakun, J. (2009). Enhancement of catalytic performance of MCM-41 synthesized with rice husk silica by addition of titanium dioxide for photodegradation of alachlor, **Environment Asia.** 2(1): 41-48.
3. Artkla, S., Grisdanurak, N., Wantala, K., Srinameb, B., Wittayakun, J. (2009). Characteristics and photocatalytic degradation of methyl orange on Ti-RH-MCM-41 and TiO<sub>2</sub>/RH-MCM-41, **Accepted.**
4. Artkla, S., Kim, W., Choi, W., Wittayakun, J. (2009). Highly enhanced photocatalytic degradation of tetramethylammonium on the hybrid catalyst of titania and MCM-41 obtained from rice husk silica, **Accepted.**